

# Resonances in Electron Impact on Diatomic Molecules\*†

George J. Schulz

Department of Engineering and Applied Science, Mason Laboratory, Yale University, New Haven, Connecticut 06520

In this review we present the energies, configuration, and other properties of resonances (also called "compound states" and "temporary negative ions") in diatomic molecules. Much of the information is presented in the form of tables and energy level diagrams. Vibrational, rotational, and electronic excitation are discussed whenever these processes have given information on resonances; often these excitation processes proceed via resonances. The paper is divided according to molecular species ( $H_2$ ,  $N_2$ ,  $CO$ ,  $NO$ ,  $O_2$ ), but the main conclusions are discussed by the nature of the processes involved.

## CONTENTS

I. Introduction	423	VI. Oxygen	468
A. Classification of Compound States	426	A. Compound State at Low Energy: $X^2\Pi_g$ (0–1 eV)	468
B. Parentage of Core-Excited Feshbach Resonances	428	1. Elastic Scattering	468
II. Hydrogen	429	2. Vibrational Excitation of $O_2$ at Low Energy (0–1.0 eV)	469
A. Resonance at Low Energy: 0–4 eV ( $^2\Sigma_u^+$ )	429	3. Potential Energy Curve for $O_2^-$ ( $X^2\Pi_g$ )	471
1. Elastic Cross Section	429	4. Equilibrium Internuclear Separation and Electron Affinity: Photodetachment Spectroscopy	471
2. Vibrational Excitation in $H_2$ via $^2\Sigma_u^+$	429	5. Three-Body Attachment in $O_2$	472
3. Rotational Excitation via the $^2\Sigma_u^+$ State and Angular Distributions	431	B. Dissociative Attachment (4.4–10 eV): $^2\Pi_u$ State	474
4. Dissociative Attachment at 3.75 eV	433	C. Core Excited Resonances	475
5. Effect of Rotational Levels of the $H_2$ Target Molecule of $H^-$ Formation near 3.75 eV	435	1. Band "a"	475
6. Associative detachment: $H^- + H \rightarrow H_2^- \rightarrow H_2 + e$	436	2. Band "b"	476
B. Resonance in the 10-eV Region ( $^2\Sigma_g^+$ )	439	VII. Conclusions	476
C. Core-excited Resonances in the 11–15 eV Region	440	A. Shape Resonances	476
1. Band "a"	444	B. Core-Excited Shape Resonances	476
2. Band "b"	445	C. Binding of Rydberg Resonances	477
3. Band "c"	446	D. Thresholds of Inelastic Cross Sections	477
4. Band "d"	446	Acknowledgments	477
5. Band "e"	447	Appendixes	
6. Band "f"	447	I. Core-Excited $H_2^-$ States	478
7. Band "g"	448	II. Core-Excited $D_2^-$ States	479
III. Nitrogen	448	III. Branching Ratios for Series "a" in $H_2$	479
A. Resonance at Low Energy (1.7–4 eV) $^2\Pi_g$	448	IV. Core-Excited Resonances in $N_2$ (11–15 eV)	480
1. Elastic Cross Section via $^2\Pi_g$	448	V. Shape Resonances Associated with $B^3\Pi_g$ and $A^3\Sigma_u^+$ States in $N_2$ (8–11 eV)	480
2. Vibrational Excitation via $^2\Pi_g$	449	VI. Resonances in $CO$ (10–15 eV)	481
3. Threshold Behavior of the Cross Section to $v=1$	457	VII. Vibrational Spacings and Franck-Condon Probabilities for Four Bands in $NO^-$	482
4. Angular Distributions	457	VIII. Resonances in $NO$ and Their Grandparents (12–18 eV)	482
5. Pure Rotational Excitation via $^2\Pi_g$	458	IX. Spacing of Vibrational States of $O_2^-$ ( $X^2\Pi_g$ )	482
B. Core-Excited Resonances in the 11–15 eV Region	458	X. Vibrational Cross Sections and Resonance Energies in $O_2^-$ at Low Energies	483
1. Band "b"– $^2\Sigma_g^+$	458	XI. Core-Excited Resonances in $O_2$	484
2. Shape Resonances and Inelastic Thresholds	459	References	484
3. Structures 5 and 6	459		
4. Bands "c" and "d"	460		
C. Bands "a" and "a'": Core-Excited Shape Resonances	460		
D. Resonances above the Ionization Potential in $N_2$	460		
IV. Carbon Monoxide	461		
A. Resonance at Low Energy (1–3 eV) $^2\Pi$	461		
1. Elastic Cross Section via $^2\Pi$	461		
2. Vibrational Excitation via $^2\Pi$	461		
3. Angular Distributions	461		
B. Dissociative Attachment (9.65–12 eV)	462		
C. Core-Excited Resonances in the 10–15 eV Region	462		
1. $^2\Sigma^+$ Resonances (10.04 eV, 10.28 eV)	462		
2. Shape Resonances and Inelastic Thresholds	463		
3. Band "a"	463		
D. Resonances above the Ionization Potential in $CO$	463		
V. Nitric Oxide, $NO$	464		
A. Compound State at Low Energy (0–1.5 eV) $X^2\Sigma^-$	464		
1. Elastic Scattering	464		
2. Vibrational Excitation (0–1.4 eV)	465		
3. Equilibrium Internuclear Separation and Electron Affinity: Photodetachment Spectroscopy	466		
B. Dissociative Attachment (7–10 eV)	466		
C. Core-Excited Resonances in $NO$	466		
1. Bands "a" to "d"	466		
2. The 12 eV–18 eV Region	467		

This paper is a continuation of the one immediately preceding, which deals with resonances occurring when electrons are incident on atoms. In the present paper we present a review of the energy levels, the designations, and the general properties of compound states in *diatomic molecules*. An attempt is made to present much of the information in the form of tables and energy level diagrams.

## I. INTRODUCTION

*Compound states* are formed by the interaction of an incident electron with a target molecule in which the incident electron is temporarily captured in the neighborhood of the molecule. The complex thus formed can also be called a *temporary negative ion* or a *resonance*.

TABLE I. Semantics of resonances.

First name	Last name	Parent	Energy <i>vis a vis</i> parent	Some characteristics	Examples
Single-particle Shape (1 particle, 0 holes)	...	Ground electronic state	above (0-4 eV)	Vibrational excitation; dissociative attachment at low energy	N <sub>2</sub> (2.3 eV) H <sub>2</sub> (2-4 eV)
Core-excited Particle-hole (2 particles, 1 hole)	Feshbach; Type I; closed-channel	Mostly Rydberg excited state	below (~0.5 eV)	Bands correlated to grandparent; sharp structure; many decay channels	N <sub>2</sub> (11.48 eV) H <sub>2</sub> (Bands "a"- "g")
	Shape; Type II; open-channel	Rydberg or valence excited state	above (0-2 eV)	Dissociative attachment	N <sub>2</sub> (9-11 eV) H <sub>2</sub> (8-12 eV)
Doubly core-excited (3 particles, 2 holes)	Feshbach	Doubly excited Rydberg and valence states	below	Above ionization; 2-electron decay	He (57.16 eV)
	Shape		above		N <sub>2</sub> (22 eV)

The latter term indicates that the attachment of the electron often occurs at a definite energy, leading to sharp structures in the cross section. However, sometimes the lifetime of the compound state is so short that the *width* of the state, as given by the uncertainty principle, is large. The terms *compound state*, *temporary negative ion*, or *resonance* are used interchangeably and authors have even used superfluous nomenclatures such as "temporary negative ion resonance."

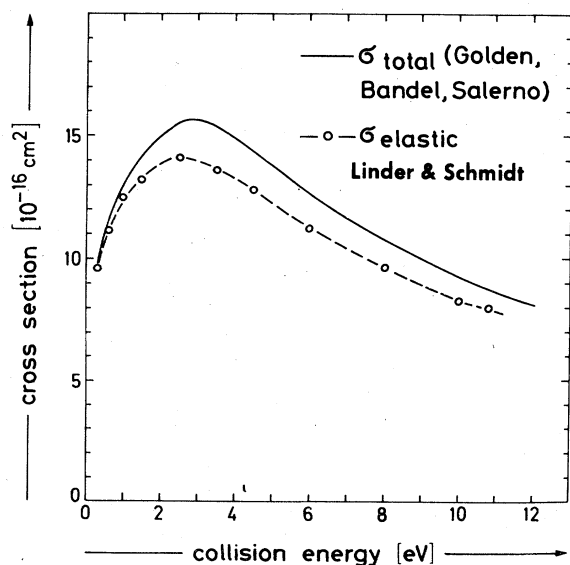


FIG. 1. Total cross section in H<sub>2</sub> (Golden *et al.*, 1966) and elastic portion alone (Linder and Schmidt, 1971a). The absolute magnitude of Linder's curve is normalized to Golden's value at the lowest energy. The difference between the two curves represents the sum of all inelastic cross sections. [From Linder and Schmidt (1971a).]

The first reference to the possibility that compound states might exist can be traced to a paper by Franck and Grottrian (1921). Experimental evidence for structure in the total cross section (e.g., N<sub>2</sub>) became available shortly thereafter, but a resonance model was not

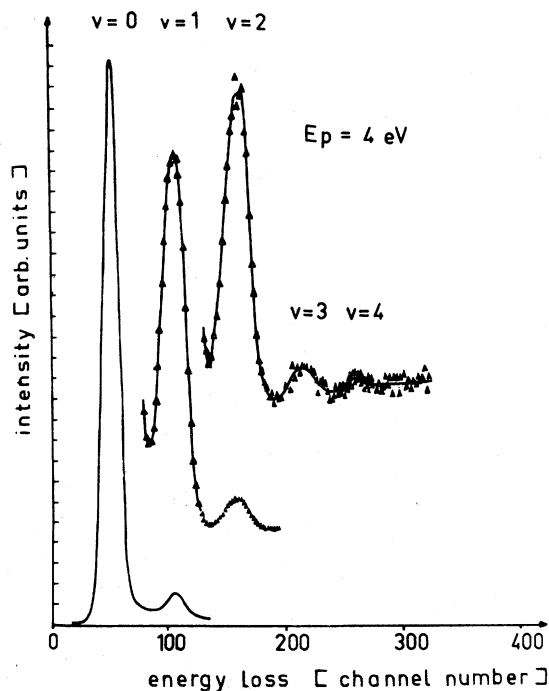


FIG. 2. Energy loss spectrum of 4-eV electrons after collision with H<sub>2</sub> molecules. The peak marked  $v=0$  represents elastic scattering. The peaks marked  $v=1, 2, 3,$  and  $4$  represent the excitation of vibrational quanta of the neutral molecule via the short-lived negative ion state  ${}^2\Sigma_u^+$ . [From Ehrhardt, Langhans, Linder, and Taylor (1968).]

applied to these observations at that time. Although there was a need to understand such structures in the cross section and also the large vibrational cross sections observed experimentally (e.g.,  $H_2$ ), the resonance model remained confined for a long time to nuclear physics alone. The application of the resonance model to molecules in the early 1960's led to a rapid progress in our understanding of electron impact on molecules and solved many long-standing puzzles in atomic physics.

Compound states in molecules which have been observed to date have a lifetime in the range  $10^{-10}$ – $10^{-15}$  sec ( $\tau = \hbar/\Gamma$ , where  $\tau$  is the lifetime and  $\Gamma$  is the width of the state). They decay by the emission of an electron into various final states which are accessible energetically. The beauty of molecules is the variety of decay

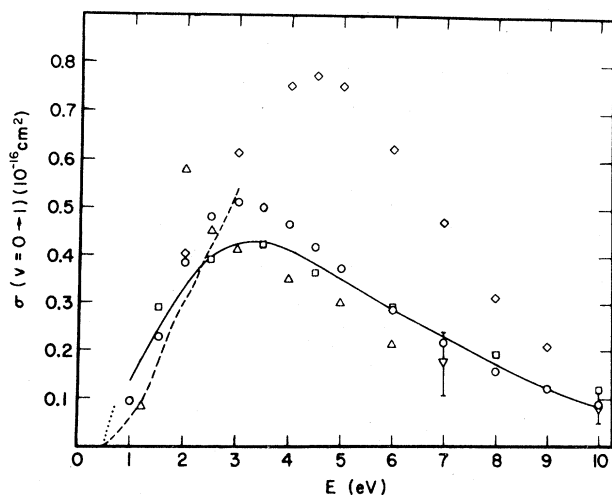


FIG. 3. Total vibrational cross section to  $v=1$  in  $H_2$ . Experimental results using double electrostatic analyzers:  $\square$  Linder and Schmidt (1971a);  $\circ$  Ehrhardt *et al.* (1968);  $\nabla$  Trajmar *et al.* (1970);  $\triangle$  Schulz (1964). Experimental results using swarms:  $\diamond$  Engelhardt and Phelps (1963);  $---$  Crompton *et al.* (1970). Experimental results using the trapped-electron method:  $\cdots$  Burrow and Schulz (1969). Theory:  $-$  Henry and Chang (1972). [From Henry and Chang (1972).]

channels that are possible for compound states: vibrational and rotational excitation, electronic excitation, elastic scattering, dissociative attachment, three-body attachment, and others. Often, a major portion of the cross section for these processes proceeds via a compound state. This is especially true in the case of vibrational excitation and in several instances of electronic excitation near threshold. Dissociative attachment can be completely understood in terms of the formation of a compound state which subsequently autoionizes and also separates into a neutral atom and a negative ion. The lifetime of the compound state, together with the separation time, determine the magnitude of the dissociative attachment cross section.

The preferential decay of some compound states into inelastic channels offers certain advantages for the

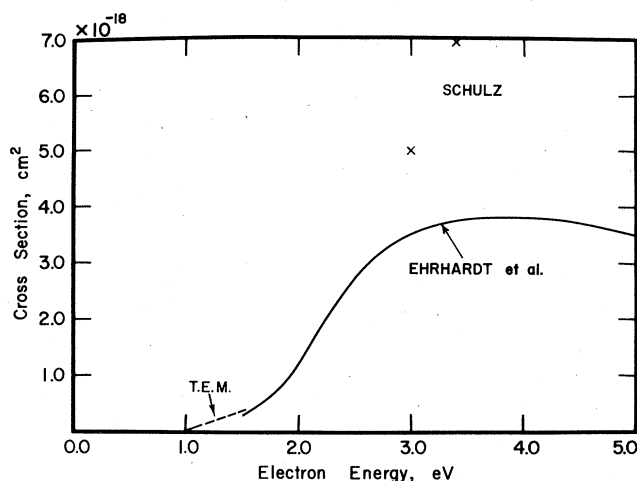


FIG. 4. Vibrational cross section to  $v=2$  in hydrogen. The slope of the cross section near threshold is determined using the trapped electron method and is indicated by the dashed lines, marked T.E.M. (Burrow and Schulz, 1969). Also shown are the double electrostatic analyzer data of Ehrhardt *et al.* (1968) and Schulz (1964a). [From Burrow and Schulz (1969).]

study of compound states. When the bulk of the inelastic cross section consists of the decay of the compound state, then the direct-scattering contribution is nearly absent and one can observe the resonant contribution alone, without interference with the non-resonant contribution. When one considers the Breit-Wigner formula, which governs the shape of single

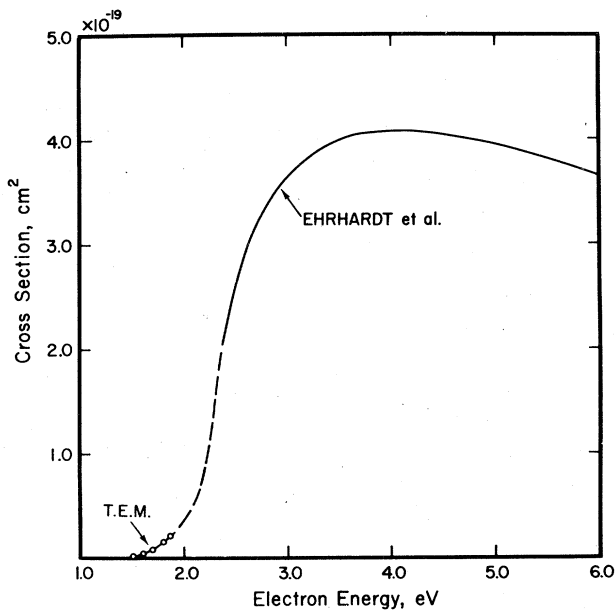


FIG. 5. Vibrational cross section to  $v=3$  in hydrogen. The cross section near threshold is determined by Burrow and Schulz (1969) using the trapped electron method, shown by the open circles. The double electrostatic analyzer data of Ehrhardt *et al.* (1968) are shown by the solid line. The dashed line is an interpolation. [From Burrow and Schulz (1969).]

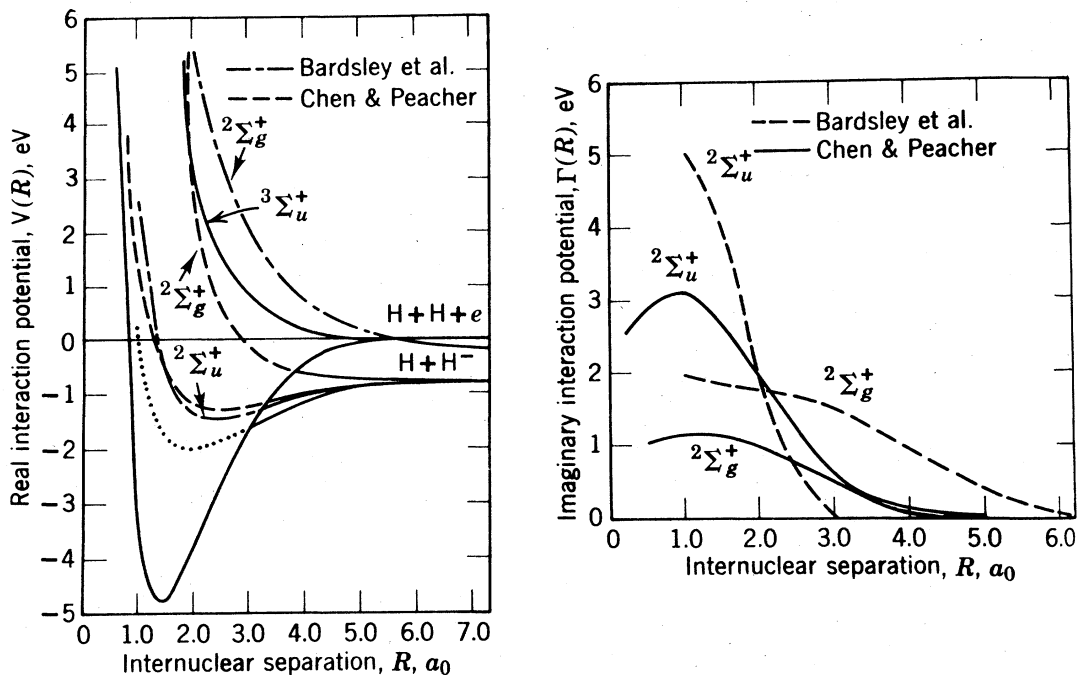


FIG. 6. The real and imaginary parts of the potential energy curves for the  $2\Sigma_u^+$  and  $2\Sigma_g^+$  states of  $H_2^-$ . On the left-hand side are shown the potential energy curves for  $H_2$  (—), and the potential energy curves for  $H_2^-$  derived by Bardsley *et al.* (1966a) and by Chen and Peacher (1968a). The dotted curve indicates the real part of the potential curve for the  $2\Sigma_u^+$  state which is needed to obtain agreement with the vibrational cross section of Ehrhardt, *et al.* (1968). The repulsive curve for  $H_2^-$  ( $2\Sigma_g^+$ ) of Chen and Peacher (1968a) is in very good agreement with the curve derived by Eliezer, Taylor, and Williams (1967), which is shown in Fig. 25(a). The potential energy curves for the lowest states of  $H_2$  ( $1\Sigma_g^+$  and  $3\Sigma_u^+$ ) are taken from Kolos and Wolnicwicz (1965). The right-hand side of the figure shows the calculated widths of the  $2\Sigma_u^+$  and  $2\Sigma_g^+$  states. [From Chen 1969.]

compound states, namely,

$$\sigma(E) \propto |A + (\Gamma_{in}\Gamma_{out})^{1/2} / (E - E_0 + \frac{1}{2}i\Gamma)|^2,$$

then the term  $A$ , representing the direct contribution to scattering, is small compared to the resonance term in inelastic processes. Above,  $\Gamma_{in}$  is the partial width for decay into the ground state,  $\Gamma_{out}$  is the partial width for decay into the excited state, and  $\Gamma$  is the total width, related to the partial widths by  $\Gamma = \Gamma_{in} + \Gamma_{out}$ .  $E_0$  is the resonant energy.

Other review papers have recently appeared: Taylor *et al.* (1966), Bardsley and Mandl (1968), Burke (1968), Massey and Burhop (1969), Chen (1969), Herzenberg (1970, 1971), Taylor (1970). The nomenclature and general approach used in this review have been strongly influenced by these papers. Phelps (1968) has recently reviewed vibrational and rotational cross sections; Takayanagi and Itikawa (1970) have reviewed rotational cross sections. Golden, Lane, Temkin, and Gerjuoy (1971) have reviewed low-energy scattering experiments and rotational excitation and have given a review of experimental techniques. The aim of the present review is the tabulation and discussion of experimental values for compound states: their positions, widths, and classifications. Theoretical considerations

are brought in only in those cases where they are needed for the discussions, but no attempt is made to include the bulk of theoretical considerations. Experimental methods are briefly discussed in the paper immediately preceding, which deals with compound states in atoms.

### A. Classification of Compound States

We can classify compound states in molecules, in an analogous manner to that in atoms (see preceding

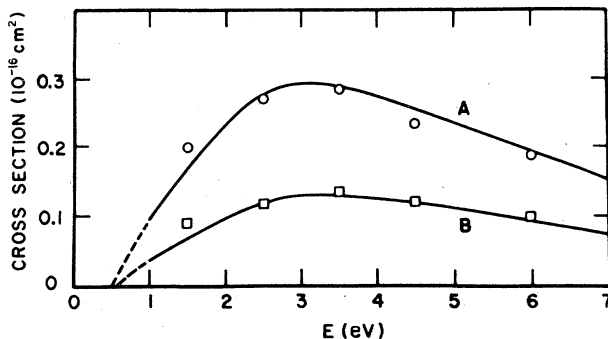
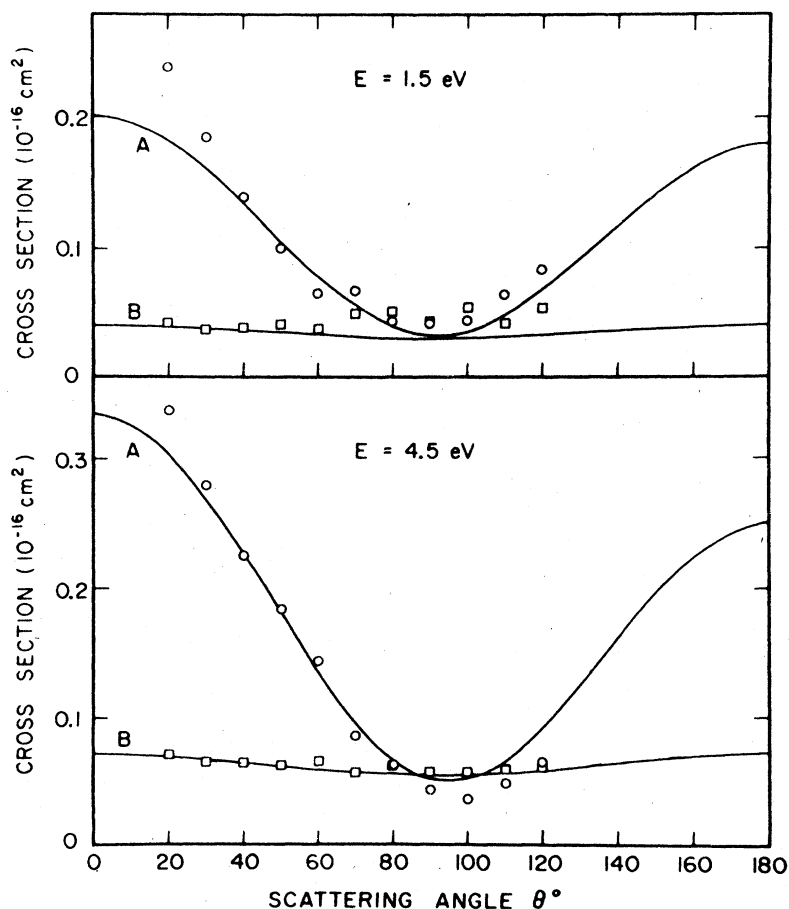


FIG. 7. Curve A: Energy dependence of pure vibrational cross section,  $\sigma(v=0 \rightarrow 1, \Delta j=0)$ . Curve B: Energy dependence of rotational-vibrational cross section,  $\sigma(v=0 \rightarrow 1, j=1 \rightarrow 3)$ . Points are experimental (Linder and Schmidt, 1971a), lines are theoretical (Henry and Chang, 1972). [From Henry and Chang (1972).]

FIG. 8. Curve A: Angular distributions for pure vibrational excitation  $\sigma(v=0 \rightarrow 1; \Delta j=0)$ . Curve B: Angular distribution for rotational-vibrational excitation  $\sigma(v=0 \rightarrow 1; j=1 \rightarrow 3)$ . Points are experimental (Linder and Schmidt, 1971a) and lines are theoretical. [From Henry and Chang (1972).]



paper), into two major categories depending on the state of the target molecule to which the incident electron attaches. Table I may serve as a helpful guide to the semantics of compound states.

When the incident electron is trapped in the potential connected with the ground electronic state, we speak of *shape resonances* or *single particle resonances*. The two terms are synonymous. In this case, the centrifugal, polarization, and exchange forces combine to create a potential with a penetrable barrier. Thus, it is the *shape* of the potential which is responsible for the trapping of the particle and for the resonance. Shape resonances associated with the ground electronic state have been substantiated in all diatomic molecules studied to date ( $\text{H}_2$ ,  $\text{D}_2$ , HD,  $\text{O}_2$ ,  $\text{N}_2$ , NO, CO). They occur at low energies (0–4 eV), exhibit a lifetime in the range  $10^{-16}$  sec to  $10^{-10}$  sec or even longer, and decay into vibrational and rotational levels of molecules and sometimes into negative ions by dissociative attachment. In all cases described in this review, vibrational excitation proceeds predominantly via shape resonances; resonances also play an important role in rotational excitation. Thus shape resonances are very important in our understanding of low-energy impact on molecules.

Since typical vibrational times are  $\sim 10^{-14}$  sec, shape resonances may be short-lived, long-lived, or comparable to vibration times. When the lifetime is short (e.g.,  $\text{H}_2$ ), the energy dependence of the vibrational cross section exhibits a broad peak; when the lifetime is long (e.g.,  $\text{O}_2$ ), the compound state itself can vibrate and the energy dependence of the cross section to a given final vibrational state exhibits a series of spikes at the location of the vibrational levels of the compound state. When the lifetime of the compound state is comparable to typical vibration times (e.g.,  $\text{N}_2$ , CO) an intermediate situation prevails. In such a case, the compound state may perform about one vibration before decaying and the cross section to the final vibrational state will exhibit several broadened spikes.

The location on the energy scale and the particular properties of shape resonances are described under a separate heading for each molecule.

*Core-excited resonances* are associated with an electronically excited state of the molecule, which is called the "parent." Core-excited resonances thus consist of a "hole" in one of the orbitals normally occupied by an electron, and of two "particles", i.e., electrons in normally unoccupied orbitals. We can also visualize reso-

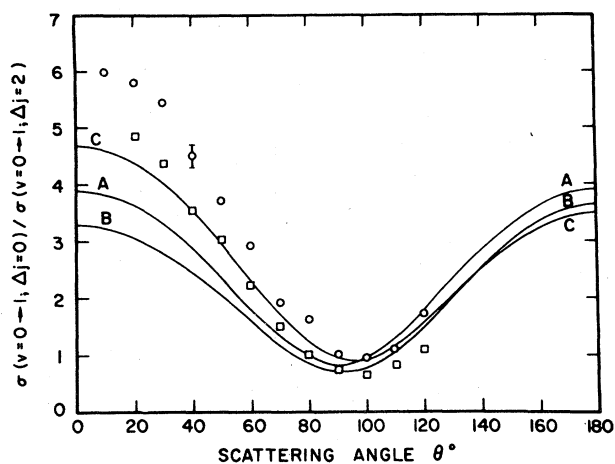


FIG. 9. Ratio  $\sigma(v=0 \rightarrow 1, \Delta j=0) / \sigma(v=0 \rightarrow 1, \Delta j=2)$  vs scattering angle at an electron energy of 4.5 eV. Experiment:  $\circ$  Ehrhardt and Linder (1968);  $\square$  Linder and Schmidt (1971); Theory: A—Abram and Herzenberg (1969); B—Henry (1970); C—Henry and Chang (1972). [From Henry and Chang (1972).]

nances consisting of two “holes” and three “particles”; such resonances have been recently postulated (Pavlovic *et al.*, 1972) and are well known in atoms (e.g., the  $2s^2 2p$  state in  $\text{He}^-$  near 57 eV). Higher hole-particle states appear to be plausible.

Core-excited resonances can lie either below or above their parent. When they lie *below* their parent, one may say that they exhibit a positive electron affinity. Such states are called Feshbach-type (after Feshbach, 1958, 1962) or Type I, or closed-channel resonances (decay into the parent state is forbidden). When core-excited resonances lie *above* their parent, they are called Type II or core-excited shape resonances. These resonances are similar to single-particle shape resonances, except that they are associated with an electronically excited state.

### B. Parentage of Core-Excited Feshbach Resonances

The parents for core-excited resonances may be, in principle, either valence or Rydberg excited states. Singly excited states of molecules may be classified into valence and Rydberg states. Both these types of excited states of the neutral molecule are formed by the promotion of a single electron from the ground state configuration into an orbital which is not filled in the ground state. When the promotion takes place into a low-lying vacant orbital, the principal quantum number of the electron does not change, and we designate the excited state as a valence state. When the principal quantum number does change by unity or more, we designate such an excited state as a Rydberg state. Rydberg states lie at higher energies and the orbitals being filled look like atomic orbitals. This gives rise to a Rydberg series of electronic states whose limit corresponds to an ionization limit of the molecules.

Calculations (Weiss and Krauss, 1970) on the binding of the additional electron show that preferentially *Rydberg excited* states have a positive electron affinity for a fixed internuclear separation in the Franck-Condon region. We therefore expect to find Feshbach-type resonances, which lie below their parent, mostly associated with Rydberg excited states. In this case, the temporary negative-ion complex consists of two electrons in Rydberg orbitals trapped in the field of a positive ion core, which is called the “grandparent” state. The parent (or parents) consists of a single Rydberg electron bound by the field of the same ionic core.

Core-excited Feshbach resonances have lifetimes ( $10^{-12}$ – $10^{-13}$  sec) which are long compared to the vibrational period of a molecule and therefore can give rise to *bands*, each of which consists of a progression of vibrational levels. Since the two Rydberg electrons trapped by the ion core are located far outside the ion core we expect the negative ion and its grandparent positive ion core to have similar vibrational spacings and Franck-Condon probabilities. One can therefore compare the vibrational spacings and Franck-Condon probabilities for a given band of negative ion vibronic states with the corresponding values for the many possible positive ion states of a molecule in order to identify the parentage and electron affinity of the band under investigation. This type of correlation has been made

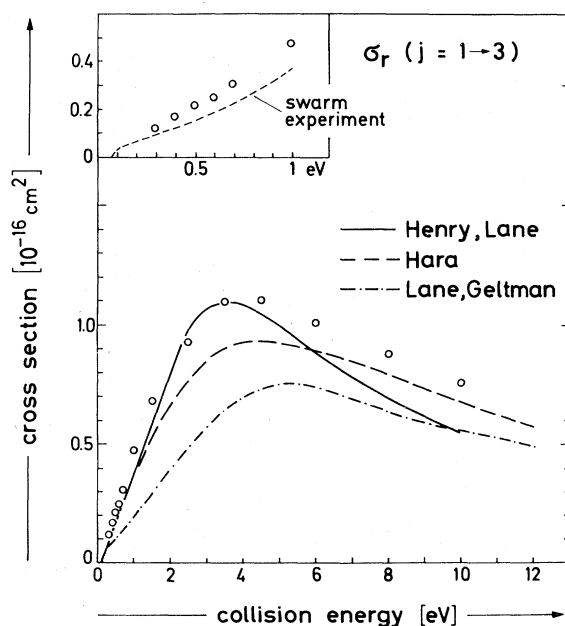
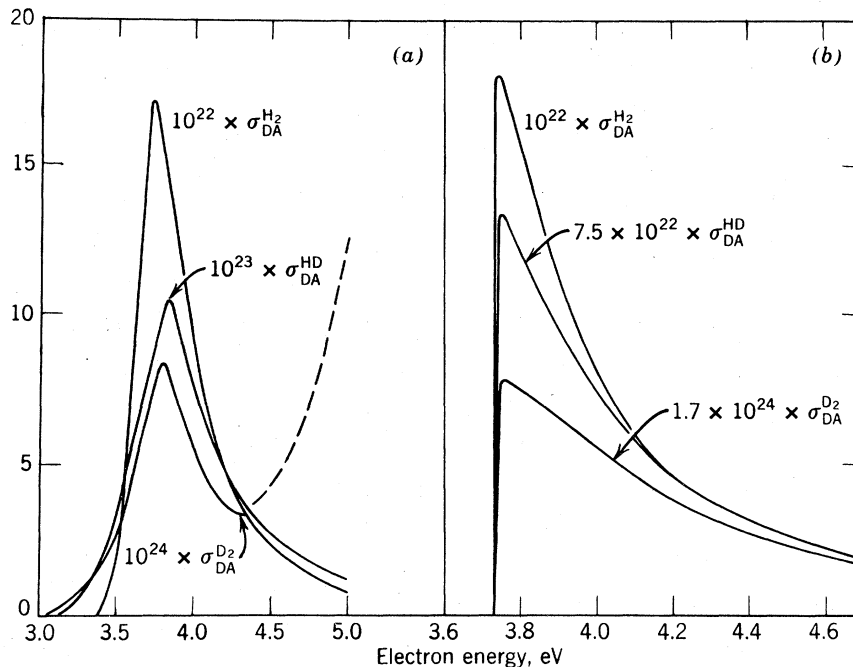


FIG. 10. Pure rotational excitation in  $\text{H}_2$ . Shown is the cross section  $\sigma_r(j=1 \rightarrow 3)$ . The circles are the experimental results of Linder and Schmidt (1971a). The lines are the theories of Henry and Lane (1969), of Hara (1969), and of Lane and Geltman (1967). The swarm data shown in the inset are recalculated for  $\sigma_r(j=1 \rightarrow 3)$  by Linder and Schmidt (1971a) from the original experiment of Crompton *et al.* (1969) which gives  $\sigma(j=0 \rightarrow 2)$ . [From Linder and Schmidt (1971a).]

FIG. 11. The energy dependence of the total cross section for dissociative attachment in  $H_2$ , HD, and  $D_2$  near 3.7 eV. The process shows a very large isotope effect and proceeds via the  ${}^2\Sigma_u^+$  states of  $H_2^-$ . Part (a) shows the experimental results of Schulz and Asundi (1967) and part (b) shows the unfolded cross sections as reported by Chen and Peacher (1968a). It should be noted that the experimental curves of Schulz and Asundi, shown on the left side of the diagram, have peak cross sections differing by orders of magnitude ( $1.6 \times 10^{-21}$  cm $^2$  for  $H_2$ ,  $1 \times 10^{-22}$  cm $^2$  for HD, and  $8 \times 10^{-24}$  cm $^2$  for  $D_2$ ). Whereas the  $H^-/H_2$  cross section was obtained with an electron energy distribution of 0.1 eV the curves for HD and  $D_2$  had to be taken with an energy distribution of 0.45 eV in order to gain sensitivity. This accounts for the difference in the threshold behavior. The rising portion of the  $D^-/D_2$  cross section, indicated by dashes, is real having been reproduced by Ziesel and Schulz (unpublished). It could result partially from the wings of the  ${}^2\Sigma_g^+$  resonance near 10 eV.



by Sanche and Schulz (1971, 1972), who find that many experimentally observed negative ion bands can be simply correlated with grandparent positive ion states. They find that the compound states usually lie about 4 eV below the grandparent from which they are derived, i.e., the binding energy of the two Rydberg electrons is 4 eV.

Resonances associated with *valence* excited states are also known, but as pointed out above, they do not seem to lead to sharp structures in cross sections. Their effect has been studied in dissociative attachment and in vibrational excitation; they may also play a role in excitation of electronic states of molecules. It is pointed out by Pavlovic *et al.* (1972) that at higher energies the density of doubly excited valence states becomes large and that resonances associated with each valence states may make a dominant contribution to excitation functions at energies in the 20-eV range.

## II. HYDROGEN

The ground state of  $H_2$  consists of two electrons in the  $1s\sigma_g$  ( $=\sigma_g1s$ ) orbital (Herzberg, 1950). The lowest unfilled orbital, in the notation of the united molecule, is  $2p\sigma_u$ , which is equivalent to  $\sigma_u1s$ . It is this orbital which the incident electron occupies when forming a resonance at low energy. In escaping from this orbital the electron must tunnel through a *p*-wave barrier. Bardsley *et al.* (1966b) and Eliezer *et al.* (1967) have shown that the ground state of  $H_2^-$  is indeed a shape resonance and that its designation is  ${}^2\Sigma_u^+$ . The angular distribution measurements of Ehrhardt *et al.* (1968) on electrons having excited the  $v=1$  vibrational state of

$H_2$  show a *p*-wave character (minimum at  $90^\circ$ ) and thus confirm the designation given above.

### A. Resonance at Low Energy: 0–4 eV ( ${}^2\Sigma_u^+$ )

#### 1. Elastic Cross Section

The lifetime of the  ${}^2\Sigma_u^+$  state is very short and the width very large; therefore there is little or no evidence for the  ${}^2\Sigma_u^+$  state in the elastic cross section (Golden and Nakano, 1966). Figure 1 shows the energy dependence of the total cross section as measured in a Ramsauer-type apparatus by Golden and Nakano and the elastic cross section only, as measured by Linder and Schmidt (1971a). No clear-cut evidence of the action of a resonance can be seen in these curves. Rather, one has to study other decay channels to establish the existence of this state. Vibrational excitation, rotational excitation (including angular distribution), as well as dissociative attachment, are the possible decay channels that can be usefully studied by electron impact in order to establish the existence of such resonances. Also, angular distribution measurements are very useful in establishing the existence of resonances. These are discussed separately for each molecule and a summary is given in Sec. VII. The experimental and theoretical considerations regarding elastic and rotational cross sections in  $H_2$  have been recently reviewed by Golden *et al.* (1971) and the reader is referred to this reference.

#### 2. Vibrational Excitation in $H_2$ via ${}^2\Sigma_u^+$

It is only in the past 10 years that experiments on vibrational excitation have led to the present-day under-

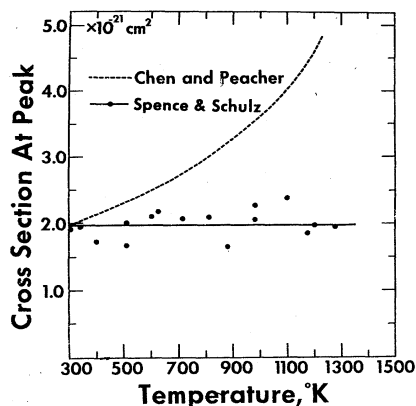


FIG. 12. Temperature dependence of the cross section for  $H^-$  formation from  $H_2$  at 3.75 eV. The experimental results (Spence and Schulz, 1971) show that the negative ion formation is independent of rotational excitation of the target, whereas the theory of Chen and Peacher (1967) shows a strong dependence. [From Spence and Schulz (1971).]

standing of the process. The first observation of a large vibrational cross section was due to Ramien (1931) whose results at 3.5 and 7 eV were essentially correct but were widely disbelieved because no simple interpretation could be found (Massey and Burhop, 1952). The use of a rather complex experimental method (Hertz diffusion) and the limited nature of the observation (only two energies given) contributed to the skepticism.

Subsequent experiments by Schulz (1964) and by Engelhardt and Phelps (1963) confirmed the large cross section for vibrational excitation, as did the experiments of Ehrhardt *et al.* (1968). This large vibrational cross section was successfully interpreted in terms of

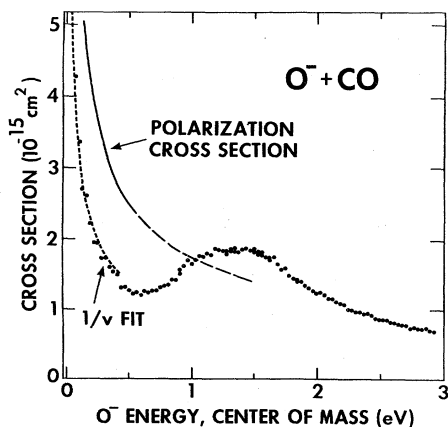


FIG. 13. The cross section for total electron detachment for the reaction of  $O^-$  with CO. The lower dashed line is the  $1/v$  fit while the upper line is the polarization cross section. The closed circles are data points. The magnitude is calibrated by assuming that the detachment rate at thermal energies is  $5.6 \times 10^{-10} \text{ cm}^2 \text{ sec}^{-1}$  (Ferguson, 1968), but this value is known to an accuracy of only  $\pm 30\%$ . The polarization cross section was calculated using  $19.5 \times 10^{-26} \text{ cm}^2$  as the polarizability of CO. [From Mauer and Schulz (1972).]

the resonance model by Bardsley, Herzenberg, and Mandl (1966b) and the energy dependence of the measured vibrational cross section could be well reproduced.

The energy-loss spectrum for 4-eV electrons in  $H_2$  is shown in Fig. 2, which clearly shows peaks due to the excitation of four vibrational states. The energy dependence of the vibrational cross section for  $v=1$  is shown in Fig. 3 in comparison with the newest theory due to Henry and Chang (1972). The theory of Faisal

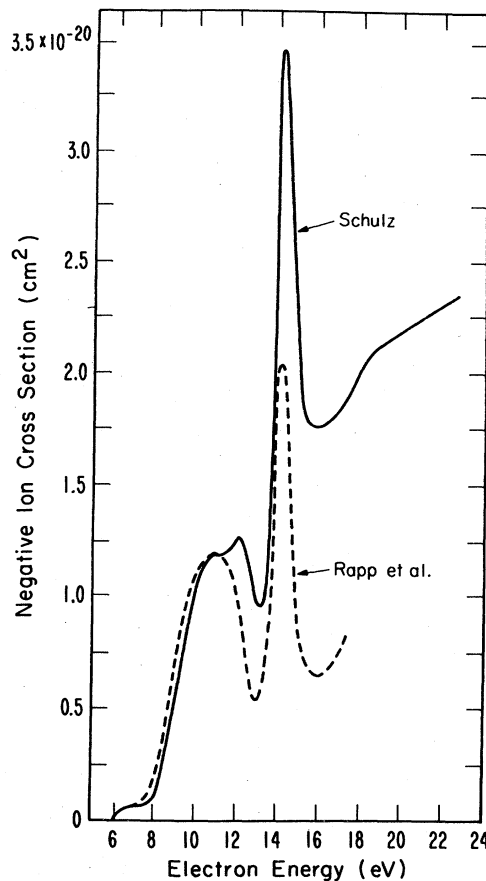


FIG. 14. Formation of stable negative ions,  $H^-$ , by dissociative attachment in hydrogen via a repulsive curve. Shown are the results of Rapp *et al.* (1965) and Schulz (1959a). The broad peak around 10 eV is interpreted as the reaction  $e + H_2 \rightarrow H_2^-(2\Sigma_g^+) \rightarrow H^- + H$ . The peak near 14.2 eV is interpreted in terms of the formation of excited H,  $e + H_2 \rightarrow H^- + H(2^3S, 2^3P)$ . The small structure near 12 eV shown on Schulz's curve has been studied in detail by Dowell and Sharp (1968) and is shown in Fig. 16.

and Temkin (1972) is also in agreement with the experiments.

Although Fig. 3 presents fairly good agreement between experiments, it is pointed out by Crompton *et al.* (1970) and also discussed by Golden *et al.* (1971) that the slope near threshold, as determined from electron beam experiments by Burrow and Schulz (1969) or by Ehrhardt *et al.* (1968) is too large to fit the measured transport coefficients. In order to perform such an

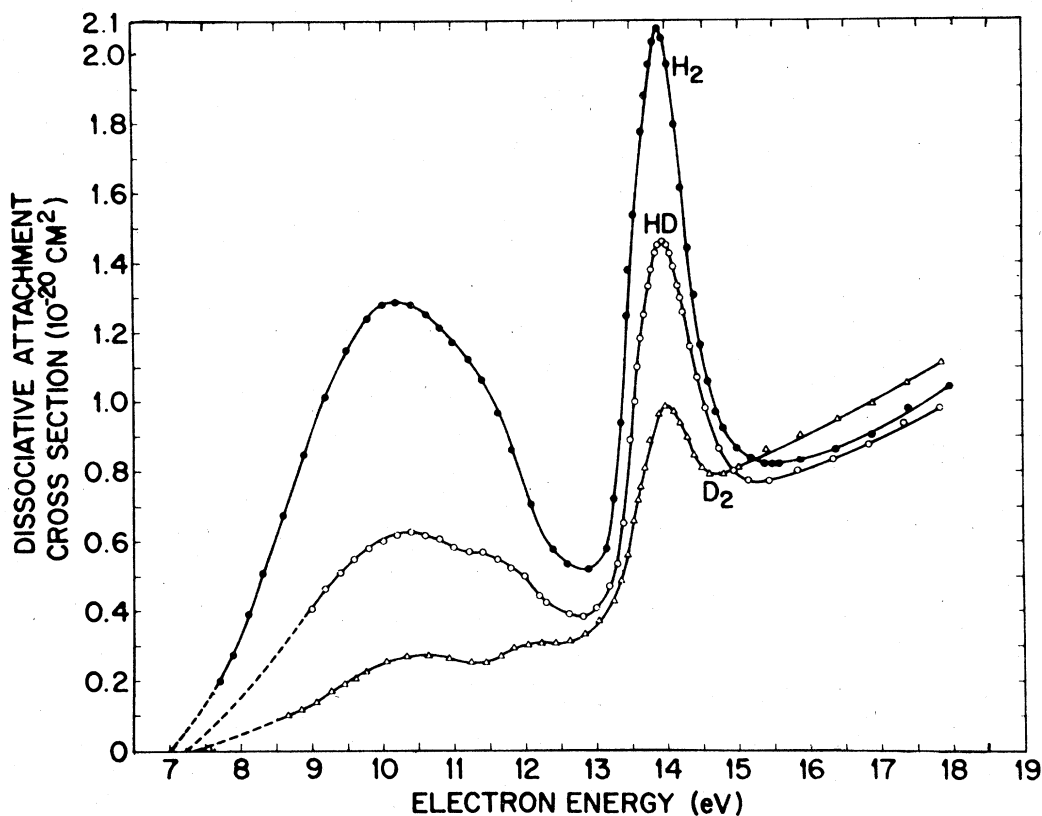


Fig. 15. Isotope effect in dissociative attachment in the neighborhood of 10 eV in  $\text{H}_2$ , HD, and  $\text{D}_2$ . [Taken from Rapp, Sharp, and Briglia (1965).]

analysis, Crompton *et al.* have to assume a reasonable energy dependence for the rotational cross section and that their approximation to the solution of the Boltzmann transport equation is applicable. To that extent, a discrepancy exists in the threshold behavior, as deduced from beam and from swarm experiments. Crompton's results based on an analysis of transport coefficients are also shown in Fig. 3.

The cross sections for excitation of the second and third vibrational states of  $\text{H}_2$  come from electron beam experiments and are shown in Figs. 4 and 5, respectively.

The experimental results presented lead to the conclusion (Bardsley *et al.*, 1966b; Eliezer *et al.* 1966) that the  ${}^2\Sigma_u^+$  state of  $\text{H}_2^-$  is involved in the excitation process. The width of this state is several eV, as can be seen in Fig. 6, which shows the dependence of the width on internuclear separation. Also, shown in Fig. 6 is the dependence on internuclear separation of the real part of the potential energy curves.

Breig and Lin (1965) and Takayanagi (1965) calculate the vibrational cross section to  $v=1$  without invoking a compound state, but they include the dependence of the polarization on the internuclear separation. Breig and Lin obtain fairly good agreement with the experi-

mental observations. (See, e.g., Chen, 1969.) The argument is sometimes made that the resonance model is not needed for an interpretation of vibrational excitation. However, it is often easier to understand the physical processes involved and the processes become more explicit and readily understandable when one uses the resonance model. There seems to be no compelling reason to "hide" the compound state. The resonance model becomes even more useful for an understanding of the isotope effect in dissociative attachment, as will be discussed below.

### 3. Rotational Excitation via the ${}^2\Sigma_u^+$ State and Angular Distributions

The general problem of rotational excitation of molecules has been very recently reviewed by Golden, Lane, Temkin, and Gerjuoy (1971) and by Takayanagi and Itikawa (1970). The reader is referred to these reviews for reference. Of interest for the present purposes is pure rotational excitation and rotational excitation which accompanies vibrational excitation, both processes proceeding via the  ${}^2\Sigma_u^+$  compound state in  $\text{H}_2$ . Figure 7 shows that the energy dependence of the cross section for simultaneous rotational and vibrational ex-

TABLE II. Summary of experimental data on  $H_2^-$ . This table gives the band designation which we use in the present review (Bands "a"–"g"). For each author, listed in the first column, we give the nomenclature he used for a given band (e.g., "Series I," "strong") and also the final state in which the band was observed (e.g.,  $X^1\Sigma_g^+$ ,  $b^3\Sigma_u^+$ ), and the energy of the first resonance, in eV.

Possible equivalence <sup>a</sup>	↓						"g"
	"a"	"b"	"c"	"d"	"e"	"f"	
Band designation	"a"	"b"	"c"	"d"	"e"	"f"	"g"
Kuyatt <i>et al.</i> (1966) (transmission)	"strong" 11.28	× <sup>e</sup>	"weak" 11.46				
Comer and Read (1971a)	$X^1\Sigma_g^+(v)$ 11.30	$X^1\Sigma_g^+$ ( $v>8$ ) 10.93 <sup>f</sup>	$X^1\Sigma_g^+(v)$ 11.19 <sup>g</sup>				
Weingartshofer <i>et al.</i> (1970)	"Series I" $X^1\Sigma_g^+$ , $b^3\Sigma_u^+$ 11.30			"Series I" $B^1\Sigma_u^+$ 11.30	"Series II" $B^1\Sigma_u^+$ 11.50	$C^1\Pi_u$ 13.63	
Sanche and Schulz (trans- mission) (1972)	11.32	×	11.43			13.66	15.09
Width, $\Gamma$ (eV)	$\leq 0.016$ ( $H_2$ ) <sup>h</sup> 0.03 ( $D_2$ )	0.03 <sup>e</sup>	$< 0.016$ <sup>h</sup>			0.08 <sup>b</sup>	
Symmetry	$^2\Sigma_g^+$	$^2\Sigma_g^+$	$^2\Sigma_g^+$ ; $^2\Pi_u$	$^2\Pi_g$ (?)		$^2\Sigma_g^+$	
Observed in	$H_2$ , HD, $D_2$	$H_2$	$H_2$ , HD, $D_2$	$H_2$	$H_2$	$H_2$ , $D_2$	$H_2$ , $D_2$
$R_g$ (Å) <sup>e</sup>	$0.97 \pm 0.01$	$1.175 \pm 0.01$		0.97			
$a$ (eV) <sup>e,d</sup>	$0.345 \pm 0.015$	$0.19 \pm 0.015$		0.345			
$b$ (eV) <sup>e,d</sup>	$0.0135 \pm 0.003$	$0.005 \pm 0.003$		0.0135			
$E_0$ (eV) <sup>e,d</sup>	11.40	11.11		11.40			

<sup>a</sup> The arrows indicate that band "a" could be identical to band "d" and that band "c" may be identical to band "e." See text.

<sup>b</sup> From Weingartshofer *et al.* (1970).

<sup>c</sup> From Comer and Read (1971a).

<sup>d</sup> Defined by the equation  $E = E_0 + a(v + \frac{1}{2}) - b(v + \frac{1}{2})^2$ .

<sup>e</sup> The symbol × indicates that band "b" is observable only in the high vibrational states ( $v > 8$ ) of the  $^1\Sigma_g^+$  state and thus cannot be observed in transmission experiments.

<sup>f</sup> Extrapolated to  $v=0$ ; see Appendix I.

<sup>g</sup> From Joyez, Comer, and Read (1973).

citation ( $v=0 \rightarrow 1$ ;  $j=1 \rightarrow 3$ ) is similar to the cross section for vibrational excitation alone ( $v=0 \rightarrow 1$ ;  $\Delta j=0$ ) and thus both processes seem to be dominated by the  $^2\Sigma_u^+$  resonance. Angular distribution measurements by Ehrhardt and Linder (1968) and by Linder (1969) (Fig. 8), shows that pure vibrational excitation exhibits a  $p\sigma$ -wave dependence, i.e., the scattered electrons exhibit a minimum at 90 degrees. These observations are in agreement with the theory which predicts an approximate angular distribution of the form  $(1 + 2 \cos^2\theta)$ . [See Bardsley and Read (1968), Ehrhardt, Langhans, Linder, and Taylor (1968), and O'Malley and Taylor (1968).]

When rotational levels are excited in addition to vibrational levels, a flat (isotropic) angular distribution is observed. Figure 8 shows the results for the transition  $\Delta j=2$ ,  $\Delta v=1$ . The ratio of the vibrational cross section without rotational excitation to that with rota-

tional excitation,  $\sigma(\Delta j=0; \Delta v=1)/\sigma(3 \leftarrow 1; \Delta v=1)$  is shown in Fig. 9 in comparison with the theories of Abram and Herzenberg (1969), of Henry (1970), and of Henry and Chang (1972). The theory of Abram and Herzenberg is based on the quantum mechanical impulse approximation and neglects the kinetic energy of rotation of the molecule during the collision. The work of Henry and Chang uses the theory of frame transformation as developed by Chang and Fano (1972). The  $p$ -wave nature of the ratio is obvious from the figure.

As far as pure rotational excitation, in which the vibrational quantum number does not change, is concerned, there are available the experimental data of Ehrhardt and Linder (1968) and the improved data of Linder and Schmidt (1971a). It is the latter data that are shown in comparison with theory in Fig. 10.

As pointed out most recently by Linder and Schmidt

(1971a), all the rotational effects can be interpreted by considering both the direct-excitation component and the resonance component to the phase shifts. The theory of Abram and Herzenberg (1969) which is based on a pure resonance model accounts well for the angular distributions observed by Linder and Schmidt (1971a) for pure rotational excitation,  $\sigma(j=1 \rightarrow 3)$ .

The suggestion has been advanced by Frommhold (1968) that electrons of thermal energy (10–100 meV) exhibit resonant behavior in exciting rotational states of  $H_2$  and  $D_2$ . Evidence for this hypothesis comes from the pressure dependence of the drift velocity, which is observed by Frommhold and by Crompton and Robertson (1971) in swarm experiments.

Recently, Raith and Land (1972) used a time-of-flight electron spectrometer to perform a transmission experiment in  $H_2$  and  $D_2$  in order to confirm the existence of resonances at very low electron energies in  $H_2$  and  $D_2$ . In  $H_2$ , they observe structures in the transmitted current at about 24 meV and in the range 60–90 meV. In  $D_2$  the results are qualitatively different, with structure appearing between 26 and 60 meV. The width of the 24-meV structure in  $H_2$  is approximately 3 meV, of which about 1.5 meV can be attributed to Doppler broadening. Rotational excitation is expected to be governed by the selection rule  $\Delta l = 0, \pm 2$ , where  $l$  is the orbital quantum number of the scattered electron. Thus we expect inelastic processes to have thresholds at 44 meV (for  $J=0 \rightarrow 2$ ) and at 75 meV (for  $J=1 \rightarrow 3$ ) in  $H_2$  and at half these values in  $D_2$ . The observed structure thus lies below the first inelastic process in  $H_2$  and above it in  $D_2$ . If the structures observed in the experiment of Raith and Land are resonances, which is by no means certain, one must await

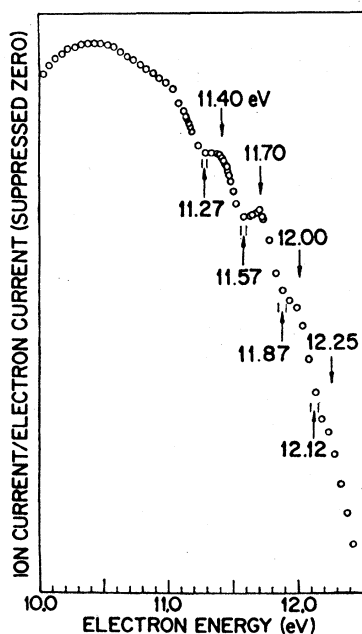


FIG. 16. Fine structure in dissociative attachment in  $H_2$ . [Taken from Dowell and Sharp (1968).]

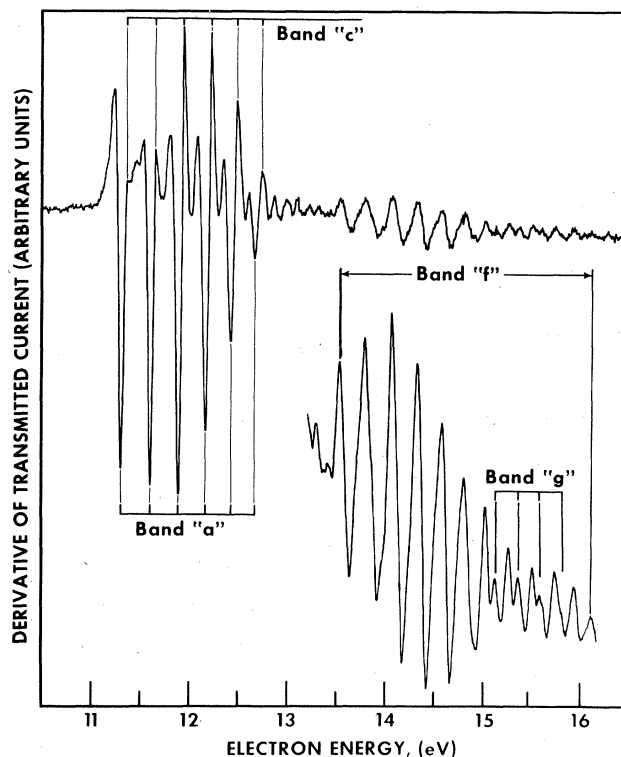


FIG. 17. Derivative of transmitted current vs electron energy in  $H_2$ . Four progressions of negative ion states are labelled "a," "c," "f," and "g." See Table II. Band "b" seems to be observable only in high vibrational states, and thus does not seem to appear in transmission experiments. Band "d," if it exists as a separate entity, is energetically coincident with band "a." For the lower portion of the figure, which shows bands "f" and "g," the gain has been increased by a factor of seven. [From Sanche and Schulz (1972).]

a theoretical interpretation for an understanding of this phenomenon.

The preliminary theoretical work by Kouri (1968) has not confirmed the reality of this process, and further developments must be awaited. At this writing, the existence of resonances in the energy range 10–100 meV is puzzling, since no molecular orbitals are available at such low energies, and since close-coupling calculations (Henry and Lane, 1969) do not give an indication for rotational resonances.

#### 4. Dissociative Attachment at 3.75 eV

The  ${}^2\Sigma_u^+$  state of  $H_2^-$  also plays a role in dissociative attachment. It is characteristic of many compound states that they decay into all channels that are energetically accessible and allowed by selection rules. The dissociative attachment channel opens up at an electron energy ( $D-A$ ), where  $D$  is the dissociation energy of  $H_2$  (4.48 eV) and  $A$  is the electron affinity of H (0.75 eV). Thus one would expect a threshold for  $H^-$  formation from  $H_2$  at 3.73 eV. Figure 11 shows the experimental result of Schulz and Asundi (1967), who ob-

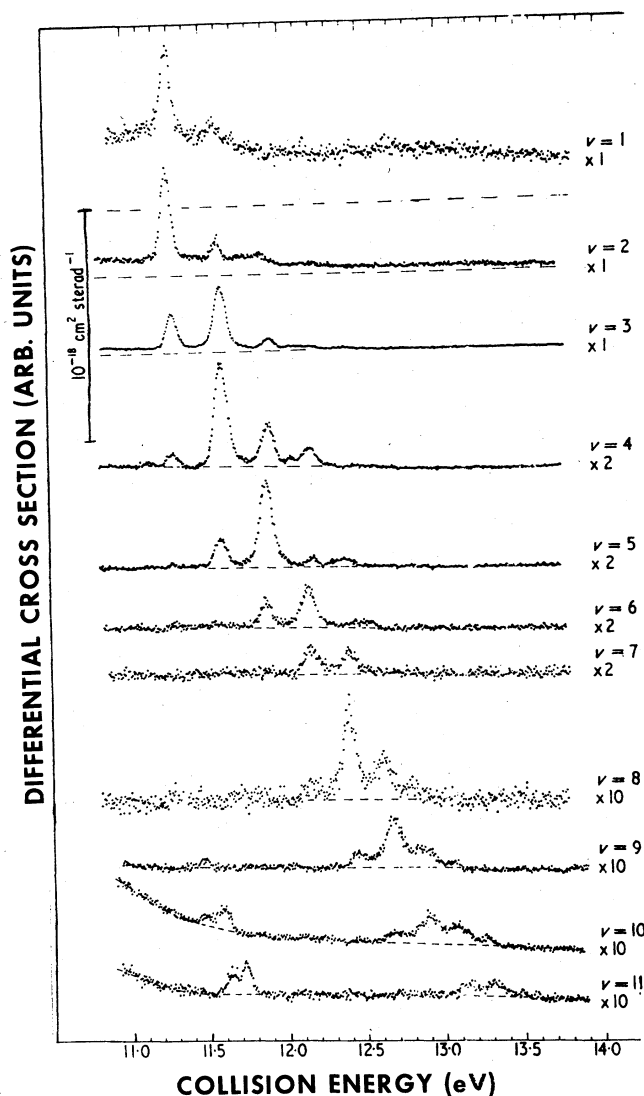


FIG. 18. Energy dependence of the absolute differential cross sections for excitation of vibrational states in H<sub>2</sub> above 11 eV. The scattering angle is 85°. For each curve the cross section scale should be multiplied by the factor indicated. The zero lines are shown broken. The structure observed in the vibrational states  $v=1$  to  $v=8$  is associated with series "a." For  $v=9$  to  $v=11$ , series "a" is visible in the energy range 12.48–13.33 eV, and series "b" appears at the low-energy end, i.e., in the energy range 11.49–11.74 eV. [From Comer and Read (1971a).]

served the onset for H<sup>-</sup> production at the predicted value. Also shown in Fig. 11 are the unfolded cross sections for the three isotopes of H<sub>2</sub> (Chen and Peacher, 1968). The isotope effect was first interpreted by Demkov (1964) as a consequence of the smaller survival probability factor for heavier atoms. Thus, D<sub>2</sub> requires a longer time to separate and remains in the region of autodetachment for a longer time than does H<sub>2</sub>. The formation of D<sup>-</sup>/D<sub>2</sub> is therefore smaller than H<sup>-</sup>/H<sub>2</sub>. Bardsley, Herzenberg, and Mandl (1966b) give a simple expression for the cross section leading to dissociative

attachment:

$$Q_{-} = Q_0 \exp - \left( \int_{R_0}^{R'} \frac{\Gamma(R) dR}{\hbar v(R)} \right).$$

Here,  $Q_0$  is the cross section for formation of the compound state and the exponential term represents the probability that the system in fact survives to a stabilization point  $R'$ . The term  $\Gamma$  is the width (and

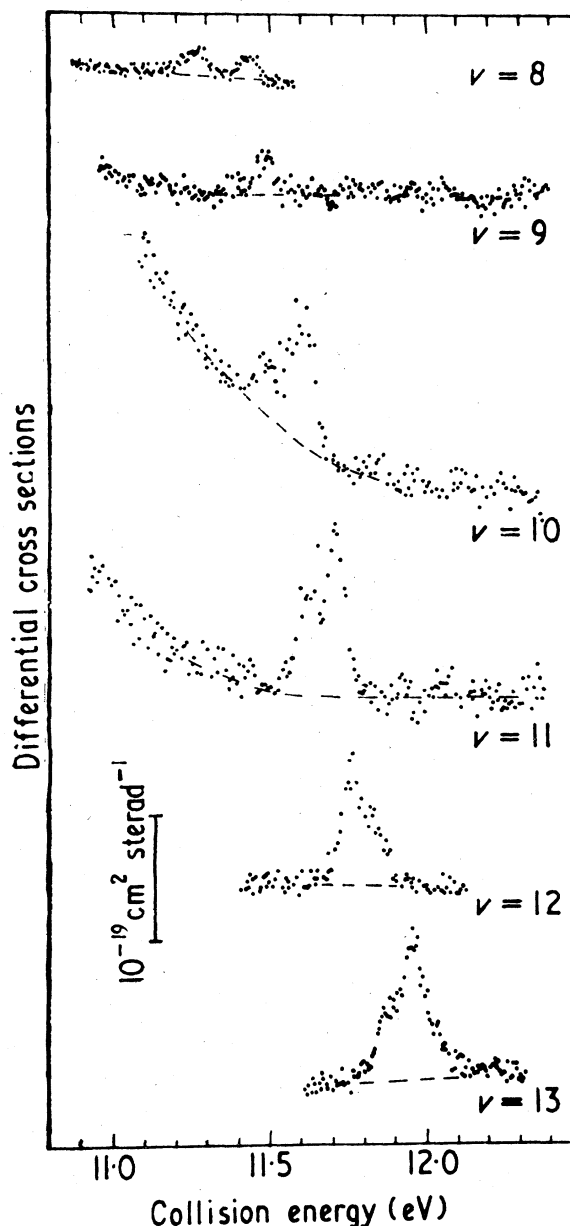


FIG. 19. Energy dependence of the absolute differential cross section for excitation of high vibrational states in H<sub>2</sub> above 11 eV. The scattering angle is 85°. The zero lines are shown broken. Only series "b" is shown. [From Comer and Read (1971a).]

$\hbar/\Gamma$  is the lifetime) of the compound state with respect to autodetachment. This width is a function of the internuclear separation  $R$ . The integration extends from the formation point  $R_0$  to the stabilization distance  $R'$  and  $v(R)$  is the relative velocity of separation of the nuclei. We can replace the exponent by the appropriate average width  $\bar{\Gamma}$  and by the time  $\tau$ , which is needed for the products to reach the stabilization point. We then write

$$Q_- = Q_0 \exp(-\bar{\Gamma}\tau/\hbar).$$

It should be noted that the total width is the sum of the partial widths for decaying into the various vibrational states of the  $(\text{H}_2+e)$  system. Separation into three particles ( $\text{H}+\text{H}+e$ ) is energetically possible at energies above 4.46 eV. In this model the isotope effect arises from the variation of the survival probability ( $\exp-\Gamma\tau/\hbar$ ) with mass. It is pointed out by Chen and Peacher (1968a) that the above expressions are only approximate and that the capture cross section, resulting from the nuclear overlap integral, becomes as sensitive to the mass as the survival probability itself. Nevertheless, the simplicity of separating the dissoci-

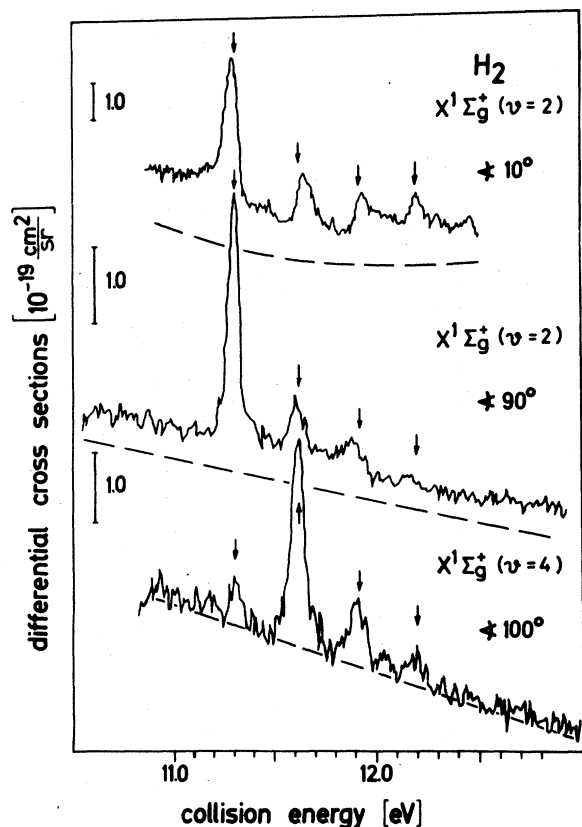


FIG. 20. Energy dependence of the absolute differential cross sections for different scattering angles and into two different exit channels,  $v=2$  and 4 of the electronic ground state. The zero lines are dashed. The length of the bars to the left represent the scaling factors in units of  $1.0 \times 10^{-19} \text{ cm}^2/\text{sr}$ . The resonances are members of band "a." [From Weingartshofer *et al.* (1970).]

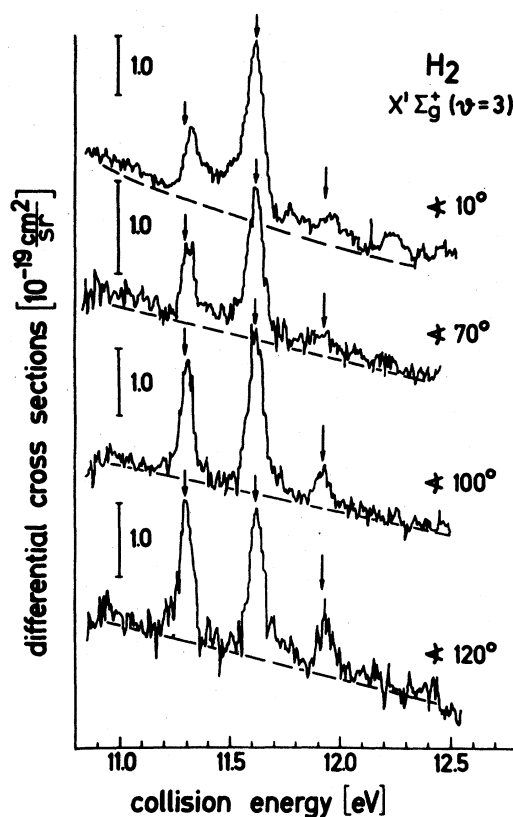


FIG. 21. Energy dependence of the absolute differential cross sections to the  $v=3$  vibrational level of the electronic ground state of  $\text{H}_2$  for four different scattering angles. The zero lines are dashed. The length of the bars to the left of each curve represents the absolute scaling factors in units of  $1.0 \times 10^{-19} \text{ cm}^2/\text{sr}$ . The resonances are members of band "a." [From Weingartshofer, Ehrhardt, Hermann, and Linder (1970).]

ative attachment cross section into two physically meaningful simple terms has accounted for the extensive use of the above expressions. Also, Chen and Peacher's considerations have not as yet been tested against experiment.

##### 5. Effect of Rotational Levels of the $\text{H}_2$ Target Molecule on $\text{H}^-$ Formation near 3.75 eV

Chen and Peacher (1967) predict theoretically a profound effect of rotationally excited levels of  $\text{H}_2$  for the reaction  $e+\text{H}_2 \rightarrow \text{H}_2^- \rightarrow \text{H}^- + \text{H}$  at 3.75 eV. In this reaction the products depart with zero kinetic energy, and Chen and Peacher predict a large increase in the survival factor leading to an increased cross section for this process as the population of higher rotational states is increased. Chen and Peacher's suggestion seems to stem from the effect of the centrifugal repulsion on the time the nuclei take to separate. To test this theory, and to determine the effect of rotational levels, Spence and Schulz (1971a) have studied the temperature dependence of the dissociative attachment cross section in  $\text{H}_2$  at 3.75 eV.

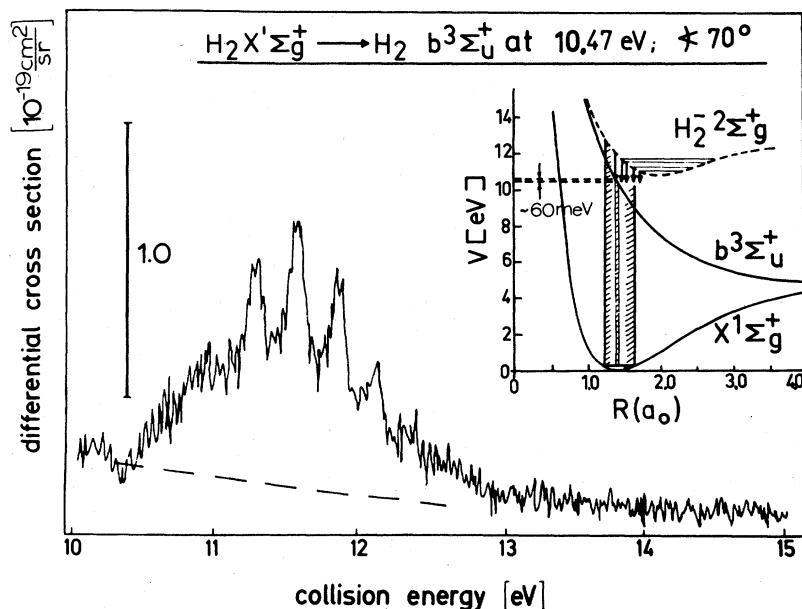


FIG. 22. Energy dependence of the absolute differential cross section for excitation into a narrow band ( $\sim 60$  meV) at 10.47 eV in  $H_2$ . The final state is the dissociative continuum,  $b^3\Sigma_u^+$ . The zero line is dashed. The length of the bar to the left of the curve represents the absolute scaling factor in units of  $1.0 \times 10^{-19}$  cm<sup>2</sup>/sr. The insert illustrates the autoionization of the  $H_2^-$  ion into the energy band. [From Weingartshofer, Ehrhardt, Hermann, and Linder (1970).]

The experimental cross section at the peak of the 3.75 eV process is plotted as a function of gas temperature in Fig. 12. Spence and Schulz (1971a) find that the cross section is independent of temperature in the range 300–1300°K and conclude that rotational excitation of  $H_2$  plays no role in the dissociative attachment process at 3.75 eV in the above temperature range. Also shown are the theoretical points calculated using the theory of Chen and Peacher (1967) normalized to the experimental data at 300°K. In this calculation it is assumed that the electron capture cross section is independent of the initial rotational state, which should be a reasonable assumption in the present case.

It is, actually, not surprising to find that the dissociative attachment cross section is independent of the rotational states of the target. The vibrational time, and thus the dissociation time, are shorter than rotational times and one would therefore suppose that the molecule is essentially nonrotating during the capture and the breakup process. In fact, Bardsley, Mandl, and Herzenberg (1966b) calculate with good success the dissociative attachment in  $H_2$  by regarding the axis of the diatomic molecule as fixed, thus ignoring rotational motion. The experimental results of Fig. 12 seem to confirm such a model.

#### 6. Associative Detachment: $H^- + H \rightarrow H_2^- \rightarrow H_2 + e$

There is a close relationship between dissociative attachment reactions at low energy, which are discussed in the preceding paragraphs, and low-energy associative detachment reactions of the type  $H^- + H \rightarrow H_2^- \rightarrow H_2 + e$ . Associative detachment is the inverse of dissociative attachment and at low energies of the colliding partners, the two processes proceed via the same compound state, in this case  $H_2^-$ . For a review of associative

detachment cross sections at thermal energy, see Ferguson (1970). In the case of  $H^- + H$ , the reaction partners approach each other along the potential energy curves  $^2\Sigma_u^+$  and  $^2\Sigma_g^+$ . The former exhibits a short lifetime for autodetachment; thus all or almost all collisions which proceed along this potential energy curve lead to associative detachment. The  $^2\Sigma_g^+$  curve is repulsive and reactions proceeding along this curve at low energy lead only to reflection or elastic scattering. One can therefore expect that the low-energy associative detachment cross section should be about one-half of that given by the Langevin polarization cross section. This prediction has been approximately checked for thermal ions (Schmeltekopf *et al.*, 1967).

Since associative detachment proceeds via the same intermediate state as dissociative attachment, there is a strong connection between the two processes. However, in associative detachment there is the probability that the resulting molecule is left in a highly excited vibrational state, provided that the compound state is short lived. Thus detailed balancing cannot be used for predicting the bulk of the associative detachment cross section from its inverse, since dissociative attachment is generally studied only for molecules in their lowest vibrational states.

For the case of  $H^- + H \rightarrow H_2 + e$ , theoretical treatments are also available. Bates and Massey (1954) and also Dalgarno (1961) have suggested that associative detachment cross sections could be large and that they could play an important role in upper atmosphere reactions. Recently, more complete theoretical treatments have become available. [Herzenberg (1967), Chen and Peacher (1968) and Browne and Dalgarno (1969), and also the review by Chen (1969)]. The main conclusions from these considerations are: At low

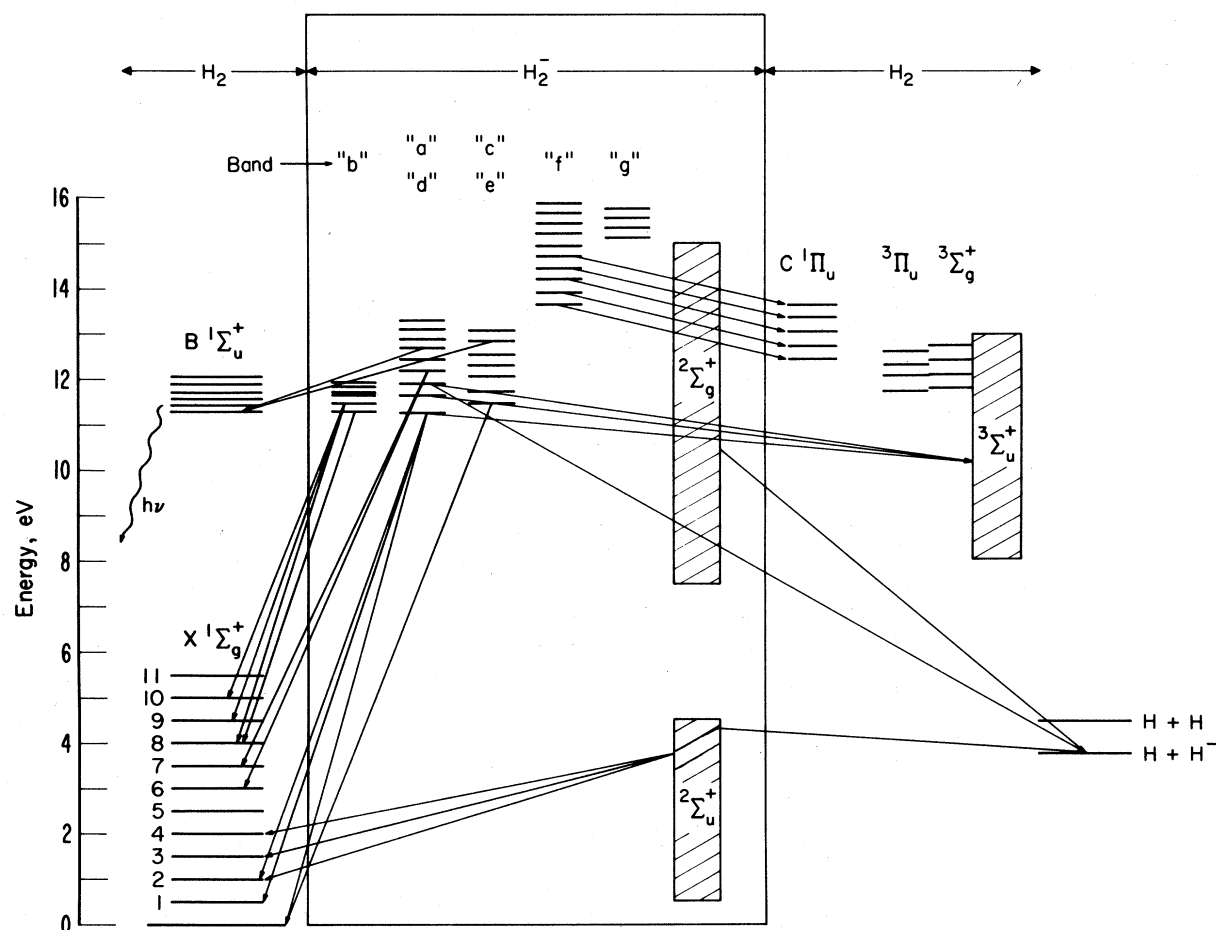


FIG. 23. A schematic summary of the decay of five energetically distinct compound states into various decay channels. In the middle of the figure we show the positions of bands "a" through "g," and on the left and right we show states of  $H_2$ . The arrows point to those decays that have been experimentally determined, but not all decay channels could be given on the figure. Band "f" seems to decay into the  $C^1\Pi_u$  state without change of vibrational quantum number, and this is properly recorded on the figure. Band "b" seems to decay only into high vibrational states of the  $X^1\Sigma_g^+$  ground state. Decay into  $H+H^-$  (dissociative attachment) is also indicated.

energy the cross section becomes very large due to Langevin spiralling arising from long-range polarization (Herzenberg, 1967); the compound state is essential for an understanding of the process; the  $H_2$  produced in the reaction is highly excited (Herzenberg, 1967; Chen and Peacher, 1968b) and an inverted population may result.

Experimentally, the reaction  $H^-+H\rightarrow H_2+e$  has not yet been studied using ion beams because of the difficulties associated with this type of experiment. However, similar reactions

(e.g.,  $O^-+CO\rightarrow CO_2^- \rightarrow CO_2+e$ ;



have been studied both in swarm experiments (see, e.g., Ferguson, 1968, Moruzzi *et al.*, 1968) and in beam experiments (Mauer and Schulz, 1973). In both these

reactions, a compound state is involved. In the case of  $CO_2^-$  the state is  $^2\Pi_u$  (Claydon, Segal, and Taylor, 1970; Krauss and Neumann, 1972), and in the case of  $H_2^-$ , the state is  $^2\Sigma_u^+$  and has been previously discussed. The  $CO_2^-(^2\Pi_u)$  state has a lifetime which is somewhat longer (Burrow and Sanche, 1972, give a width,  $\Gamma=0.13-0.26$  eV) than the compound state in  $H_2$  ( $\Gamma\sim 1$  eV).

The experiments of Mauer and Schulz (1972) show that at very low energies, the cross section is given by a  $1/v$  functional form, where  $v$  is the relative velocity. Thus polarization dominates, consistent with previous swarm experiments (Moruzzi *et al.*, 1968; Ferguson, 1970). Because Mauer and Schulz used a beam experiment, they could extend the range of incident ion energies; they find that at higher energies (e.g., 1.5 eV in the center of mass for the reaction  $O^-+CO$ ) the cross section rises and exhibits a maximum, as shown

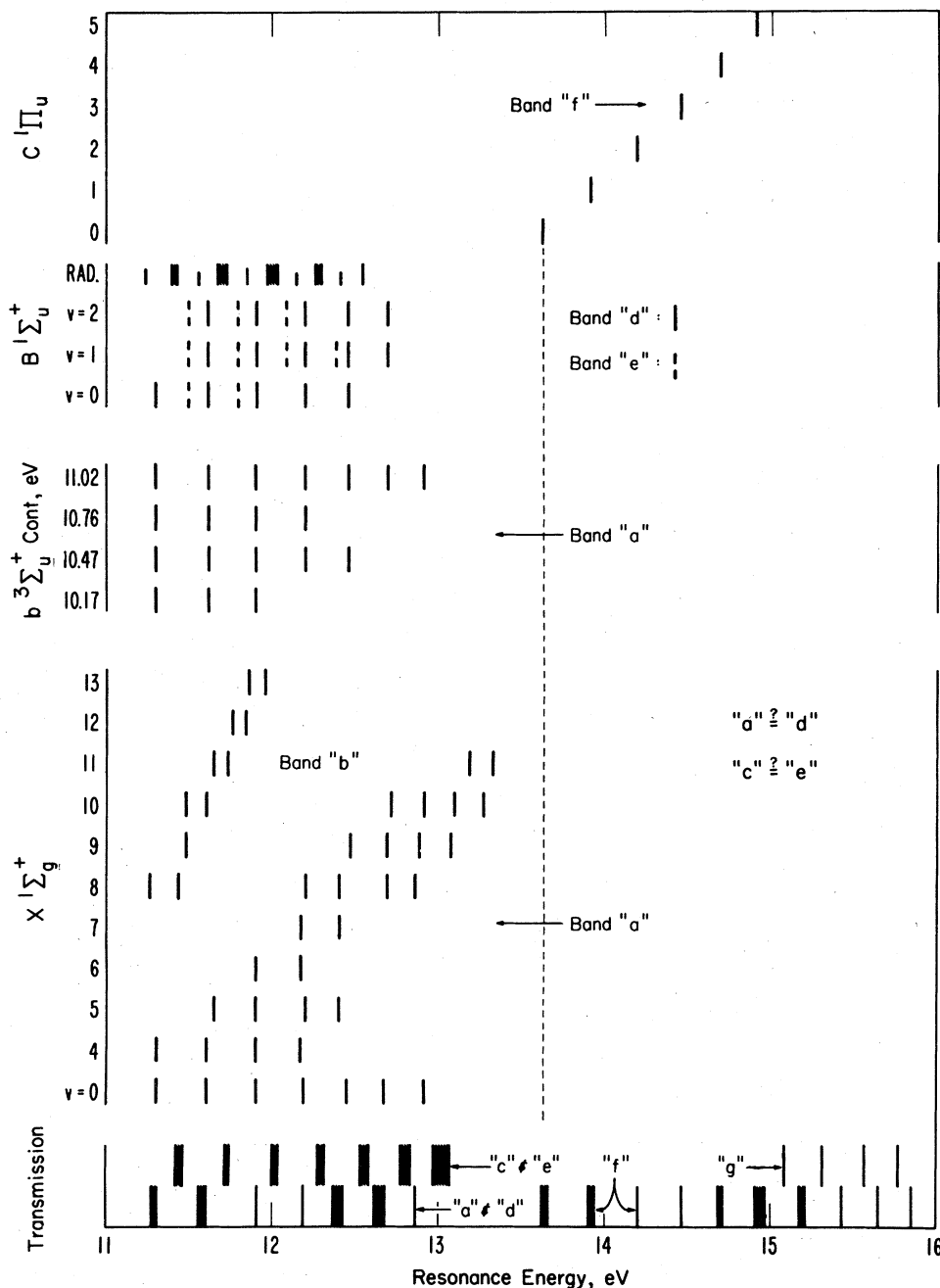


FIG. 24. Position of compound states, as observed in various decay channels. On the bottom, the position of various bands is shown, as observed in transmission experiments. The shaded region shows the extent of the discrepancy between experiments. Higher on the figure, we show the positions of the compound states as observed in various excited states and in the emission of radiation (marked RAD). The assignment to various bands is noted.

in Fig. 13. This rise is due mainly to the following effect: At very low ion energies, ions can reach the region of large associative detachment, which occurs at relatively small internuclear separations, only via an attractive curve. Ions entering the process along repulsive curves cannot get close enough for associative detachment to take place. However, at higher kinetic energies, even ions entering the reaction along repulsive curves can get close enough to the neutral species to

detach. Thus, the cross section exhibits a subsidiary rise at 1.5 eV in the case of  $O^- + CO$  and at 0.25 eV in the case of  $O^- + H_2$ .

Mauer and Schulz (1972) also performed an energy analysis of the detached electrons and found that the reaction leads predominantly to very low-energy electrons, near zero eV. Thus very high vibrational states of CO<sub>2</sub> are excited.

The experimental evidence from the reaction  $O^- +$

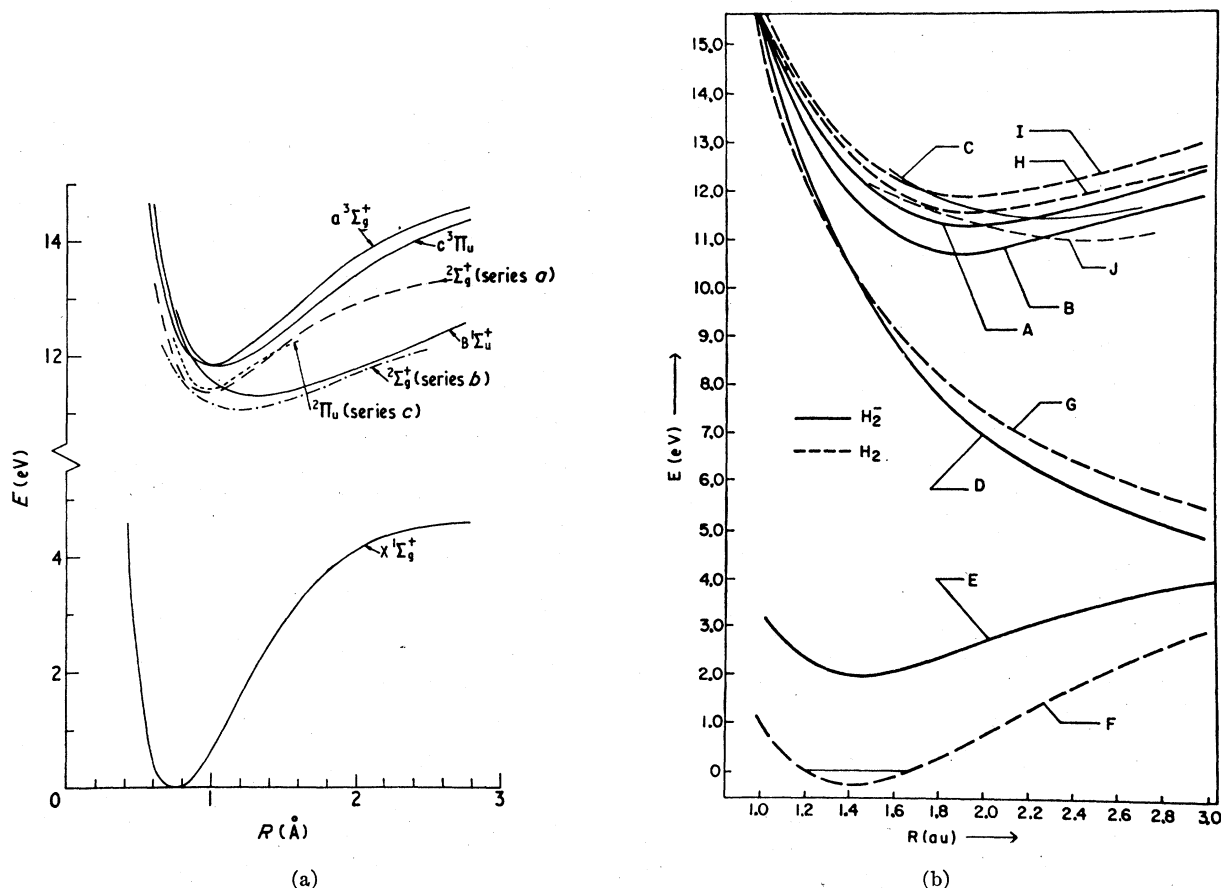


FIG. 25. (a) Potential energy curves for  $H_2^-$  state (broken curves) which give the best fits to experimental data. Corresponding curves for some  $H_2$  states (full curves) are also shown (Sharp, 1971). It should be noted that the energy scale is taken with respect to the bottom of the ground-state potential curve. [From Comer and Read (1971a).] (b) Potential energy curves for  $H_2^-$  derived from calculations. The full curves represent the calculated compound states and the dashed curves are some of the parent  $H_2$  states. (A)  $H_2^- 2^3\Sigma_g^+$  consisting of  $C^1\Pi_u + \pi_u 2p'$ ; (B)  $H_2^- 2^3\Sigma_g^+$  consisting of  $C^3\Pi_u + \pi_u 2p'$ ; (C)  $H_2^- 2^3\Sigma_g^+$  consisting of  $B^1\Sigma_u + \sigma_u 1s'$ ; (D)  $H_2^- 2^3\Sigma_g^+$  consisting of  $3^3\Sigma_u + \sigma_u 1s'$ ; (E)  $H_2^- 2^3\Sigma_u^+$  consisting of  $X^1\Sigma_g^+ + \sigma_u$ ; (F)  $H_2 X^1\Sigma_u^+$ ; (G) One configuration result for  $H_2 3^3\Sigma_u^+ 1\sigma_g 1\sigma_u$ . This curve lies about 0.32 eV above the "exact"  $3^3\Sigma_u^+$  curve, but is used as a comparison with the  $H_2^-$  calculation consisting of this configuration plus an extra electron; (H) Two configuration result for  $H_2 3^3\Pi_u(1\sigma_g 1\pi_u + 1\sigma_u 1\pi_g)$ . The minimum of this curve lies about 0.14 eV above the experimental minimum. The  $H_2 a^3\Sigma_g^+$  curve lies so close to this one that they are indistinguishable on this scale; (I) Same as H for  $C^1\Pi_u$  and  $E^1\Sigma_g^+$ ; (J)  $H_2 B^1\Sigma_u^+$ . [From Eliezer, Taylor, and Williams (1967).]

$CO \rightarrow CO_2 + e$  indicates that the theoretical predictions for  $H^- + H, \rightarrow H_2 + e$ , as outlined above, are probably correct.

### B. Resonance in the 10-eV Region ( $2^3\Sigma_g^+$ )

The first excited state of  $H_2$  is the  $(1\sigma_g)(2p\sigma_u)^3\Sigma_u^+$  state. In the notation for separated atoms this becomes  $(\sigma_g 1s)(\sigma_u 1s)^3\Sigma_u^+$ . The dominant configurations of the compound state associated with this excited state is  $(1\sigma_g)(2p\sigma_u)^2 2^3\Sigma_g^+$  or, in the notation of separated atoms,  $(\sigma_g 1s)(\sigma_u 1s)^2 2^3\Sigma_g^+$ . Agreement exists on this assignment (Bardsley, Herzenberg, and Mandl, 1966a; Eliezer, Taylor, and Williams, 1967; Bardsley and Mandl, 1968).

When the real part of the potential energy curve for the  $2^3\Sigma_g^+$  is calculated as a function of internuclear separation,

it is found (Bardsley and Mandl, 1968; Eliezer *et al.*, 1967) that the potential energy curve crosses the potential energy curve of the parent, i.e., the  $3^3\Sigma_u^+$  state. As long as the potential energy curve for  $H_2^-$  lies below the parent we are dealing with a core-excited resonance of the Feshbach type. When the potential energy curve lies above the parent we are dealing with a core-excited shape resonance. In this case the assignment varies as a function of internuclear separation.

Information regarding the  $2^3\Sigma_g^+$  state of  $H_2^-$  comes from experiments on dissociative attachment. In other channels, this state has not yet been observed. A comparison of two recent experiments on negative ion formation with  $H_2$  in the range 7–17 eV is shown in Fig. 14. An interesting isotope effect, not as dramatic as the one for the  $2^3\Sigma_u^+$  state, has been discovered by Rapp

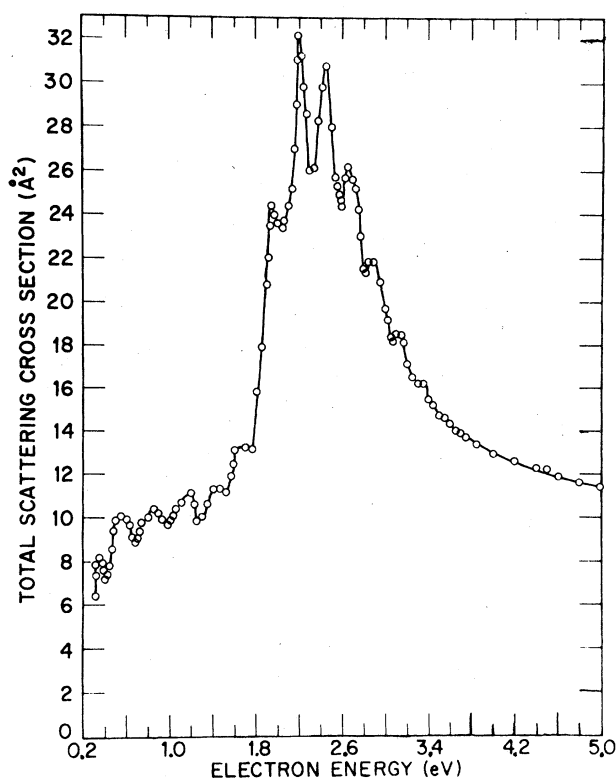


FIG. 26. The absolute total cross section for scattering of electrons on  $N_2$ , as obtained using a modified Ramsauer technique. The total cross section includes elastic and inelastic components. The structure above 1.8 eV is indicative of the pseudovibrations of the  ${}^2\Pi_g$  compound state. The structure below 1.8 eV has not been substantiated by other experiments, although attempts at confirming it have been made. The structure below 1.8 eV must be considered in doubt at the present time. [From Golden (1966).]

*et al.* (1965). These results are shown in Fig. 15. Similar considerations as those discussed in Sec. IIA4 also apply here. In fact, Bardsley, Herzenberg, and Mandl (1966b) have obtained a good theoretical fit to the curves of Fig. 15, and they point out that decay of the  ${}^2\Sigma_g^+$  state of  $H_2^-$  to the  ${}^3\Sigma_u^+$  excited state is more probable than decay to the ground state. The overlap is more favorable when the compound state can decay into its parent ( ${}^3\Sigma_u^+$ ) state. This may explain why it has not been possible to detect the decay of the  $H_2^-({}^2\Sigma_g^+)$  state to the ground electronic state. The total width of the  ${}^2\Sigma_g^+$  state is estimated to be  $\Gamma=0.8$  eV and the entry width from the ground electronic state is 0.004 eV.

The potential energy curves for the  ${}^2\Sigma_u^+$  and the  ${}^2\Sigma_g^+$  states, derived by Bardsley *et al.* (1966a) and by Chen and Peacher (1968a), have already been discussed in connection with Fig. 6. Also shown are the imaginary parts of the potential curves, i.e., the width  $\Gamma$ , as a function of internuclear separation. The potential energy curves of Eliezer *et al.* (1967) are shown in Fig. 25(b).

The  $H^-$  formation via the  ${}^2\Sigma_g^+$  state extends well

into the 11–12 eV region, in which a multitude of resonances are observed in elastic and inelastic scattering (see Sec. IIC). It is therefore not surprising that high-resolution experiments on negative ion formation would show structure in the 11–12 eV region. The decay of bound compound states into the dissociative attachment channel was observed by Dowell and Sharp (1968) and is shown in Fig. 16. The mechanisms for this coupling have been discussed by Eliezer *et al.* (1967) in terms of a radiationless intramolecular transition.

The structure shown in Fig. 16 is further discussed in Sec. IIC.

### C. Core-Excited Resonances in the 11–15 eV Region

Resonances of the core-excited (Feshbach) type in  $H_2$  were discovered by Kuyatt, Mielczarek, and Simpson (1964) in the energy range 11.62 to 13.31 eV by

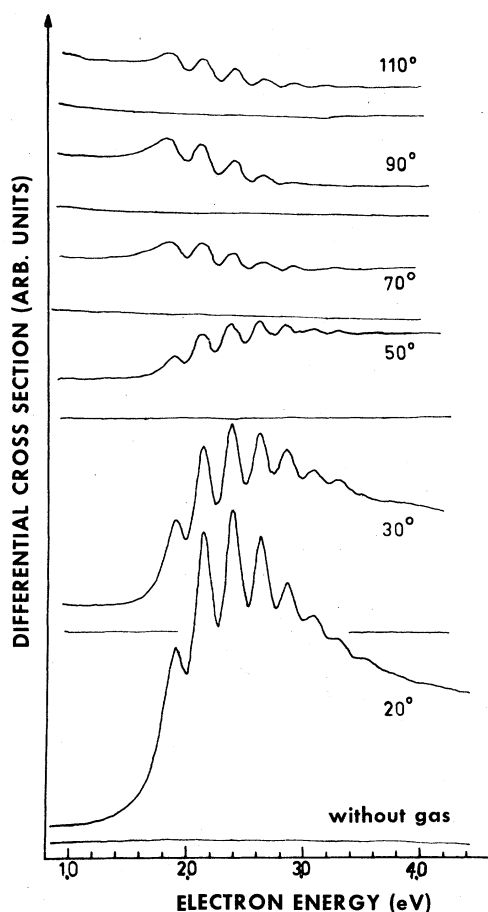


FIG. 27. Energy dependence of the “elastic” cross section in  $N_2$  at various angles of observations. The experiment uses an electrostatic monochromator and an electrostatic analyzer, which accepts only “elastically” scattered electrons. Since the resolution is not sufficiently good to resolve rotational states, all rotational transitions are included in the measurement. [From Ehrhardt and Willmann (1967).]

observing elastically scattered electrons. These structures were confirmed by Golden and Bandel (1965) in a Ramsauer-type experiment for both  $H_2$  and  $D_2$ . Menendez and Holt (1966) found the structure in the excitation of the  $v=1$  and  $v=2$  vibrational states of the ground electronic state,  $H_2(X^1\Sigma_g^+)$ , thus indicating a decay of the resonances into vibrational states. Heideman, Kuyatt, and Chamberlain (1966) were the first to observe the decay of these compound states into electronically excited states of  $H_2$  by studying the energy dependence of the  $v=0$  and  $v=1$  vibrational states of the  $B^1\Sigma_u^+$  state of  $H_2$ . Also, it was understood both theoretically (Eliezer *et al.*, 1967) and experimentally (Kuyatt *et al.*, 1966) that more than one compound state contributes to the observed structure, and that the isotopes HD and  $D_2$  exhibit a set of similar structures but that they show differences in the relative strength of the series.

Experimentally, five series of resonances have been definitely identified, and as many as seven can be invoked to explain the experimental data. Comer and Read (1971a) have suggested a classification scheme,

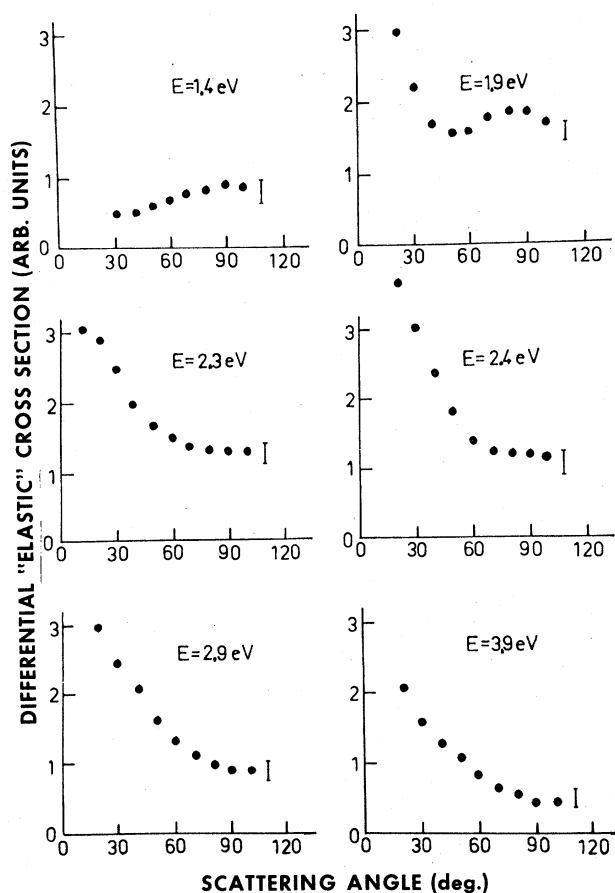


FIG. 28. Angular dependence of "elastically" scattered electrons at various fixed electron energies  $E$ . A common scale is used for all curves. [From Ehrhardt and Willmann (1967).]

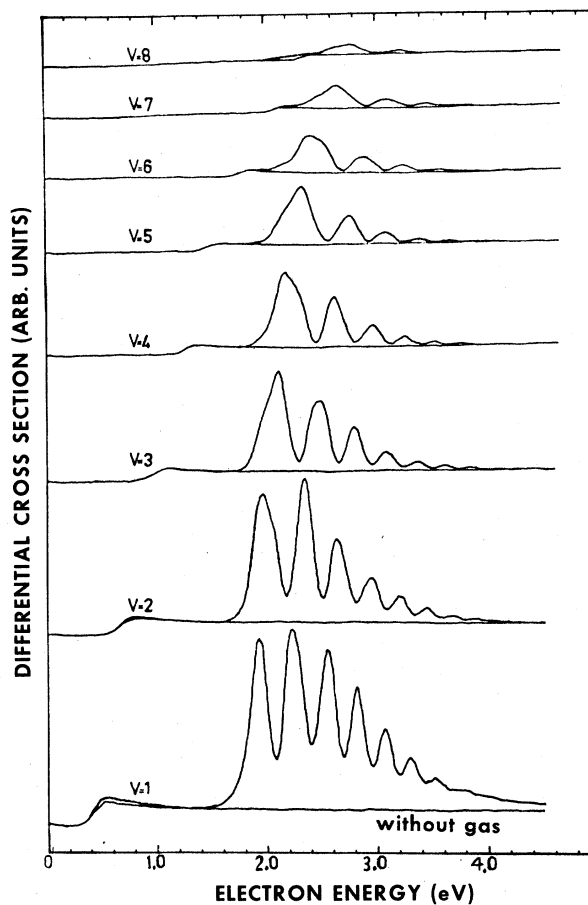


FIG. 29. Energy dependence of the vibrational excitation in  $N_2$  at a scattering angle of  $20^\circ$ . Excitation to eight vibrational states ( $v=1-8$ ) is observed in the region of the  $^2\Pi_g$  compound state. [From Ehrhardt and Willmann (1967).]

which was later adopted by Sanche and Schulz (1972), and which is followed in the present review. We designate the different bands with the letters "a" to "g." Table II provides a listing of the bands and indicates the names given to the bands by different authors, the decay channel in which the bands were observed, and the energy of the first feature. The table is presented to provide a "dictionary" which is helpful in reading the original literature.

It should be noted that series "a" and "d" have the same starting energy and the same spacing. The need for postulating two separate series with similar molecular parameters is brought about by angular distribution measurements (Comer and Read, 1970). Series "a" is of the  $\Sigma$ -type and thus is expected to exhibit an isotropic behavior. Weingartshofer *et al.* (1970) observe structure in the  $B^1\Sigma_u$  state at the positions of the resonances in series "a." However, the angular distribution in this channel of decay is *not* isotropic. Therefore, Comer and Read find it necessary to postulate a state of  $\Pi$  symmetry around 11.40 eV. They have considered the possibility that the observed anisotropy

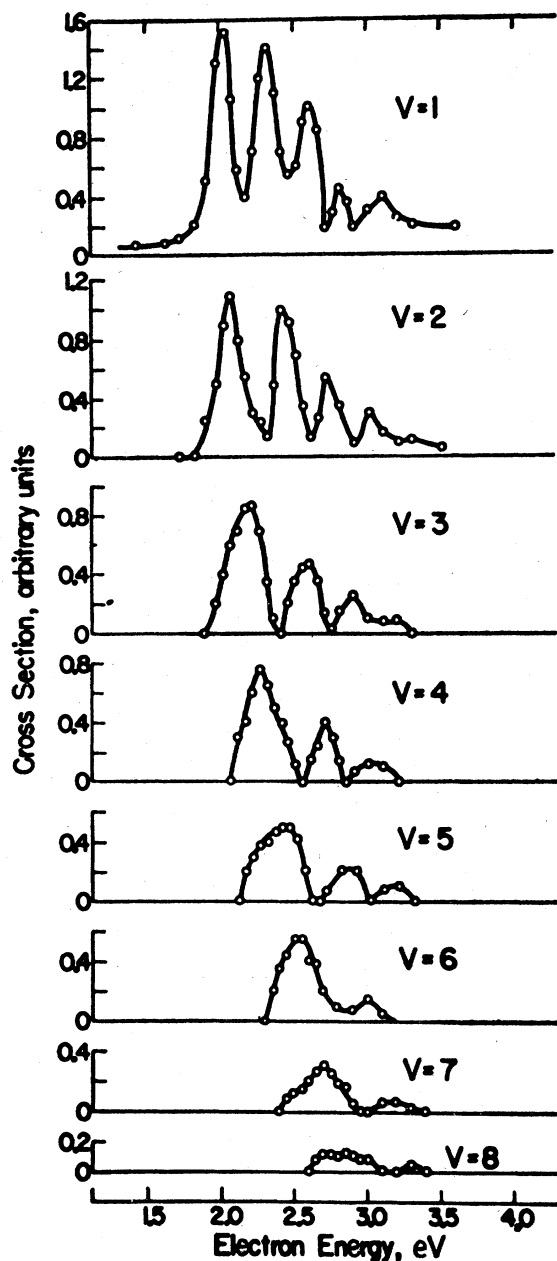


FIG. 30. Energy dependence of the vibrational excitation in  $N_2$ . The angle of observation was 72 degrees. As in Fig. 29, eight vibrational states are visible in the region of the  ${}^2\Pi_g$  compound state. The similarity of the curves with those shown in Fig. 29 indicates that the structures in the vibrational cross sections are independent of angle of observation. [From Schulz (1964).]

of the resonances in the  $B^1\Sigma_u^+$  states results from a  $d$ -wave component in the entrance channel, but have discarded this interpretation because it leads to an unreasonably large  $d$ -wave amplitude in the entrance channel.

The above considerations rely heavily on angular distribution measurements which, in molecules, may

not be as well understood as one would wish. For example, Black and Lane (1971) point out that in certain decay channels transitions may show preference for a change in rotational quantum number, e.g.,  $j=0 \rightarrow j=1$ . Such an effect would upset the simple interpretation of angular distribution measurements and may render unnecessary the assignment of a separate series for bands "d" and "e." More detailed analysis must be awaited.

These uncertainties are taken into account in Table II. Arrows point to series "a" and "d" and to series "c" and "e," indicating that future consideration may show that "a"="d" and "c"="e." In energy, these two sets of series ("a" and "d"; "c" and "e") are almost coincident.

Samples of recent experimental results, as observed in different decay channels, are shown in Figs. 17–22. Figure 17 shows the results of a transmission experiment by Sanche and Schulz (1972) in which the derivative of the transmitted current is measured directly. This experiment, following closely in concept the experiments of Kuyatt *et al.* (1964) and Schulz (1964), exhibits higher sensitivity to sharp structures than previous transmission experiments. In the experiment of Sanche and Schulz (1972), optical focussing effects are largely eliminated by the use of an axial magnetic field and the detection sensitivity is enhanced by modulating the electron energy in the collision chamber. The advantage of the transmission experiment is the overview that it provides for a large region of energy. However, many details of resonances, such as the decay channel and the angular distribution of scattered electrons, cannot be easily extricated from transmission experiments.

Figures 18 and 19 show the results of Comer and Read (1971a) for which a double electrostatic analyzer was used. By studying resonances in high vibrational states of the electronic ground state, Comer and Read are able to eliminate all interference effects between resonant and nonresonant scattering; in fact they discovered series "b" by observing resonant structure in vibrational levels above  $v=8$ , as is shown in Fig. 19. It

TABLE III. Position of maxima in the elastic and inelastic cross sections of  $N_2$  (Ehrhardt and Willmann, 1967).

$v'$	Energy, eV	
	$v=0$	$v=1$
0	1.89	1.93
1	2.15	2.24
2	2.40	2.55
3	2.65	2.82
4	2.89	3.07
5	3.13	3.31
6	3.36	3.53
7	3.58	3.76

should be noted that most of the structure visible in the lower vibrational states of Fig. 18 consists of series "a". The values of the resonant energies obtained by Comer and Read are tabulated for  $\text{H}_2^-$  in Appendix I, and for  $\text{D}_2^-$  in Appendix II. The results for  $\text{D}_2^-$  are very similar to those for  $\text{H}_2^-$ .

Studies similar to those of Comer and Read, using a similar technique had been previously undertaken by Weingartshofer *et al.* (1970). Their results (in absolute units) at different angles of observation are shown in Figs. 20 and 21. In addition to the  $X^1\Sigma_g^+$  decay channel, Weingartshofer *et al.* examined other decay channels: the dissociation continuum,  $b^3\Sigma_u^+$  (see Fig. 22);  $c^3\Pi_u$ ;  $a^3\Sigma_g^+$ ; and several vibrational levels of the states  $C^1\Pi_u$ ,  $B'^1\Sigma_u^+$ , and  $D^1\Pi_u$ . The branching ratios for the decay into some of these channels are listed, in absolute units, in Appendix III. Molecular radiation emanating from the  $B^1\Sigma_u^+$  state of  $\text{H}_2$  and  $\text{D}_2$  also shows the appropriate resonances, as has been shown by McGowan and Williams (1969) and by Pichanick *et al.* (1971).

Figure 23 shows a schematic diagram of the five energetically distinct compound states of  $\text{H}_2^-$  and some of the decay channels. Figure 24 shows the energies at which various resonances have been observed in different channels of decay. On the bottom of the

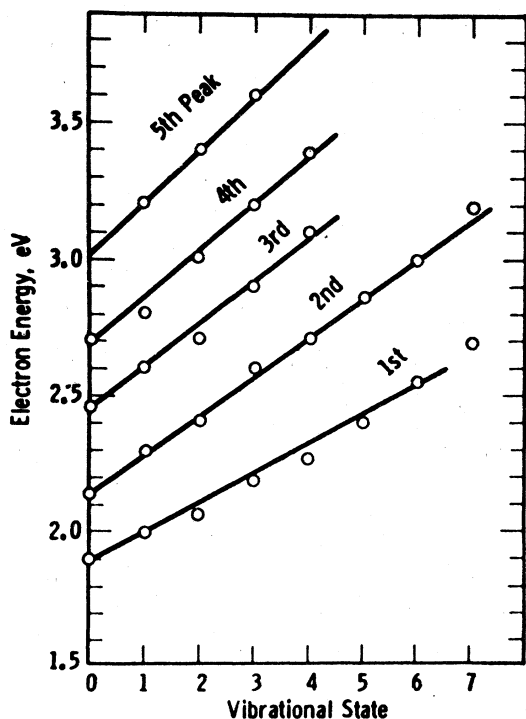


FIG. 31. Position of the peaks in the cross section vs quantum number of the final state. If the  $^2\Pi_g$  compound state were long-lived compared to vibrational times, the solid lines would be horizontal, i.e., the peaks would occur at the same energy regardless of the final vibrational state. The effect shown on this figure indicates that the lifetime of the  $^2\Pi_g$  compound state is comparable to a vibrational period. [From Schulz (1964).]

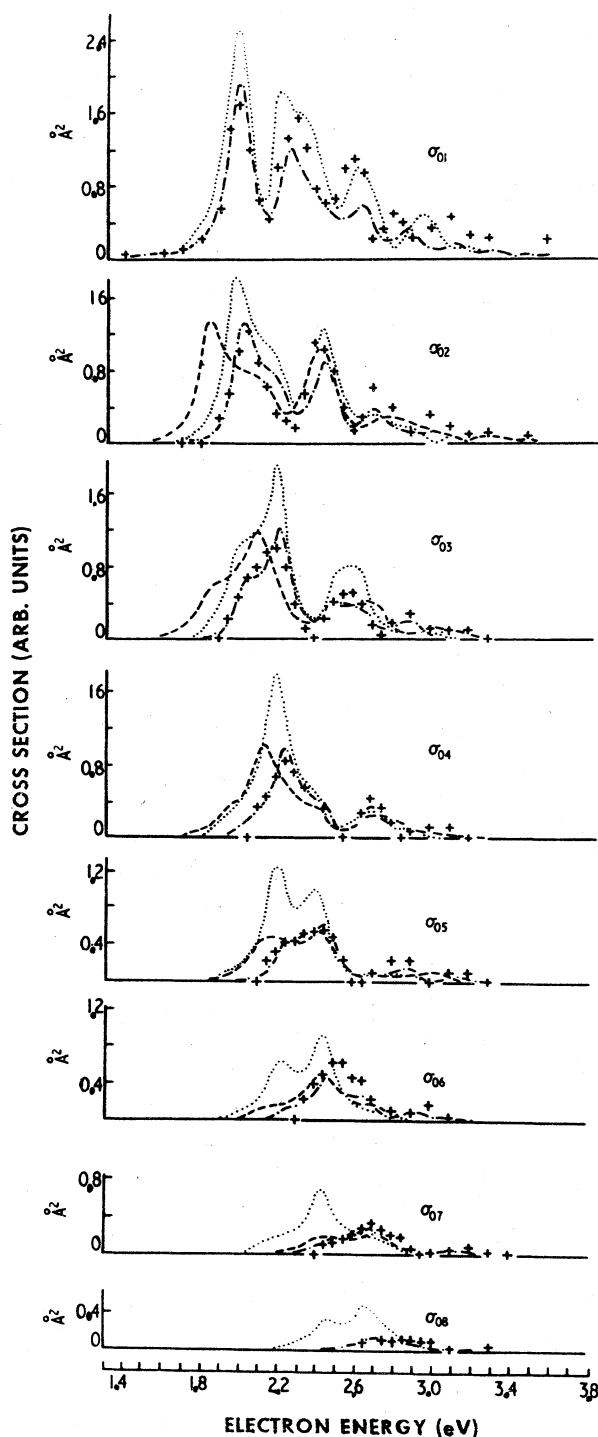


FIG. 32. Comparison of experimental and theoretical vibrational cross sections for resonant  $e\text{-N}_2$  scattering. Crosses are the experimental results of Schulz (1964). The curves show various theoretical attempts to fit the experimental cross sections without allowing for the variation of  $\Gamma$  with internuclear separation. None of these theoretical curves reproduce the regularity of the experimental structure. The broken curve: Herzenberg and Mandl (1962); chain curve: Chen (1964); dotted curve: Hasted and Awan (1969). [From Birtwistle and Herzenberg (1971).]

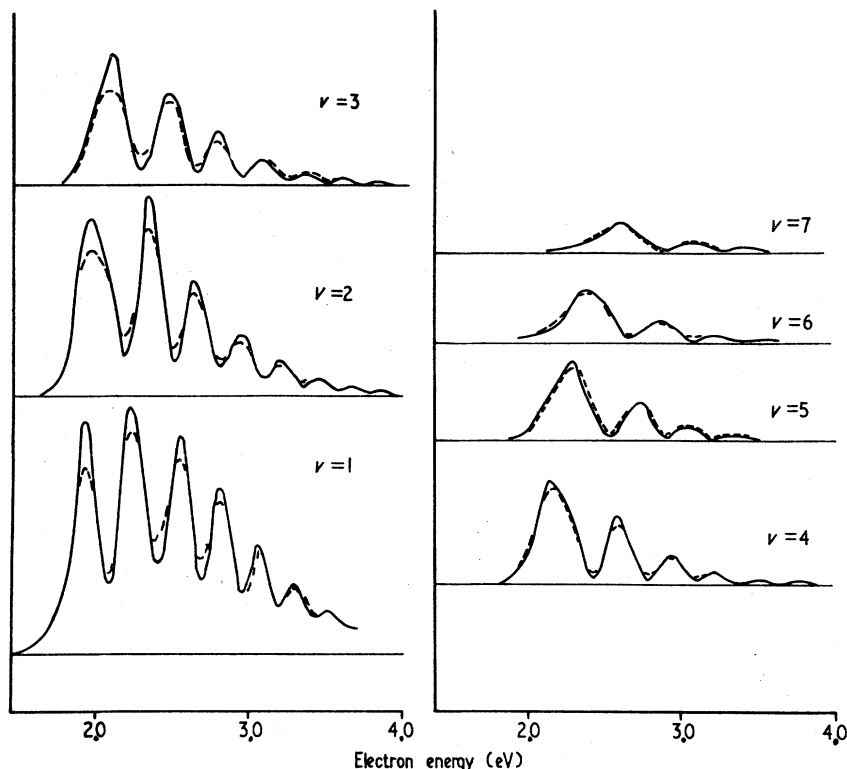


FIG. 33. Comparison of the theoretical cross section for vibrational excitation using a variable  $\Gamma$ . The dashed curve (Birtwistle and Herzenberg, 1971) is theoretical, using a variable  $\Gamma$ , and the full curve is experimental (Ehrhardt and Willmann, 1967). The theoretical cross section is calculated using the parameters of Table IV. [From Birtwistle and Herzenberg (1971).]

figure, the position of resonances is indicated as they appear in transmission experiments. The energy positions of the transmission experiments of Kuyatt *et al.* (1966) and of Sanche and Schulz (1972) are shown. The shaded region indicates the spread of values, which rarely exceeds 50 meV. Thus the agreement is considered excellent.

Higher on Fig. 24, we show decay into high vibrational states of the ground electronic state, into the  $b^3\Sigma_u^+$  continuum, and the  $B^1\Sigma_u^+$  state as well as the  $C^1\Pi_u$  states in the low vibrational levels.

Decay into the  $B^1\Sigma_u^+$  state followed by the emission of a photon is also indicated. Whereas McGowan and Williams (1969) observe a "strong" and a weak series, Pichanick *et al.* (1971) observe only the "strong" series. The shaded area indicates the degree of uncertainty between the two above-mentioned experiments. The short lines indicate the positions of the "weak series" in the radiation. The "strong" lines agree best with series "c" (or "e") and the weak ones with series "a" (or "d"). Why this is so, i.e., why one band seems to dominate in radiative decay when it is not observed in inelastic channels, is not understood.

Below we discuss some of the more prominent features of the different bands. Appendixes I and II list the energies in tabular form for  $H_2$  and  $D_2$ .

A set of potential energy curves has been derived from purely experimental information by Comer and Read (1971a) and is shown in Fig. 25(a). A quasi-

variational calculation of Eliezer *et al.* (1967) gives very good agreement with some of the experimental observations and points to the proper designation of the states. Eliezer *et al.* find that the lowest two compound states have  $^2\Sigma_g^+$  symmetry and that they consist of the  $C^3\Pi_u$  and  $C^1\Pi_u$  states, respectively, with an electron attached which has  $(\pi_u 2p')$  symmetry. See Fig. 25(b).

#### 1. Band "a"

Band "a" seems to decay into all possible decay channels. The agreement between various groups as to

TABLE IV. Characteristics of  $N_2^-$  ( $^2\Pi_g$ ) resonance at 2.3 eV.

	Birtwistle and Herzenberg (1971)	Krauss and Mies (1970)
$R_0^- - R_0$ (cm) <sup>a</sup>	$0.095(\pm 0.003) \times 10^{-8}$	$0.12 \times 10^{-8}$
$\hbar\omega$ (eV) <sup>b</sup>	$0.244 \pm 0.003$	0.24
$x_e$ <sup>c</sup>	$0.0051 \pm 0.0017$	0.0046
$\Gamma(R_0)$ (eV) <sup>d</sup>	$0.57 \pm 0.02$	0.8

<sup>a</sup>  $R_0^-$ ,  $R_0$  are the equilibrium internuclear separations for  $N_2^-$  and  $N_2$ , respectively.

<sup>b</sup>  $\hbar\omega$  is the vibrational spacing of  $N_2^-$ .

<sup>c</sup>  $x_e$  is the anharmonic constant.

<sup>d</sup>  $\Gamma(R_0)$  is the width at  $R_0$ .

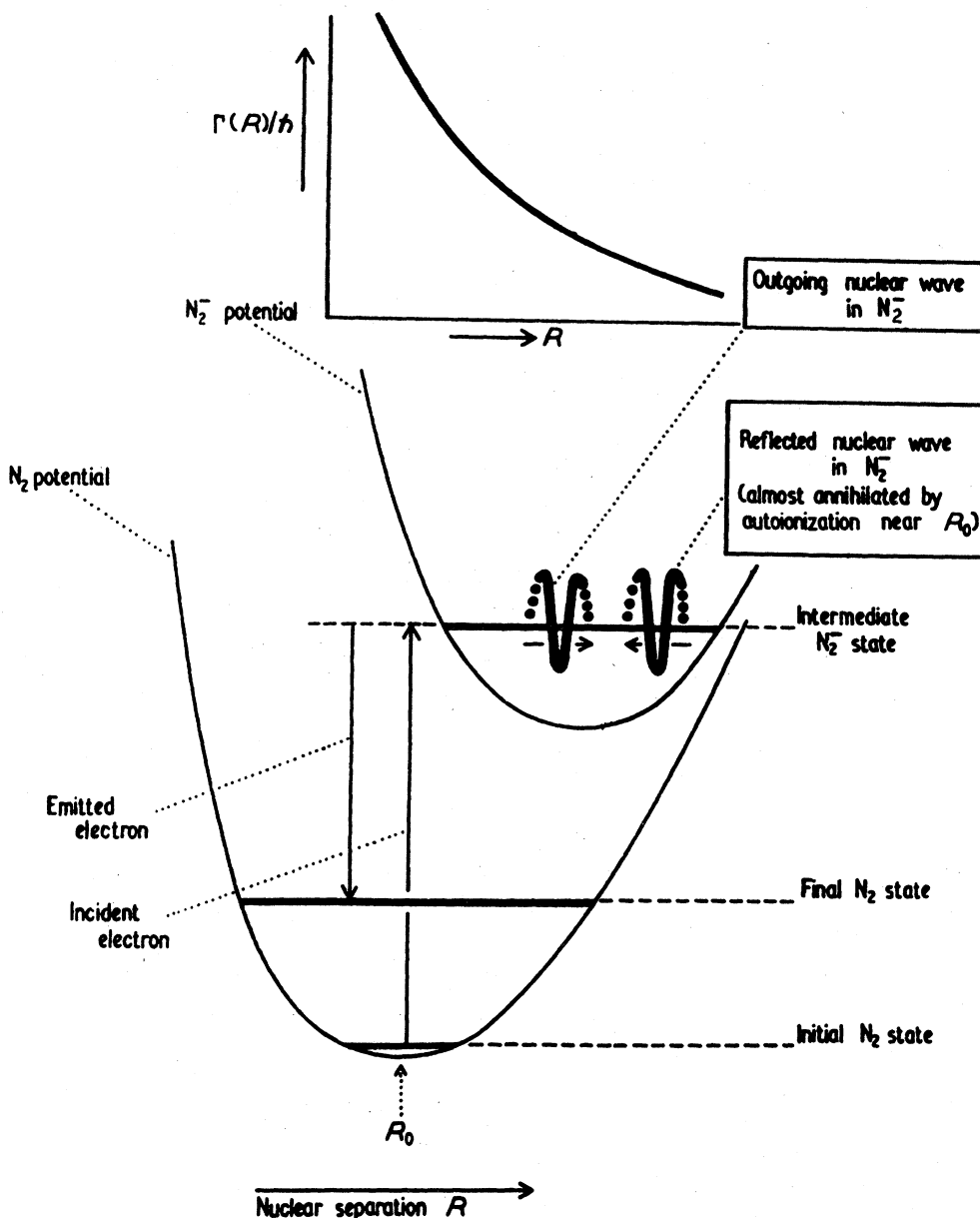


FIG. 34. The "boomerang" model of the nuclear wave function applied to the  $N_2^-$  ion. This schematic model is discussed by Herzberg (1968). It is based on the assumption that the magnitude and  $R$  dependence of  $\Gamma(R)$  are such that only a single outgoing and a single reflected wave matter. [From Birtwistle and Herzberg (1971).]

the location on the energy scale is very satisfactory. Small discrepancies in energy probably result from the method of evaluating the position of the resonances. Also, interference effects can shift the position of the peaks, which are not necessarily the true positions of the resonances. The results of Weingartshofer *et al.* (1970) and of Comer and Read (1970a), who observe resonances in those channels in which very little interference takes place (e.g., high vibrational states), are free from such errors.

Eliezer *et al.* (1967) assign to this band the configuration  $(\sigma_g 1s)(\pi_u 2p)(\pi_u 2p')^2 \Sigma_g^+$ , consisting predominantly of  $(C^3\Pi_u + e)$ . When one arbitrarily adds 0.25 eV to Eliezer's calculated values, excellent agreement

exists between theory and experiment. (see Appendix I). In any case, the spacing calculated by Eliezer *et al.* for band "a" agrees with experiment and thus the assignment appears convincing. Comer and Read obtain values of 0.975 Å and 11.40 eV for the equilibrium internuclear separation and the energy minimum, respectively, whereas the values deduced by Eliezer *et al.* are 1.03 Å and 11.18 eV. Band "a" seems to be firmly established.

## 2. Band "b"

Band "b" has been observed only by Comer and Read (1971a) in high vibrational levels of the ground state of  $H_2$ . They obtained a natural width of 30 meV

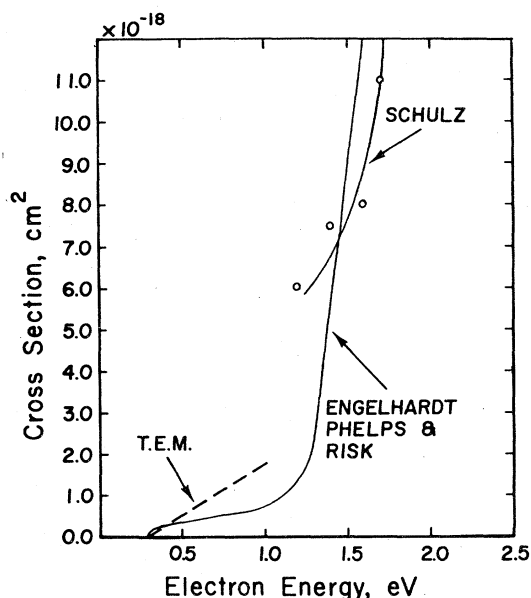


FIG. 35. Excitation function for  $v=1$  in  $N_2$  near threshold. Shown are the results of Engelhardt, Phelps, and Risk (1964) obtained from an analysis of swarm experiments, the double electrostatic analyzer measurements of Schulz (1964), and the slope near threshold obtained using the trapped-electron method (TEM) by Burrow and Schulz (1969). The low-energy portion of the theoretical cross section (Chen, 1964a) is identical to that of Engelhardt, Phelps, and Risk below 1.2 eV. [From Burrow and Schulz (1969).]

for band "b" and suggested that the new resonance has the configuration  $(\sigma_g 1s)(\sigma_u 1s)^2 {}^2\Sigma_g^+$ , representing an electron bound to the  $B {}^1\Sigma_u^+$  excited state of  $H_2$ . This band has not been observed in any transmission experiment. The assignment is still in doubt, especially since the potential energy curve for the  $(\sigma_g 1s)(\sigma_u 1s)^2$  compound state should have a larger equilibrium internuclear separation than the parent  $B {}^1\Sigma_u^+$  state (H. S. Taylor, private communication). In order to interpret their experiment, Comer and Read (1971a) must assign a smaller equilibrium internuclear separation to the  $(\sigma_g 1s)(\sigma_u 1s)^2$  state compared to the parent  $B {}^1\Sigma_u^+$  state, as shown in Fig. 25(a).

### 3. Band "c"

Band "c" has been observed in the transmission experiments of Kuyatt *et al.* (1966) and of Sanche and Schulz (1972) in both  $H_2$  and  $D_2$ . In their early work, Comer and Read (1971a) observed band "c" only in  $D_2$  and not in  $H_2$ . They assign to band "c" the configuration  $(\sigma_g 1s)(\pi_u 2p)(\sigma_g 2s) {}^2\Pi_u$ . Recently, however, Joyez, Comer, and Read (1973) were able to observe band "c" in a high resolution experiment in  $H_2$ . Their value for the width is  $\Gamma \leq 16$  meV and the starting energy is about 11.19 eV, with subsequent values at 11.50, 11.80, and 12.07 eV. If the starting value of 11.19 for band "c" is substantiated, then the quantum numbers for band "c" as assigned by the other investi-

gators listed in Appendix I will have to be incremented by unity.

As pointed out previously, band "c" appears strongly in vacuum uv emission.

The calculated progression of Eliezer *et al.* (1967) for the configuration  ${}^2\Sigma_g^+(\sigma_g 1s)(\pi_u 2p)(\pi_u 2p')$  agrees well with most of the experimental energy positions, as shown in Appendix I. However, there is a problem in understanding the angular dependences found by Comer *et al.*

The detailed understanding of bands "c" and "e" is still missing and the above considerations must be considered as preliminary.

### 4. Band "d"

This band was postulated by Comer and Read (1971a) from an analysis of the results of Weingartshofer *et al.* (1970). On the basis of the angular distribution of electrons observed by Weingartshofer *et al.* in the  $B {}^1\Sigma_u$  exit channel, Comer and Read suggest that the compound state involved must have  ${}^2\Pi_g$  symmetry. Although the results of Weingartshofer are coincident in

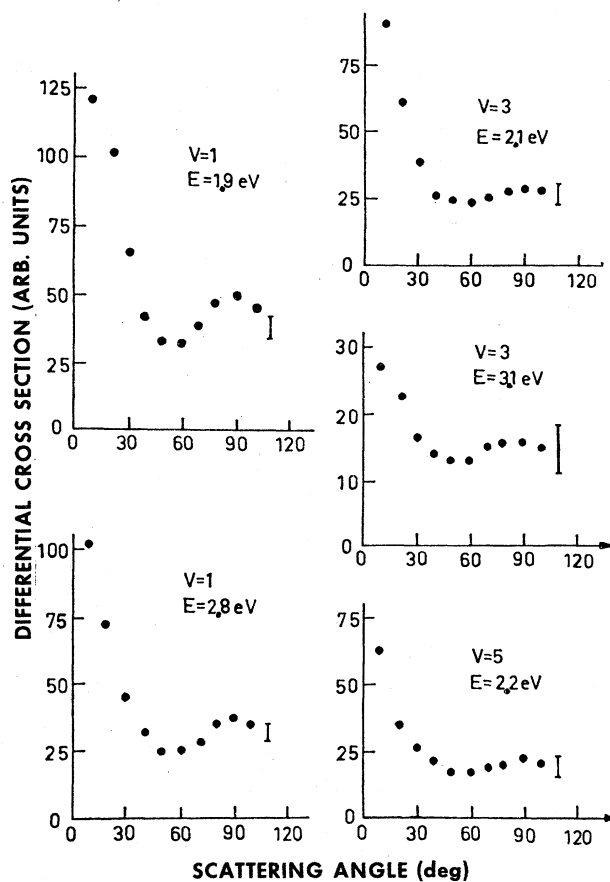


FIG. 36. Angular dependence of the cross section for vibrational excitation to  $v=1, 3$ , and  $5$  in  $N_2$ . The electron energy is indicated. The subsidiary peaks near  $90^\circ$  result from  $d$ -wave scattering. [From Ehrhardt and Willmann (1967).]

energy with series "a," Comer and Read suggest that the compound state is not the same since series "a" involves a  ${}^2\Sigma_g^+$  state. However, Black and Lane (1971) have recently pointed out that angular distributions are not a simple guide to the assignment of symmetries because different rotational transitions may be dominant in various decay channels. Thus Black and Lane show that the rotational transition  $j=0 \rightarrow j=1$  dominates in the process  $e + \text{H}_2(X\ {}^1\Sigma_g^+) \rightarrow \text{H}_2^-(e + C\ {}^1\Pi_u) \rightarrow \text{H}_2(B\ {}^1\Sigma_u^+) + e$ . If such mechanisms are present, angular distributions will have to be analyzed in more detail.

### 5. Band "e"

Under the heading of band "e" we list the measurement of Weingartshofer *et al.* (1970) who observed inelastically scattered electrons having excited the  $B\ {}^1\Sigma_u^+$  state.

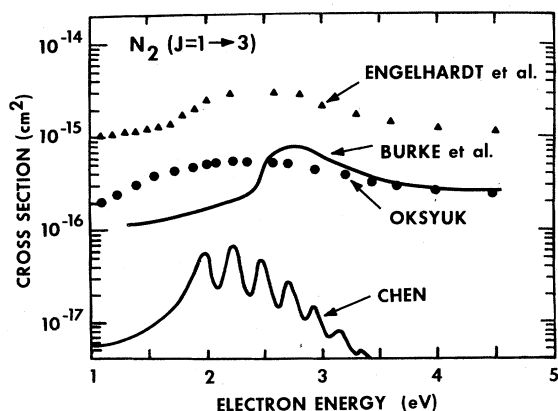


FIG. 37. Pure rotational excitation ( $J=1 \rightarrow 3$ ) in the region of the  ${}^2\Pi_g$  compound state in  $\text{N}_2$ . Shown are the theoretical results of Oksyuk (1966), Burke and Sinfailam (1970), and Chen (1966b), and the momentum transfer cross section of Engelhardt, Phelps, and Risk (1964).

Comer and Read advocate such a separation because of a discrepancy in the energy scale, but there is a good possibility that band "e" may be the same progression as band "c".

### 6. Band "f"

Band "f" extends from approximately 13.5 to 16 eV in  $\text{H}_2$  and from 13.5 to 14.5 eV in  $\text{D}_2$ . This band corresponds to the 13.63-eV progression found by Ehrhardt and Weingartshofer (1969) in the  $C\ {}^1\Pi_u$  decay channel of  $\text{H}_2$ . It has also been observed by Golden (1971) in a transmission experiment using a derivative technique similar to that of Sanche and Schulz (1972). In transmission experiments, band "f" exhibits a width of about 90 meV in both  $\text{H}_2$  and  $\text{D}_2$ , in good agreement with the natural width of 80 meV estimated by Ehrhardt *et al.* (1969). The  ${}^2\Sigma_g^+$  symmetry for band "f" was assigned by these authors.

Band "f" shows peculiar characteristics: it decays

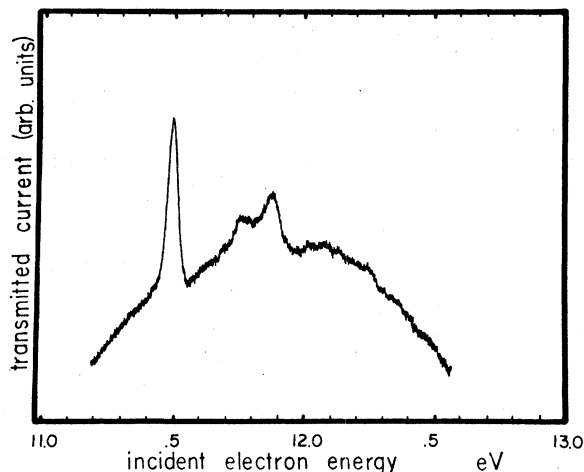


FIG. 38. Transmission of electrons by  $\text{N}_2$ , showing a sharp "window"-type resonance at  $11.48 \pm 0.05$  eV. The zero of current has been displaced. Additional structure occurs at 11.75 and 11.87 eV. The latter is partly due to an inelastic threshold ( $E\ {}^2\Sigma_g^+$ ). The nitrogen pressure was  $\sim 0.04$  Torr. [From Heide-man, Kuyatt, and Chamberlain (1966a).]

preferentially to identical vibrational levels of the  $C\ {}^1\Pi_u$  state, i.e., in the decay process the vibrational quantum number does not change (Weingartshofer *et al.*, 1970). This is clearly evident from Figs. 23 and 24. It is therefore likely that the potential energy curve responsible for band "f" has the same shape and the same equilibrium internuclear separation as the  $C\ {}^1\Pi_u$  or  $D\ {}^1\Pi_u$  states.

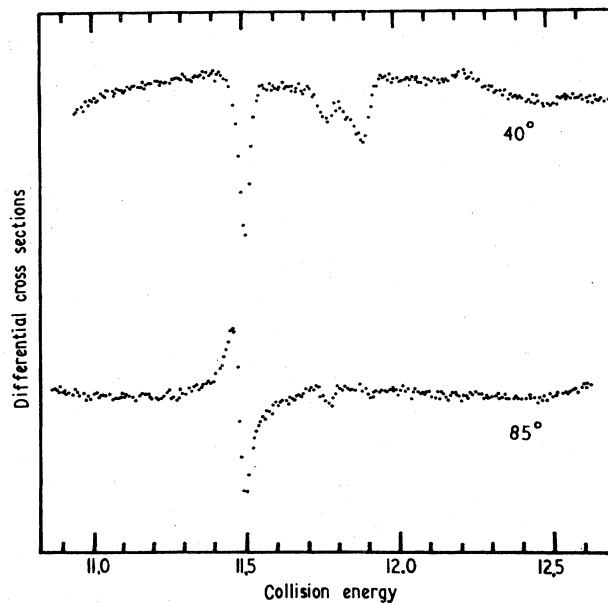


FIG. 39. Energy dependence of the differential elastic cross section for  $\text{N}_2$  at  $40^\circ$  and  $85^\circ$ . The largest structure shown occurs at 11.48 eV and is coincident in energy with the transmission peak shown in Fig. 38. The designation is  ${}^2\Sigma_g^+$ . The energies of the other structures are listed in Appendix V. [From Comer and Read (1971b).]

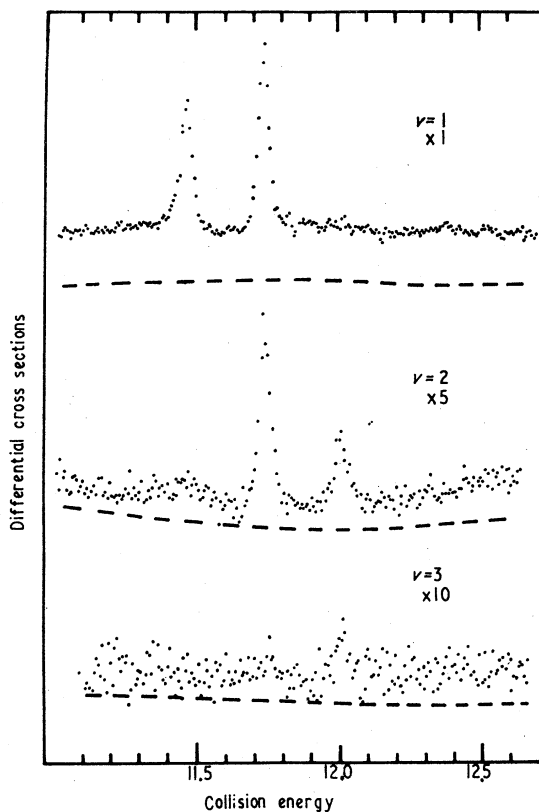


FIG. 40. Energy dependence of the differential vibrational cross sections for scattering of electrons from  $N_2$ . The exit channels are vibrational levels of the electronic ground state and the scattering angle is  $70^\circ$ . The curves do not have the same cross section scale but the peak intensities can be obtained from Table II. The zero lines are shown broken. [From Comer and Read (1971).]

### 7. Band "g"

Figure 17 shows that band "f" appears perturbed by the presence of other structures. This new band is labelled "g" and tabulated in Appendix I. It appears much more clearly in  $D_2$  where bands "f" and "g" do not overlap. Three features around 16 eV in the data of Golden (1971) in  $H_2$  which he attributed to autoionization could be members of band "g."

## III. NITROGEN

### A. Resonance at Low Energy (1.7–4 eV) ${}^2\Pi_g$

The earliest experiments on the total cross section in  $N_2$  showed a broad peak in the region around 2.3 eV in  $N_2$  (Ramsauer and Kollath, 1931), but it was not until the early 1960's that an understanding of this effect became available, largely as a result of improved experimental techniques and the pioneering theoretical contribution of Herzenberg and Mandl (1962). From an experimental viewpoint one obtains the most detailed information on the nature of the compound state involved by studying structure in the elastic and vibra-

tional cross sections vs energy and by studying angular distributions of the scattered electrons. It should be recalled that, in the case of  $H_2$ , the dissociative attachment decay channel provided valuable understanding. However, since no stable  $N^-$  ion exists, such a study is not feasible in  $N_2$ .

The history of this discovery has been well reviewed by Massey and Burhop (1969), by Chen (1969), by Birtwistle and Herzenberg (1971), and by Bardsley and Mandl (1968). Following the total cross section measurements by Ramsauer and Kollath (1931), Haas (1957) established that the vibrational cross section exhibits a peak in the 2.3-eV energy range and that a temporary negative ion is involved. Schulz (1959) confirmed these observations using the trapped-electron method, but not until he used double electrostatic analyzers (Schulz 1962a, 1964a, 1966) could he establish the details of the resonance process.

The nitrogen molecule has the configuration  $(\sigma_g 1s)^2 (\sigma_u 1s)^2 (\sigma_g 2s)^2 (\sigma_u 2s)^2 (\pi_u 2p)^4 (\sigma_g 2p)^2$ . The first unfilled orbital is  $\pi_g 2p$  ( $= 3d\pi_g$  in the united-molecule notation) and the incident low-energy electron temporarily occupies this orbital. As the electron escapes, it encounters a  $d$ -wave barrier through which it must tunnel. This shape resonance has a symmetry  ${}^2\Pi_g$  and it is centered around 2.3 eV. It dominates the low-energy electron impact cross sections in  $N_2$ , as shall be discussed in the following sections. A summary of shape resonances in other molecules is given in Sec. VII.

#### 1. Elastic Cross Section via ${}^2\Pi_g$

The energy dependence of the total scattering cross section, obtained by Golden (1966) using a modified Ramsauer apparatus, is shown in Fig. 26. The structure in the cross section above 1.8 eV is clearly visible. This structure can be observed in a Ramsauer-type apparatus when the energy distribution of the electrons

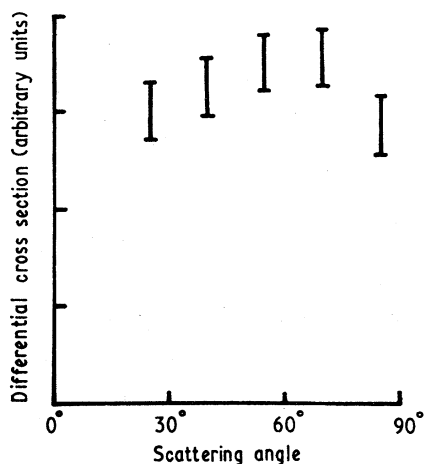


FIG. 41. Angular distribution for the two resonant peaks observed in the  $\nu=1$  exit channel (see Fig. 40). [From Comer and Read (1971b).]

is narrow. The structure above 1.8 eV had been previously observed in the vibrational cross section by Schulz (1964) and interpreted as evidence for the  ${}^2\Pi_g$  compound state, which in  $N_2$  is sufficiently long-lived to show vibrational structure. Below 1.8 eV, Schulz did not observe any structure or other evidence for a compound state, whereas the total cross section of Golden, shown in Fig. 26, exhibits such structure below 1.8 eV.

In order to resolve this discrepancy, Ehrhardt and Willmann (1967) re-examined the elastic and inelastic differential cross sections as well as the total cross section, but were unable to reproduce the structures below 1.8 eV. In order to insure the proper working order of their apparatus, Ehrhardt and Willmann studied the low-energy structure in NO, which had previously been measured by Boness and Hasted (1966), and confirmed this structure both in the total cross section as well as in the elastic cross section. Thus it is highly probable that the structure below 1.8 eV, shown in Fig. 26, is spurious.

The differential elastic cross section at different scattering angles is shown in Fig. 27 and the angular distribution is shown in Fig. 28.

The structure in the elastic cross section above 1.8 eV, as well as in the vibrational excitation indicates the existence of a compound state whose lifetime is comparable to or longer than a vibrational period. The compound state is formed by the addition of an electron in a  $\pi_g$  orbital to the ground electronic state of  $N_2$  (Gilmore, 1965; Krauss and Mies, 1970), and this

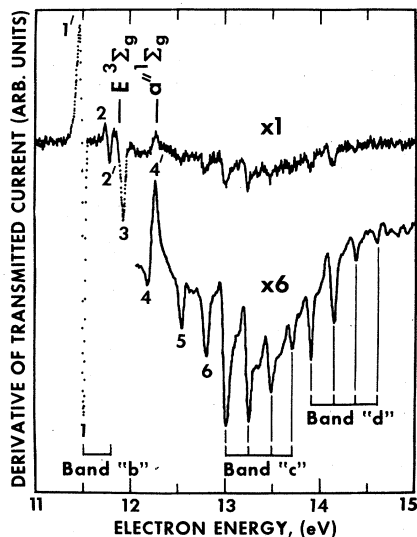


FIG. 42. Derivative of the transmitted current vs electron energy in  $N_2$  (11–15 eV). The giant resonance marked 1–1' is the  ${}^2\Sigma_g^+$  state and forms the starting member of band "b," whose parents are the  $E^3\Sigma_g^+$  and  $a^1\Sigma_g^+$  Rydberg states of  $N_2$ . The grandparent is the ground state of  $N_2^+$ . Structures 3 and 4 are shape resonances. The other resonances, including bands "c" and "d" which appear on the higher sensitivity run on the bottom of the figure, have the  $A^2\Pi_u$  state of  $N_2^+$  as a grandparent. [From Sanche and Schulz (1972).]

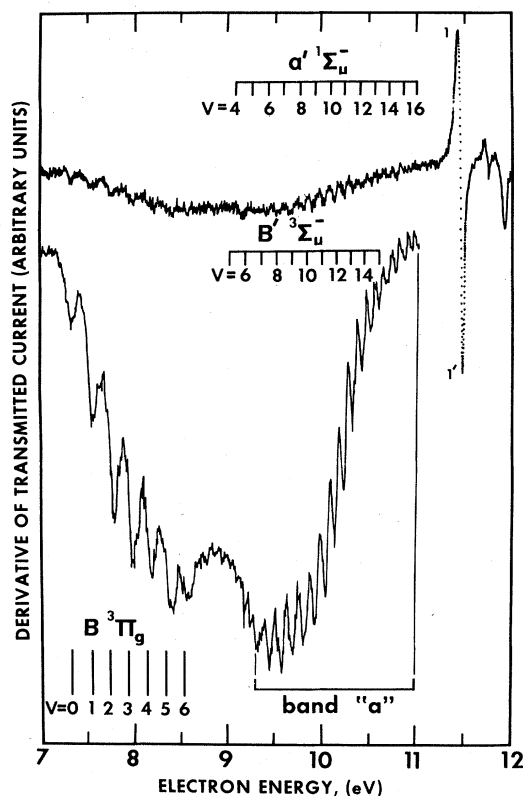


FIG. 43. Derivative of the transmitted current vs electron energy in  $N_2$  (7–12 eV). Structure in the region 7–9 eV is due to inelastic processes involving the  $B^3\Pi_g$  state of  $N_2$ . The locations of the  $B^3\Pi_g$  state, the  $B^1\Sigma_u^-$  state, and the  $a^1\Sigma_u^-$  state of  $N_2$  are indicated. Band "a" is a progression of core-excited shape resonances associated with the  $B^3\Pi_g$  state, and the large structure (1–1') is the first Feshbach resonance,  ${}^2\Sigma_g^+$ . The bottom trace is taken with a higher sensitivity. [From Sanche and Schulz (1972).]

assignment is proven by angular distribution studies (Ehrhardt *et al.*, 1967, 1968) of inelastically scattered electrons.

## 2. Vibrational Excitation via ${}^2\Pi_g$

The vibrational excitation cross sections for the excitation of the first eight levels of the ground electronic state of  $N_2$  clearly show structure which is characteristic of the compound state. Figures 29 and 30 show the vibrational cross sections at  $20^\circ$  and  $72^\circ$ , respectively, as obtained by two different groups. The shape and general behavior of the cross sections are in good agreement. Table III lists the positions of the maxima of the features, as observed in the  $v=0$  and  $v=1$  decay channels. Actually, the positions of the peaks occur at different positions, depending on the channel of observation, i.e., the peaks shift to higher energies for higher vibrational states. This effect, first discussed by Schulz (1964), is shown in Fig. 31. This feature, as well as the regularity of the structure in the vibrational cross section, stimulated theoretical interest in the

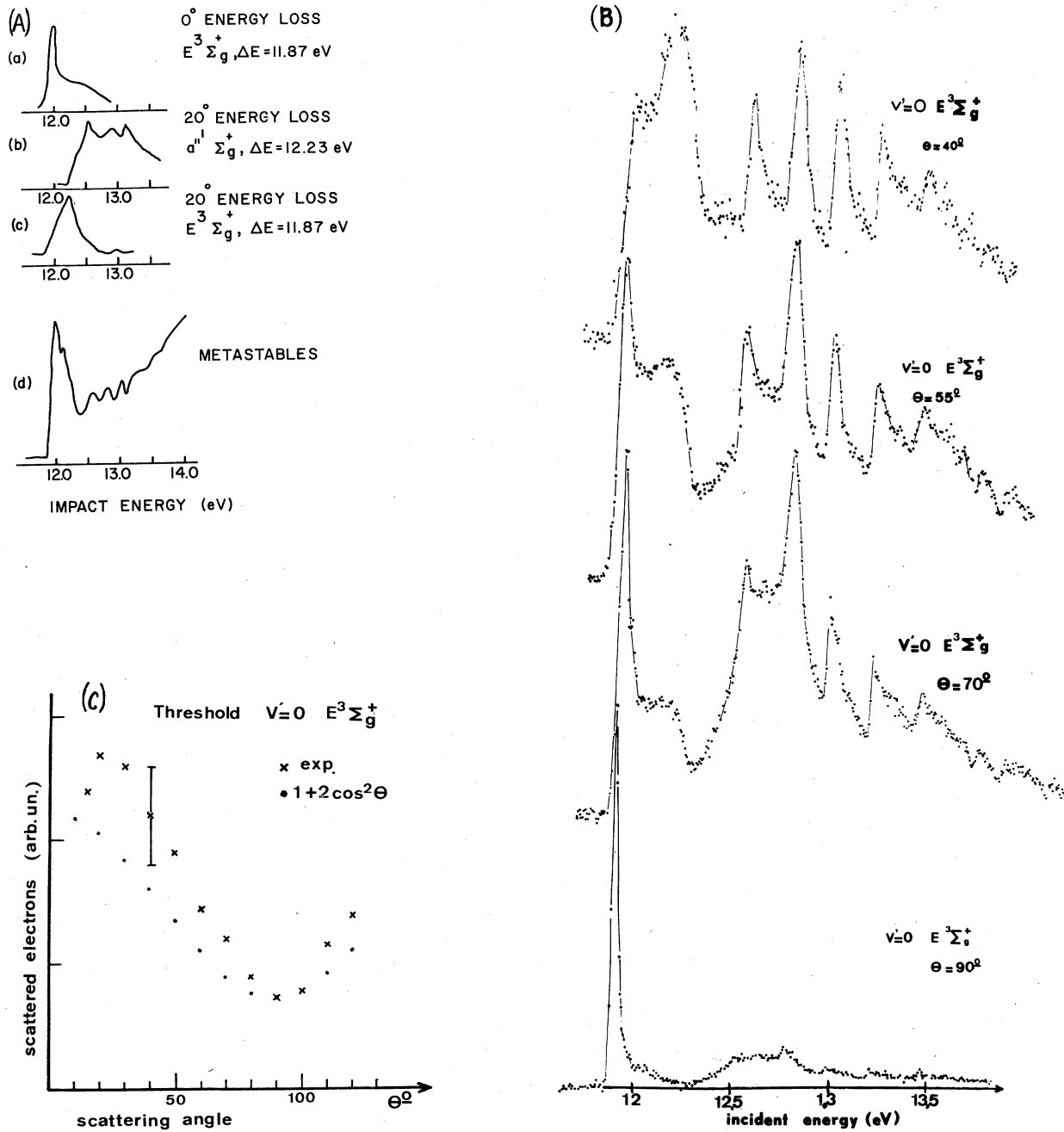


FIG. 44. (A) Threshold region for excitation of the  $E^3 \Sigma_g^+$  and  $a''^1 \Sigma_g^+$  states of  $N_2$ . Shown are the differential cross sections of Heidemann *et al.* (1966a) at  $0^\circ$ , and Ehrhardt and Willmann (1967) at  $20^\circ$ . Also shown is the excitation function for metastables (Lawton and Pichanick, 1973). [From Lawton and Pichanick (1973).] (B) Energy dependence of the differential excitation cross section for the  $E^3 \Sigma_g^+(v=0)$  state of  $N_2$ , at different angles of observation. The sharp peak near 11.90 eV has a half-width of  $35 \pm 5$  meV at  $90^\circ$  and exhibits the angular behavior shown in Fig. 44(C). [From Mazeau, Hall, Joyez, Landau, and Reinhardt (1972b).] (C) Angular distribution of electrons having excited the  $E^3 \Sigma_g^+(v=0)$  state in  $N_2$  at 11.90 eV. Also shown is an angular distribution of the form  $(1+2 \cos^2 \theta)$ , normalized to the experimental data at  $90^\circ$ . The good agreement between the angular distributions points to a  $p\sigma$  partial wave, indicating that the threshold behavior is dominated by a shape resonance. [From Mazeau, Hall, Joyez, Landau, and Reinhardt (1972b).]



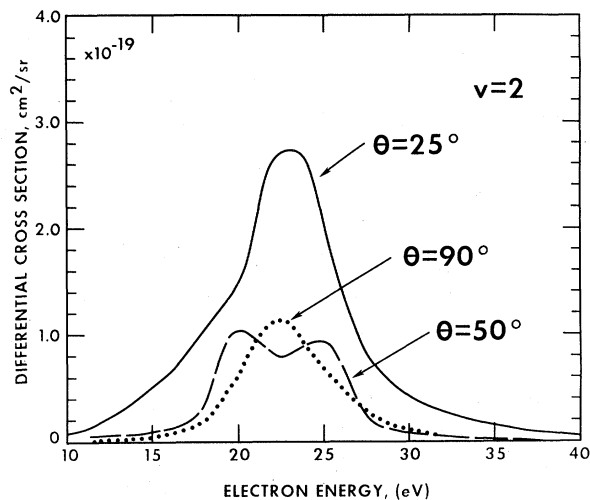


FIG. 45. Energy dependence of the differential cross section for vibrational excitation to  $v=2$  in  $N_2$  for three angles of observation. The energy range is 15 to 30 eV. The peak in the vibrational cross section possibly indicates the existence of a high density of overlapping compound states around 20 eV. The curves for  $v=1$  and  $v=3$  are similar to that shown. [From Pavlovic, Boness, Herzenberg, and Schulz (1972).]

problem. However, the early theoretical approaches, although correct in principle, could not reproduce unambiguously these properties (Herzenberg and Mandl, 1962; Chen, 1964; Hasted and Awan, 1969).

It was pointed out by Herzenberg (1968) that it is essential to consider the variation of the width  $\Gamma$  with

TABLE V. Derived properties of the 11.48-eV core-excited Feshbach resonance in  $N_2^-$ .<sup>a</sup>

Symmetry	${}^2\Sigma_g^+$
Parent	$E {}^3\Sigma_g^+$
$R_e$ (Å)	$1.115 \pm 0.01$
$a$ (eV)	$0.270 \pm 0.02$
$b$ (eV)	$0.002 \pm 0.002$
$\Gamma$ (eV)	$6 \times 10^{-4}$
$E_0$ (eV)	11.345

<sup>a</sup> The quantities  $a$  and  $b$  are the Morse parameters of the potential curve defined so that the energy  $E$  of the vibrational level  $v$ , with respect to the  $v=0$  level of the ground state, is given by  $E = E_0 + a(v + \frac{1}{2}) - b(v + \frac{1}{2})^2$ .  $R_e$  is the equilibrium internuclear separation. [From Comer and Read (1971).]

internuclear separation. Such a variation is expected from the dependence of the penetrability of the centrifugal barrier with the energy of the emitted electron, which varies with  $R$ . Without allowing for such a variation, theory cannot reproduce the simplicity and regularity of the experimental results (see Fig. 32), and it certainly cannot reproduce the simple shift in peaks shown in Fig. 31.

Birtwistle and Herzenberg (1971) used a variable  $\Gamma$  in their theory and obtained excellent agreement with experiment, as shown in Fig. 33.

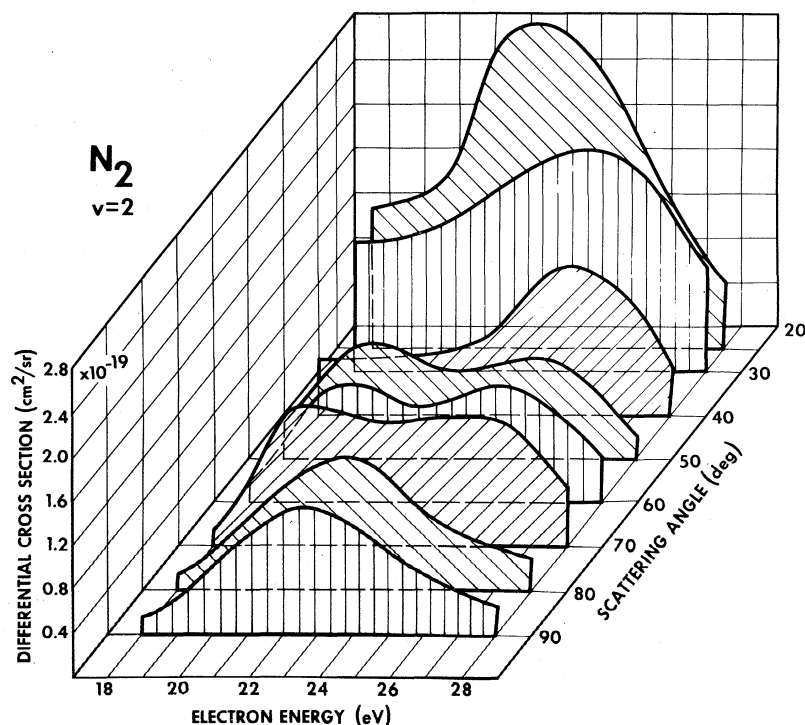


FIG. 46. Combined angular and energy dependence of the differential cross section for vibrational excitation to  $v=2$  in  $N_2$ . The energy dependence of the process observed depends on the angle of observation. The complexity of the curves makes it probable that a superposition of many compound states is involved. [From Pavlovic, Boness, Herzenberg, and Schulz (1972).]

TABLE VI. Genealogy of Feshbach resonances in  $N_2^-$ .

Resonance $N_2^-$			Grandparent $N_2^+$			Binding eV
Designation	Energy, eV	Spacing	Designation	Energy, eV	Spacing	
"b" ( $^2\Sigma_g^+$ )	11.48	0.27	$X^2\Sigma_g^+$	15.6	0.27	4.1
	11.75					
	12.02					
"5"	12.64	0.23	$A^3\Pi_u$	16.7	0.23	4.1
"6"	12.87					
"c"	13.00					
"d"	13.88					

The best fit to the experiment was obtained when Birtwistle and Herzenberg (1971) used the parameters for  $N_2^-$  shown in Table IV. For comparison, Table IV also shows the parameters for the  $N_2^-$  state from ab initio calculation of Krauss and Mies (1970). The excellent agreement obtained from these completely independent approaches is most gratifying.

The model of Birtwistle and Herzenberg (1971) leads to the conclusion that the  $N_2^-$  compound state has only

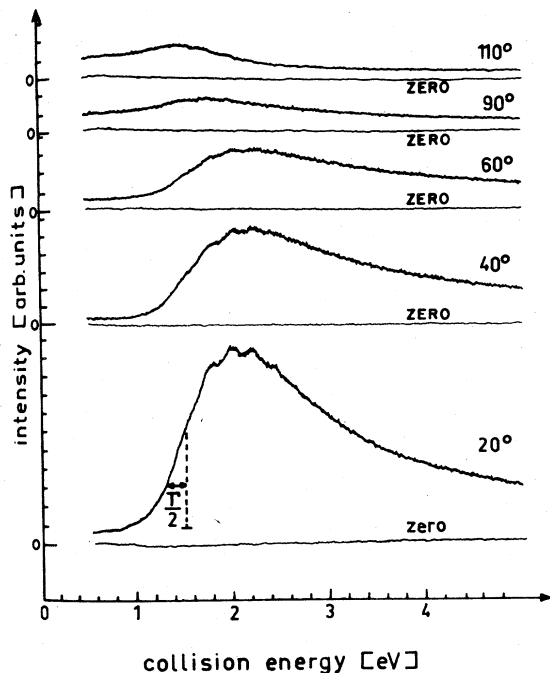


FIG. 47. Energy dependence of the elastic differential cross section for CO at different scattering angles. The first peak is only weakly indicated as a shoulder at 1.5 eV.  $\Gamma/2$  is an approximate measure of the half-width of the compound state. The structures are better developed in the vibrational cross section (see Fig. 48). The intensity scales for all curves are the same. [From Ehrhardt, Langhans, Linder, and Taylor (1968).]

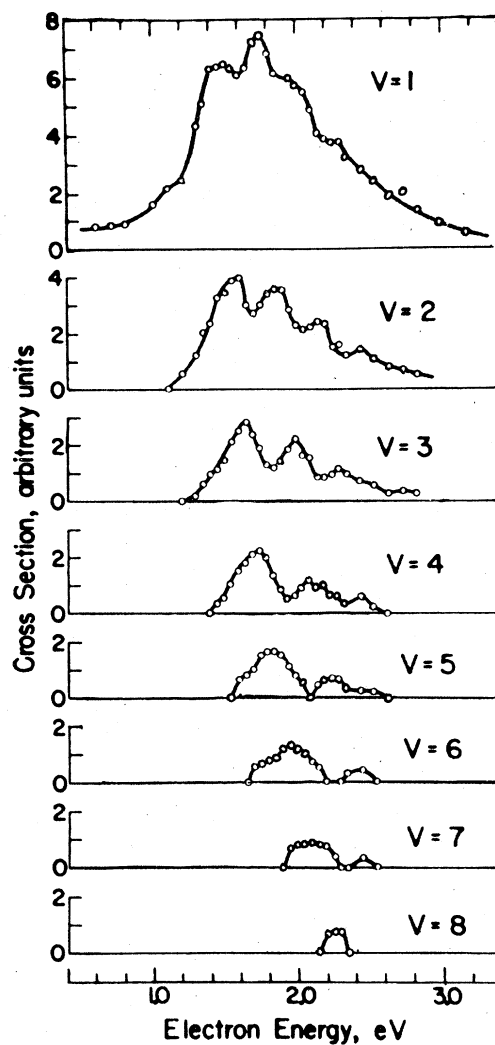


FIG. 48. Energy dependence of differential vibrational excitation in CO at an angle of observation of  $72^\circ$ . The structure resulting from the  $^3\Pi$  compound state is more pronounced than in elastic scattering but broader than the equivalent structure in  $N_2$ . [From Schulz (1964).]

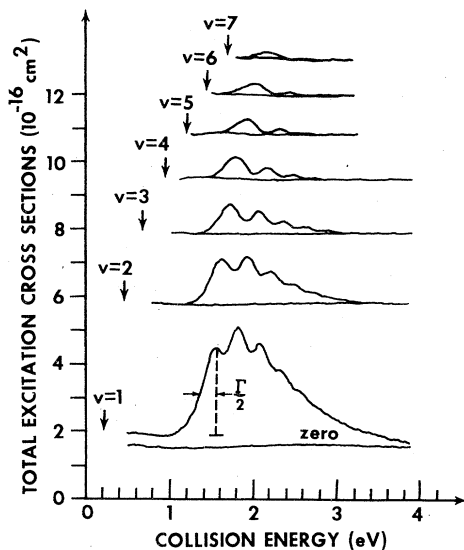


FIG. 49. Absolute cross sections for vibrational excitation of the CO molecule. The arrows point to the threshold energies of the individual vibrational states. [From Ehrhardt, Langhans, Linder, and Taylor (1968).]

time enough to vibrate once before autoionization takes place. Thus the  $N_2^-(^2\Pi_g)$  state lies intermediate in lifetime between long-lived compound states [e.g.,  $O_2^-(X^2\Pi_g)$ ] and short-lived compound states [e.g.,  $H_2^-(^2\Sigma_u^+)$ ]. This “boomerang” model is shown schematically in Fig. 34.

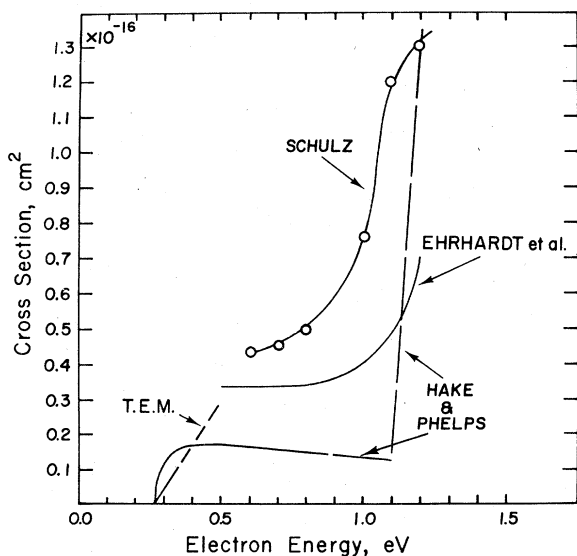


FIG. 50. Threshold behavior of the cross section for exciting the  $v=1$  state in CO. Shown are the results of Hake and Phelps (1967). The portion of the data by Hake and Phelps indicated by the dashed line are only approximate. Also shown are the results of Ehrhardt *et al.* (1968), Schulz (1964), and the trapped-electron data (marked TEM) giving the slope near threshold (Burrow and Schulz, 1969). [From Burrow and Schulz (1969).]

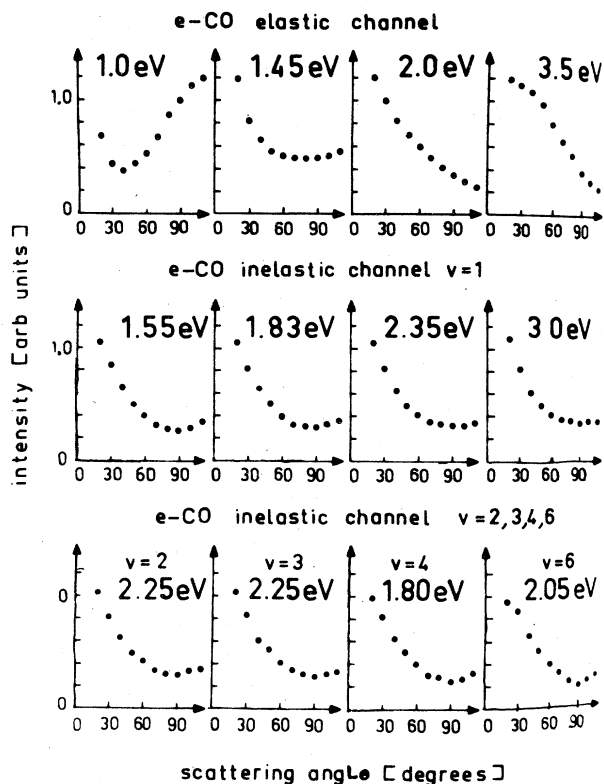


FIG. 51. Angular dependences of elastic and inelastic scattering of electrons by CO molecules at different collision energies. In the elastic channel (upper row) the angular dependence changes rapidly with energy since the scattering contains several partial waves with varying phase shifts (energy close to threshold). The constancy of the curve shapes for all inelastic channels at energies within the resonance region demonstrates that a compound state with a well-defined set of quantum numbers exists. [From Ehrhardt, Langhans, Linder, and Taylor (1968).]

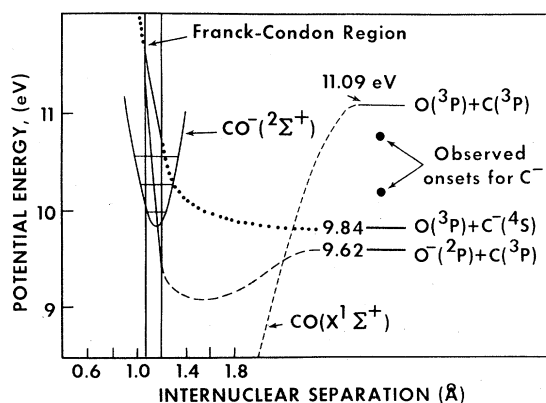


FIG. 52. Hypothetical potential energy curves for  $CO^-$  systems showing the possible decay of the  $^2\Sigma^+$  resonance at 10 eV into the  $O(^2P)+C(^3P)$  and  $O(^3P)+C(^4S)$  dissociative attachment channels. The onsets for the negative ions are taken from the work of Stamatovic and Schulz (1970). [From Sanche and Schulz (1972).]

FIG. 53. Formation of  $O^-$  from CO by dissociative attachment. Shown are the curves of Stamatovic and Schulz 1970 (points) and their calibration against the onset of  $Xe^+$ . Also shown are the results of Chantry (1968) by the dashed line and of Rapp and Briglia (1965) by the crosses. The structure near 10 eV on the curve by Stamatovic and Schulz is caused by the  $^2\Sigma^+$  resonance existing at 10.04 eV. [From Stamatovic and Schulz (1970).]

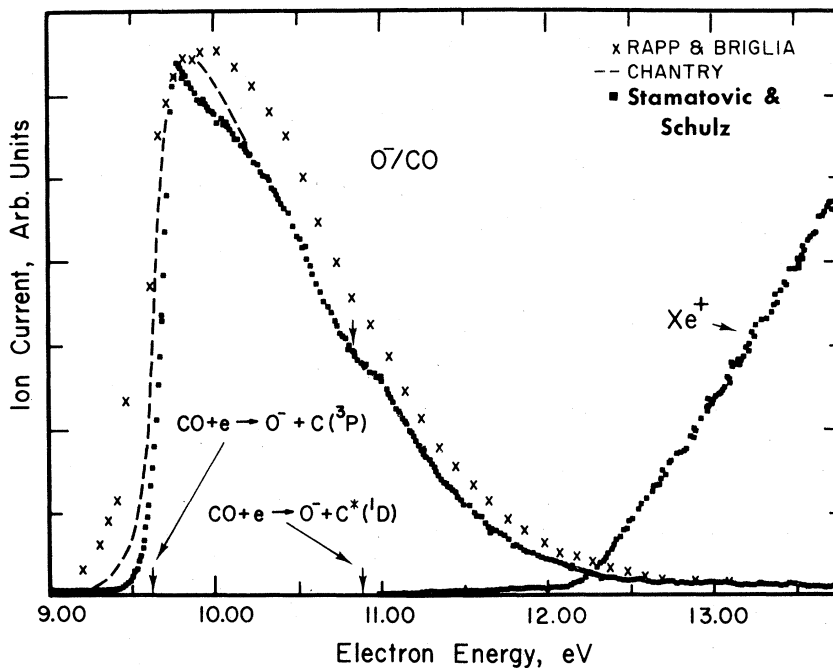
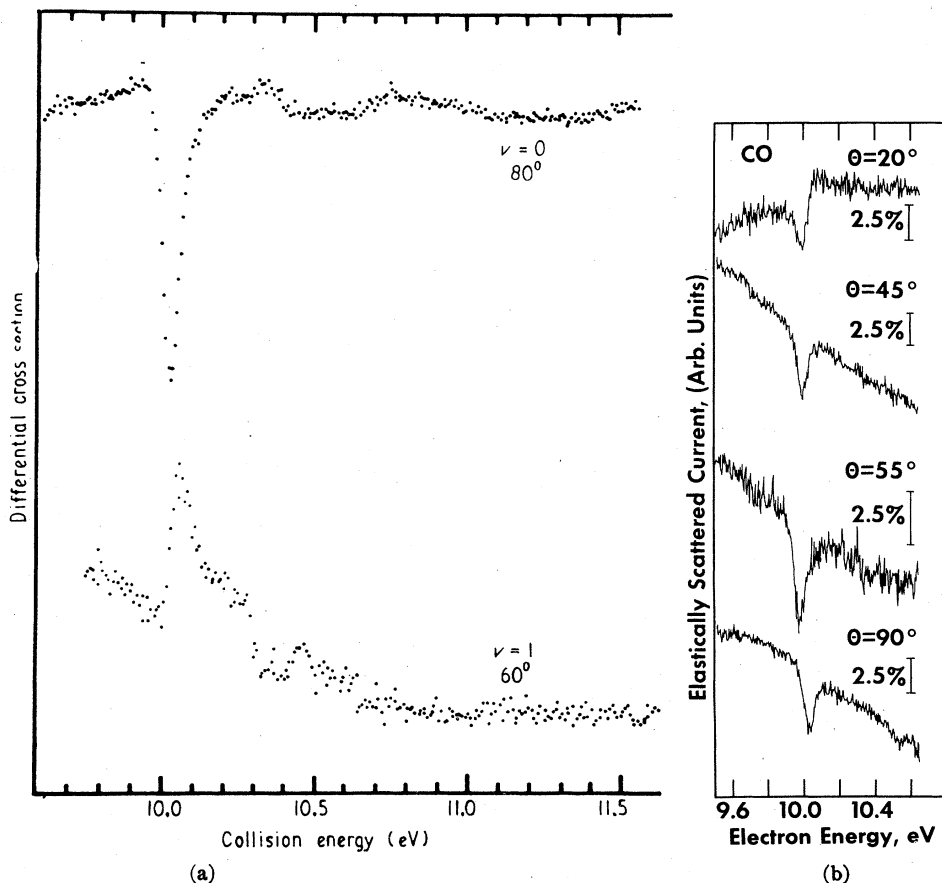


FIG. 54. (a) Energy dependence of the differential cross section in CO. The exit channels are the  $v=0$  and  $v=1$  vibrational states of the ground electronic state. The positions of the resonances are listed in Appendix VI. [From Comer and Read (1971c).] (b) Energy dependence of the elastic cross section in the vicinity of the  $^2\Sigma^+$  resonance at 10.04 eV at different angles of observation. The shape is characteristic of an  $s$ -wave resonance. [From Pavlovic (to be published).]



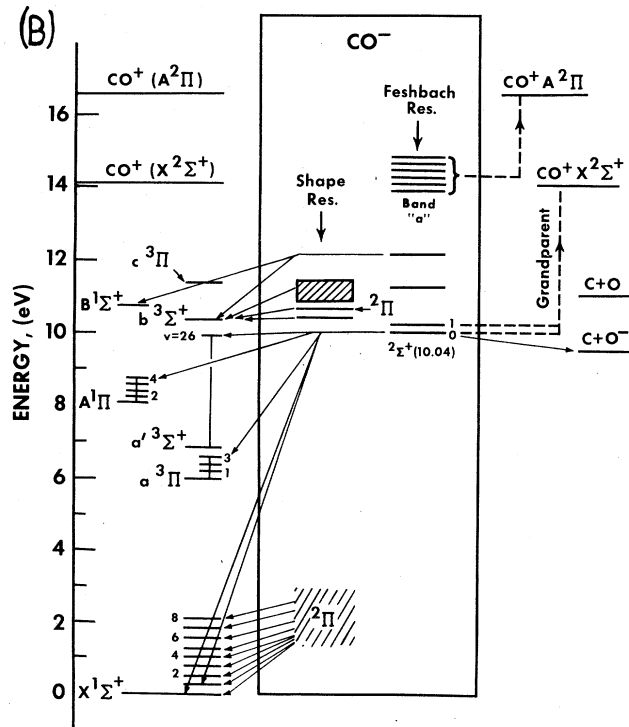
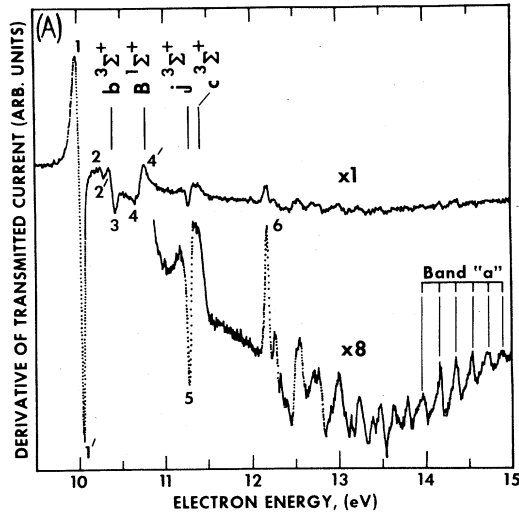
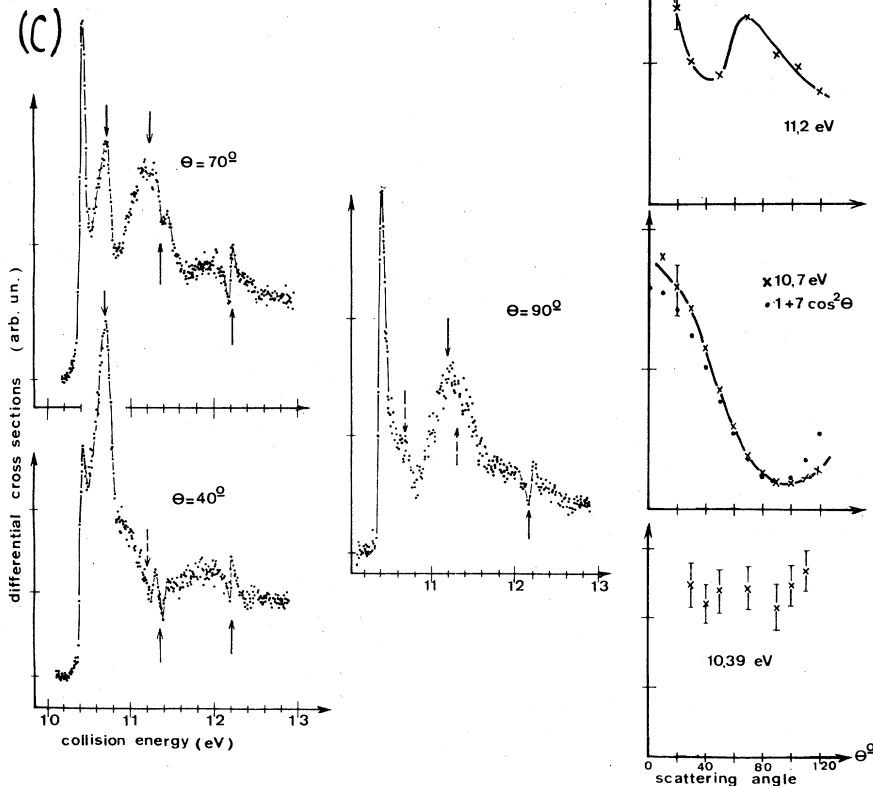


FIG. 55. (A) Derivative of transmitted current vs electron energy in CO. Resonances 1-4 are associated with the  $b^3\Sigma^+$  and  $B^1\Sigma^+$  parent states of CO. The locations of these states and the  $j$  and  $c$  states are indicated. Band "a" whose grandparent is the  $A^2\Pi$  state of  $\text{CO}^+$ , appears near the end of the spectrum. The gain on the lower curve has been increased by a factor of 8. The smaller structures on that curve represent variations in the transmitted current of about 0.01% which is the detection limit of the present experiment. [From Sanche and Schulz (1972).] (B) Schematic energy level diagram of CO and the compound states. The lines with the arrows show the preferred decay channels for the compound states. On the left side of the diagram are shown the low states of CO, i.e.,  $a^3\Pi$  (6.01 eV);  $a'^3\Sigma^+$  (6.86 eV);  $A^1\Pi$  (8.03 eV);  $b^3\Sigma^+$  (10.39 eV); and  $B^1\Sigma^+$  (10.78 eV). The preferential decay is based on the work of Comer and Read and of Mazeau *et al.* The decay into  $\text{C}+\text{O}^-$  (dissociative attachment) is shown on the right side. (C) Differential excitation functions for the  $b^3\Sigma^+$   $v'=0$  level in CO. The curves on the left show the energy dependence at  $40^\circ$ ,  $70^\circ$ , and  $90^\circ$ . The downward pointing arrows point to shape resonances at 10.7 and 11.2 eV. The upward pointing arrows indicate Feshbach resonances (11.3 and 12.2 eV). The diagrams on the right side show angular distributions at specified electron energies. The points on the diagram in the center (10.7 eV) represent the function  $(1+7 \cos^2\theta)$ , normalized at  $90^\circ$ . [From Mazeau, Gresteau, Joyez, Reinhardt, and Hall (1972a).]



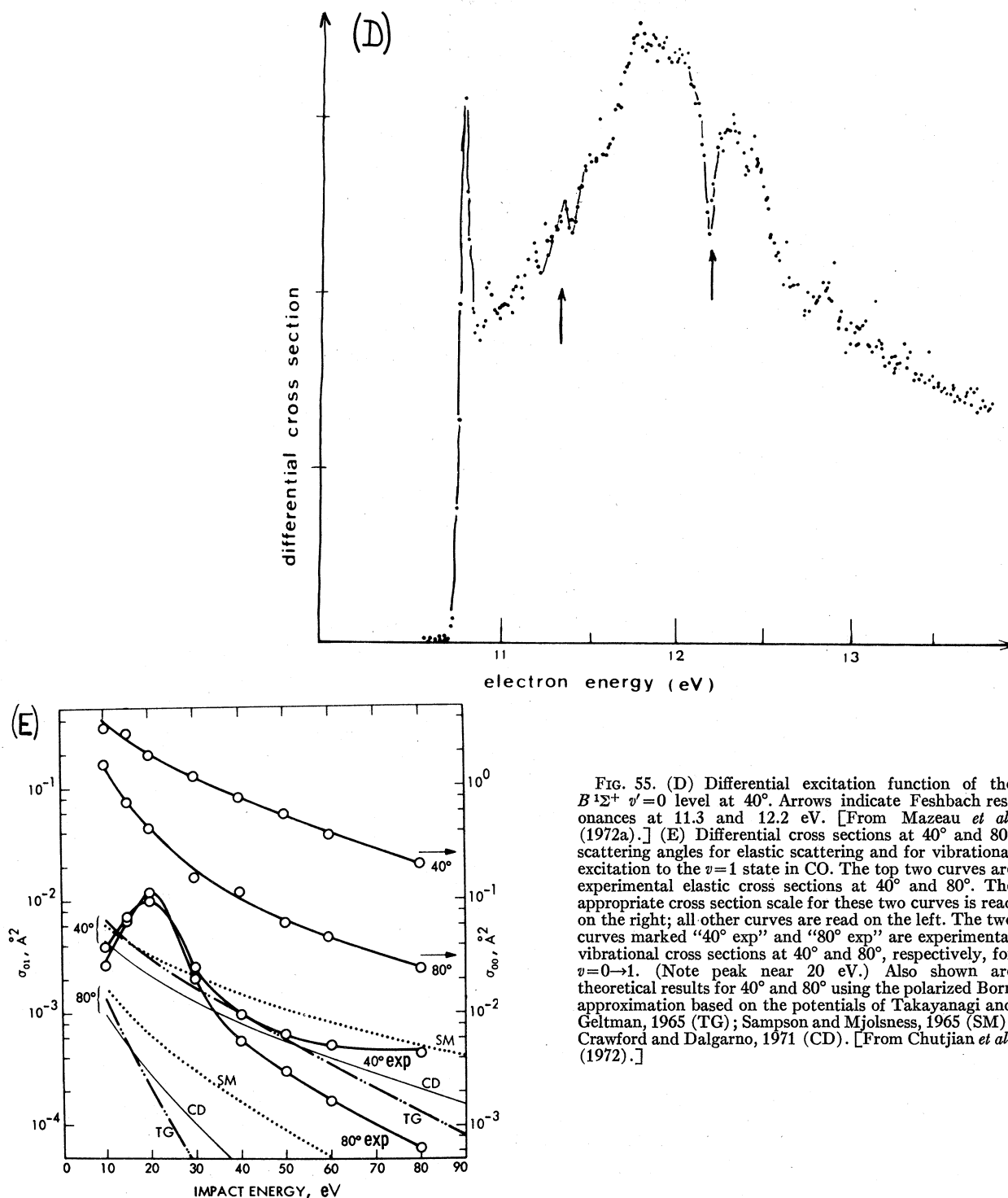


FIG. 55. (D) Differential excitation function of the  $B^1\Sigma^+ v'=0$  level at  $40^\circ$ . Arrows indicate Feshbach resonances at 11.3 and 12.2 eV. [From Mazeau *et al.* (1972a).] (E) Differential cross sections at  $40^\circ$  and  $80^\circ$  scattering angles for elastic scattering and for vibrational excitation to the  $v=1$  state in CO. The top two curves are experimental elastic cross sections at  $40^\circ$  and  $80^\circ$ . The appropriate cross section scale for these two curves is read on the right; all other curves are read on the left. The two curves marked " $40^\circ \text{ exp}$ " and " $80^\circ \text{ exp}$ " are experimental vibrational cross sections at  $40^\circ$  and  $80^\circ$ , respectively, for  $v=0 \rightarrow 1$ . (Note peak near 20 eV.) Also shown are theoretical results for  $40^\circ$  and  $80^\circ$  using the polarized Born approximation based on the potentials of Takayanagi and Geltman, 1965 (TG); Sampson and Mjolsnes, 1965 (SM); Crawford and Dalgarno, 1971 (CD). [From Chutjian *et al.* (1972).]

### 3: Threshold Behavior of the Cross Section to $v=1$

The "direct" component of the vibrational cross section in  $N_2$  is small and therefore the onset of an appreciable cross section for vibrational excitation is delayed. This can be seen in Fig. 35, which compares three measurements in the threshold region. The small cross

section near threshold may be due to direct excitation or to the residual effect of the compound state.

### 4. Angular Distributions

It has already been pointed out that angular distribution measurements are a powerful tool for the deter-

mination of the symmetry of compound states. Under favorable circumstances the angular distribution of inelastically scattered electrons is determined uniquely by comparing the symmetries of the resonant state, the initial state, and the final state. The conditions under which a unique angular distribution can be obtained from symmetry considerations are listed by Bardsley and Read (1968) and by O'Malley and Taylor (1968):

(a) The scattering must be dominated by a single resonant state, so that nonresonant scattering and the contributions from other resonances are both negligible. This situation is often found in the study of inelastic collisions, but for elastic scattering there are always considerable nonresonant contributions.

(b) The molecule does not rotate appreciably during the lifetime of the resonant state.

(c) It must be assumed that when the resonant state is expanded in spherical harmonics the contribution from the lowest allowed value of  $l$  are dominant. For resonances at low energies this is nearly always true.

(d) It must also be assumed that the Born-Oppenheimer separation of electronic and vibrational motion is valid.

In the case of the  $N_2^-(^2\Pi_g)$  resonance near 2.3 eV, the extra electron must go into the  $\pi_g$  orbital. It must have even orbital angular momentum ( $l \geq 2$ ) and the projection of the angular momentum on the molecular axis must be unity. We may speak of a  $d\pi$ -wave. The expected  $d$ -wave behavior of the cross section to various vibrational states of  $N_2$  should show a subsidiary peak near  $90^\circ$ . The experimental results of Ehrhardt *et al.* (1968), shown in Fig. 36, exhibit such behavior, and thus the angular distribution measurements confirm the designation of  $^2\Pi_g$  for the first shape resonance in  $N_2$ .

### 5. Pure Rotational Excitation via $^2\Pi_g$

Pure rotational transitions can also be excited by compound states. It has already been pointed out that experiments on the "elastic cross section" exhibit structure in the energy dependence which can be attributed to the  $^2\Pi_g$  resonance. However, beam experiments do not have the resolution necessary for a study of rotational excitation, or for distinguishing rotational levels in vibrational transitions. Thus, in the case of  $N_2$  and in fact all molecules except  $H_2$ , one has to rely on theory. The results of the theory, for rotational excitation  $J=1 \rightarrow 3$ , are shown in Fig. 37. Wide discrepancies exist in the region of the  $^2\Pi_g$  compound state. The results of Chen (1966b) using projection operators seem to be much below the close-coupling results of Burke and Sinfaillam (1970) and those of Oksyuk (1966). It should be noted that in the resonance region quantum jumps  $J=0 \rightarrow 4$  or  $J=1 \rightarrow 5$ , i.e.,  $\Delta J=4$ , are possible in addition to the usual quantum jumps,  $\Delta J=2$ . Chen (1966b) has calculated the cross sec-

tions for these transitions, with and without vibrational excitation.

### B. Core-Excited Resonances in the 11–15 eV Region

As pointed out previously, Feshbach-type resonances are more likely to occur below Rydberg excited states of molecules. In  $N_2$ , the lowest Rydberg state is the  $E^3\Sigma_g^+$  state (Mulliken, 1957) at 11.87 eV and one would expect that a sharp resonance would occur about 0.5 eV below this state. Such is actually the case. Heidermann, Kuyatt, and Chamberlain (1966a) discovered a very sharp resonance at 11.48 eV, using a transmission experiment (Fig. 38). Comer and Read (1971b) performed a different scattering experiment in which the decay of the resonance could be observed for  $v=0, 1, 2$ , and 3 of the ground electronic state. Their results are shown in Figs. 39 and 40 and the angular distributions for electrons having excited the  $v=1$  state are shown in Fig. 41. From these observations, Comer and Read deduce that the symmetry of the 11.48-eV resonance is  $^2\Sigma_g^+$  and that the most likely parent is the  $E^3\Sigma_g^+$  state. Actually, Fig. 40 shows that a progression is involved here, of which the 11.48-eV state is the first member. The other members of this band, which we choose to call band "b" are listed in Appendix IV in comparison with other experiments. Table V lists the parameters of the  $^2\Sigma_g^+$  state. It should be noted that the 11.48-eV  $^2\Sigma_g^+$  resonance has also been observed as a sharp peak in the optical excitation function ( $\lambda=3371 \text{ \AA}$ ) of the  $C^3\Pi_u$  state (Kisker, 1972).

The results of the recent transmission experiment of Sanche and Schulz (1972) are shown in Figs. 42 and 43. The features are numbered and the more obvious progressions are given letter names. The energy values are tabulated in Appendix IV, in comparison with other experiments.

The total production of metastable states has been measured by Lawton and Pichanick (1972) and their results are shown in Fig. 44(A). The differential inelastic cross sections to the  $E^3\Sigma_g^+$  ( $v=0$  and  $v=1$ ),  $a'^1\Sigma_g^+$  ( $v=0$ ), and other electronically excited states, have been studied by Mazeau *et al.* (1972b). Samples of their results on the energy dependence and the angular distribution of scattered electrons are shown in Figs. 44(B)–(E). Figure 44(F) is a schematic energy level diagram of the  $N_2$  and  $N_2^-$  systems and the decay scheme for various resonances. We have indicated in separate columns shape resonances and Feshbach resonances.

Below we discuss the properties of individual bands, as deduced from the various experiments. In Appendixes IV and V we list the energies of the resonances.

#### 1. Band "b", $^2\Sigma_g^+$

Three members of band "b" are listed in Appendix IV. The  $^2\Sigma_g^+$  resonance at 11.48 eV consists of two

electrons of the Rydberg orbital symmetry  $3s\sigma_g$  temporarily bound in the field of the grandparent  $X^2\Sigma_g^+$  core of  $N_2^+$ . This is evidenced by the fact that both the spacing between the vibrational levels of band "b" and the amplitudes of the structures are close in magnitude to the corresponding values for excitation of the ground state  $X^2\Sigma_g^+$  of  $N_2^+$ . The spacing between the structures of band "b" is 270 meV and the ratio of magnitudes of the two peaks is  $10 \pm 0.5$ . These experimental results agree well with the values for the  $X^2\Sigma_g^+$  state of  $N_2^+$ , which has a spacing of 271 meV between the  $v=0$  and  $v=1$  states and which has a ratio of 9.96 for the Franck-Condon probabilities for exciting these vibronic states.

Table VI shows these comparisons: The binding between the lowest member of band "b" and the grandparent  $X^2\Sigma_g^+$  state of  $N_2^+$  is 4.1 eV. This value represents the binding of the two  $3s\sigma_g$  electrons to the positive ion core. It is noteworthy that the value of about 4.1 eV does not change as different grandparents are considered, and in fact the value remains constant even for other molecules (see Table X). But the value is applicable only to the lowest band. The same grandparent can give rise to other bands, lying higher in energy.

Only the zeroth level of the  $X^2\Sigma_g^+$  grandparent state is strongly excited in molecular transitions from the ground state of  $N_2$  and we would expect that a similar situation prevails for the resonances associated with the  $X^2\Sigma_g^+$  grandparent state. Thus we would not expect to observe a long progression of vibronic states of the  $^2\Sigma_g^+$  resonance.

## 2. Shape Resonances and Inelastic Thresholds

Structures 3 and (4-4') of Fig. 42 (at 11.92 and 12.2 eV) have been identified as  $p$ -wave shape resonances associated with the  $E^3\Sigma_g^+$  Rydberg state of  $N_2$  (Sanche and Schulz, 1972). The first of these lies near the threshold for the  $E^3\Sigma_g^+$  state (11.87 eV), so that one would expect a dramatic influence of the 11.92-eV  $p$ -wave shape resonance on the threshold behavior of the  $E^3\Sigma_g^+$  state. That the  $E^3\Sigma_g^+$  state and also the  $a''^1\Sigma_g^+$  state at 12.26 eV show a very sharp rise near threshold has been observed by many investigators (Heideman *et al.*, 1966a; Ehrhardt and Willmann, 1967; Swanson *et al.*, 1971; Mazeau *et al.*, 1972b; Lawton and Pichanick, 1973).

Figures 44(A) and 44(B) clearly show that the cross section as well as the differential cross section to the  $E^3\Sigma_g^+$  state rise very steeply near threshold. *A priori*, a sharp rise near threshold can arise from three causes:

- (i) The existence of a shape resonance just above the threshold. The angular distribution in this case would exhibit a  $p$ -type (e.g.,  $p\sigma$ ) behavior.
- (ii) The existence of a Feshbach-type resonance

below the threshold can influence the inelastic cross section above threshold (Ehrhardt and Weingartshofer, 1969; Taylor, 1970). In the case of  $N_2$ , we would be dealing with the "wings" of the  $^2\Sigma_g^+$  resonance which lies 390 meV below the  $E$  state. Herzenberg and D. Ton-That point out that the opening of a new channel of decay (as is the case when the electron energy passes through the energy of an excited state) leads to an abrupt increase in the total width  $\Gamma$ . This effect is especially pronounced when the electronic state is the "parent" of the resonance, since the decay width into the parent is generally large. Herzenberg and D. Ton-That have worked out these considerations for the case of the  $^2S$  resonance in helium decaying into the  $2^3S$  state, showing that a sharp peak in the excitation cross section of the  $2^3S$  state near threshold results. It is expected that the model will be valid in other cases as well. It leads to an  $s$ -wave behavior in the angular distribution of inelastically scattered electrons.

(iii) The existence of a "virtual" state, similar to one existing near the  $2^1S$  threshold in helium (see preceding paper).

In order to distinguish between the three possibilities outlined above, Mazeau *et al.* (1972b) studied the angular distribution of the electrons having excited the  $E^3\Sigma_g^+$  ( $v=0$ ) state. Figure 44C shows that the angular distribution near the threshold of the  $E$  state approximates the shape expected for a  $p\sigma$ -wave. This experiment demonstrates that the threshold behavior of the  $E^3\Sigma_g^+$  state is dominated by the  $p$ -wave resonance near 11.9 eV, and also confirms the assignment given to this resonance by Sanche and Schulz (1972).

The resonance (4-4') of Fig. 42, which lies between 12.1-12.2 eV, is also believed to be a shape resonance (Mazeau *et al.*, 1972b; Sanche and Schulz, 1972), probably of  $^2\Pi$  symmetry. The angular distribution of the scattered electrons having excited the  $E^3\Sigma_g^+$  ( $v=0$ ) state near 12.1 eV exhibits, approximately, the shape characteristic of a  $p\pi$ -wave (Mazeau *et al.*, 1972b).

The sharp onset of the excitation function is characteristic of the  $E^3\Sigma_g^+$  and the  $a''^1\Sigma_g^+$  states at 11.87 and 12.26 eV, respectively. Other inelastic cross sections, examined by Swanson *et al.* (1971), ( $A^3\Sigma_u^+$ ,  $B^3\Pi_g$ ,  $B'^3\Sigma_u^-$ ,  $a'^1\Sigma_u^-$ ,  $a^1\Pi_g$ ,  $C^3\Pi_u$ ,  $E^3\Pi_g$ ,  $a''^1\Sigma_g^+$ ) do not exhibit a sharp rise near threshold.

## 3. Structures 5 and 6

The energy of the lowest Feshbach resonance composed of two Rydberg electrons trapped in the field of the  $A^2\Pi_u$  core of  $N_2^+$  can be estimated by adding to the energy of the  $^2\Sigma_g^+$  resonance (11.48 eV) the difference between the ionization potential for the  $X^2\Sigma_g^+$  and the  $A^2\Pi_u$  states of  $N_2^+$ . Such an estimate gives 12.62 eV for the energy of that  $^2\Pi_u$  resonant state which would consist of two  $3s\sigma_g$  electrons bound to the  $A^2\Pi_u$  core. Resonances 5 and 6 of Fig. 42 (at 12.64 and 12.87 eV) probably belong to that state. In fact,

resonance 5 lies at 12.64 eV, only 20 meV above the estimated position (Sanche and Schulz, 1972). The parent of these structures can be the  $F^3\Pi_u$  state lying at 12.75 eV. This state has a  $^3\Pi_u$  core with an extra  $3s\sigma_g$  electron attached. Mazeau *et al.* (1972b) suggest that the  $G(^3\Pi_u)$  state at 12.8 eV could be admixed.

Structures 5 and 6 are also replicated in the differential cross section of the  $E^3\Sigma_g^+$  ( $v=0$ ) state and these structures appear at 12.54 and 12.78 eV, respectively, as shown in Fig. 44(B) and in Appendix IV. Structures 5 and 6 are not visible in the  $E^3\Sigma_g^+$  ( $v=1$ ) decay channel.

#### 4. Bands "c" and "d"

Two short bands ("c" and "d") in the 13–15 eV energy range are shown in Fig. 42. They start at 13.00 and  $13.88 \pm 0.05$ , respectively. Here the overlap between the different resonances makes an accurate reading of the spacing between the vibrational members of each band difficult. Nevertheless, the average spacing of  $230 \pm 5$  meV for band "c" and  $225 \pm 5$  meV for band "d" lies close to the value of 228 meV for the corresponding average spacings of the vibrational levels of the  $A^3\Pi_u$  state of  $N_2^+$  which is the suggested grandparent for the two bands. Mazeau *et al.* (1972b) suggest that the parent of band "c" is the state  $H$  which they have recently discovered. The state  $H$  is a triplet, and its  $v=0$  level lies at  $13.15 \pm 0.01$  eV. The spacing of the two lowest vibrational levels is 240 meV.

The band "c" has been observed in the decay channels  $E^3\Sigma_g^+$  ( $v=0, v=1$ ),  $a'^1\Sigma_g^+$  ( $v=0$ ), and also  $C^3\Pi_u$  by Mazeau *et al.* (1972b). The energies of bands "c" and "d" are listed in Appendix IV.

#### C. Bands "a" and "a'": Core-Excited Shape Resonances

At lower energies (7–11 eV) other structures are visible in the total scattering cross section of  $N_2$ . These structures are clearly seen in derivative transmission spectra for  $N_2$  shown in Fig. 43. The progression of dips between 7 and 9 eV in the transmission spectrum is interpreted predominantly as the excitation of vibrational levels of the  $B^3\Pi_g$  valence state of  $N_2$  and indicates that the cross section for excitation of the  $B$  state rises sharply at threshold. This finding confirms similar conclusions derived from studies using the trapped-electron method (Brongersma and Oosterhoff, 1969, 1967; Hall *et al.*, 1970).

The next structures (band "a" in Fig. 43) form a very well-developed progression of 18 vibrational levels which extends from 9 to 11 eV. The energy of each structure and the corresponding spacings are given in Appendix V. When one attempts to correlate the energies of this progression with vibrational energy levels of the known states in this energy region, namely the  $B^3\Sigma_u^+$ ,  $a'^1\Sigma_u^+$ ,  $a^1\Pi_g$ , and  $W^1\Delta_u$  valence excited states, it is found that none of these states nor any

combination of them could reproduce the spacing of band "a" (Sanche and Schulz, 1972).

Structures at the same energies as band "a" have also been observed, superimposed on a continuum, in the excitation function to various vibrational states ( $v=1-5$ ) of the  $B^3\Pi_g$  valence state of nitrogen. This is shown in Fig. 44D.

We are dealing here with a vibrational progression of core-excited shape resonances, similar to those existing near 2.3 eV in  $N_2$ , i.e., the  $^2\Pi_g$  state of  $N_2^-$ . Many of the features of band "a", when observed in the decay into the  $B^3\Pi_g$  parent state are reminiscent of the features already discussed in connection with the 2.3-eV shape resonance in  $N_2$ . The position on the energy scale of the peaks observed in different vibrational decay channels of the  $B^3\Pi_g$  state shift. This can be clearly seen in Fig. 44D and in Appendix V, where the energy values are tabulated. The shifting of the peaks is reminiscent of a similar effect already discussed in connection with the 2.3-eV shape resonance in nitrogen (see Figs. 31 and 33), and the Boomerang model (Fig. 34) developed by Herzberg (1968) and by Birtwistle and Herzberg (1971). A band similar to band "a" is also associated with the  $A^3\Sigma_u^+$  state, as evidenced by the structure in the cross section to various vibrational states of the  $A^3\Sigma_u^+$  final state, in the energy range 8.22–9.57 eV (Fig. 44E). As in the case of band "a", the locations of the peaks shift on the energy scale. The parent of this band is the  $A^3\Sigma_u^+$  state. Appendix V gives the energies of the structures, as observed in the  $v=2-6$  states of the  $A^3\Sigma_u^+$  electronic state.

The energy level diagram, Fig. 44F, indicates schematically some of the decay channels. The core-excited shape resonance associated with the  $A^3\Sigma_u^+$  state is marked "a'".

#### D. Resonances above the Ionization Potential in $N_2$

Pavlovic *et al.* (1972) have observed vibrational excitation for the levels  $v=1, 2, 3$  in  $N_2$  in the energy range 20–24 eV. They also observed the angular distribution of electrons having excited these states and found that the angular distribution depends strongly on the incident energy, and in fact the shape of the energy dependence depends on the angle of observation. These anomalies in the angular distribution, coupled with the large size of the observed cross section, led Pavlovic *et al.* to prefer an interpretation in terms of resonances associated with doubly excited states of the nitrogen molecule rather than singly excited Rydberg states. Further experimental work will, however, be needed before this model is reliably proved.

Resonances associated with doubly excited states of atoms (e.g.,  $2s^22p$  in the case of He) are well known. In the case of small systems such as helium, one expects these resonances to be spaced well apart compared to their width, whereas in systems with more electrons (e.g.,  $N_2$ ) there is the possibility of many doubly ex-

cited states which are closely spaced ( $\sim 0.25$  eV), each of which may have an associated compound state. Thus it may not be possible to resolve individual states, especially since the states themselves may be relatively broad.

The resonances discussed above would have two holes in the normally filled shells of  $N_2$ ,  $(KK)(\sigma_g 2s)^2(\sigma_u 2s)^2(\sigma_g 2p)^2(\pi_u 2p)^4$  and would have three electrons in the vacant orbitals,  $(\pi_g 2p)$  and  $(\sigma_u 2p)$ . Pavlovic *et al.* (1972) calculate that, in the 22-eV region, the spacing of such resonances is less than 0.25 eV.

We note that the resonances discussed in the previous section (core-excited shape resonances,  $a$  and  $a'$ , connected with the  $A^3\Sigma_u^+$  and  $B^3\Pi_g$  states, respectively) have one hole in the normally filled shell and two electrons in the vacant orbitals, whereas the resonances near 2.3 eV (connected with the ground  $X^1\Sigma_g^+$  state of  $N_2$ ) have zero holes and one electron in the vacant orbitals. Thus the shape resonances invoked by Pavlovic *et al.* follow logically from the two types already discussed.

Figures 45 and 46 show the energy dependence and the angular dependences observed by Pavlovic *et al.* (1972) for the excitation of  $v=2$ . The energy dependence of the cross section for exciting  $v=1$  and  $v=3$  is very similar to that shown.

A measurement and an analysis of the angular distribution of electrons having excited the  $v=1$  vibrational state of  $N_2$  (and also CO) has been performed by Truhlar *et al.* (1972) with the aim of testing whether a simple nonresonant mechanism can explain the vibrational excitation near 20 eV. Such a model appears to be applicable in the 20-eV energy range in the case of  $H_2$  (Trajmar *et al.*, 1970). Truhlar *et al.* find that a resonance model must be involved in the case of  $N_2$  and CO in order to interpret the experimental results on vibrational excitation near 20 eV. It should be noted that the *experimental* results of Truhlar *et al.* (1972) are in good agreement with those of Pavlovic *et al.* (1972).

#### IV. CARBON MONOXIDE

The electron configurations and the resulting levels of compound states of diatomic molecules are determined essentially by the number of electrons. Therefore  $N_2$  and CO, being isoelectronic molecules, should exhibit very similar properties. In fact this is the case. However, the positions of the compound states and their widths differ somewhat.

The CO molecule is not symmetric with respect to inversion so that the  $g-u$  symmetry is not preserved. Also, the permanent dipole of CO often cannot be ignored. The following review of the carbon monoxide molecule follows closely the discussion of  $N_2$ .

##### A. Resonance at Low Energy (1–3 eV) $^2\Pi$

The configuration of CO is identical to that already listed for  $N_2$ , except that the subscripts  $g$  and  $u$  now

lose their meanings (see Table IX). As a consequence, the  $3d\pi$  orbital contains a  $p$ -wave component (Bardsley and Mandl, 1968; O'Malley and Taylor 1968; Read, 1968). Thus the trapped electron tunnels through a  $p$ -wave barrier which is not as high as a  $d$ -wave barrier and, as a result, the width of the state is expected to be larger (the lifetime is shorter) than in  $N_2$ . These expectations agree with the experimental results.

##### 1. Elastic Cross Section via $^2\Pi$

The energy dependence of the differential elastic cross section for CO is shown in Fig. 47. Compared to  $N_2$ , the structure in the cross section is less pronounced, although the peak in the neighborhood of 2 eV is especially clear at 20 and 40 degrees. The individual resonances become more obvious when the vibrational cross sections are studied. Ehrhardt *et al.* (1968) estimate the width at 0.4 eV.

##### 2. Vibrational Excitation via $^2\Pi$

The energy dependence of the vibrational cross section, as observed at an angle of 72 degrees, is shown in Fig. 48. This curve, obtained by Schulz (1964) is in all respects similar to the curve obtained at 20 degrees (Ehrhardt *et al.*, 1968), indicating that the shape of the cross section does not depend on angle. The sum of all vibrational cross sections has a relatively smooth behavior, with a single peak at 1.7 eV and a magnitude

$$\sum_{v=1}^8 \sigma_v = 3.5 \times 10^{-16} \text{ cm}^2.$$

In obtaining this value, Ehrhardt *et al.* (1968) took into account the variation of the cross sections with angle. The vibrational cross sections in absolute units is shown in Fig. 49.

A notable difference exists between  $N_2$  and CO if one observes that the cross section for  $v=1$  has a long tail which extrapolates to the onset for  $v=1$  (see Phelps, 1968) whereas  $N_2$  shows a tail which is smaller by an order of magnitude. A direct dipole-type process is probably responsible for the difference. Figure 50 shows the details of the threshold region for excitation of  $v=1$  in CO, as determined by different methods of measurement.

The other notable difference between  $N_2$  and CO is the larger width of the observed structure. As already noted, this larger width is a result of the barrier being predominantly of a  $p$ -wave character in CO, with  $d$  wave mixed in. In  $N_2$ , the barrier is predominantly  $d$  wave.

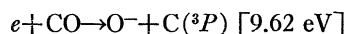
##### 3. Angular Distributions

Figure 51 shows the angular distributions obtained by Ehrhardt *et al.* (1968) for electrons which are scattered elastically and inelastically. Qualitatively, the curves for the inelastically scattered electrons show a  $p$ -type behavior of the curves, with a minimum at 90 degrees.

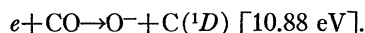
A fairly good, but not perfect, fit to the experimental curves was obtained by O'Malley and Taylor (1968) whose theory gives the angular distribution in the form  $(1+7 \cos^2\theta)$ . The deviation between this expression and the experiment is of the order of 10%. Read (1968) was able to improve the fit to the angular distribution of inelastically scattered electrons in CO, using a mixture of  $p\pi$  and  $d\pi$  waves. The mixing of the  $p\pi$  and  $d\pi$  waves is left as a parameter and the mixing parameters are adjusted until a good fit to the experimental angular distribution is obtained.

### B. Dissociative Attachment (9.65–12 eV)

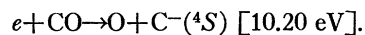
Dissociative attachment in CO leads to the formation of  $O^-$  via the reactions (Chantry, 1968)



and



A much smaller cross section ( $\sim 6 \times 10^{-23} \text{ cm}^2$ ) exists for the reaction (Stamatovic and Schulz, 1970)



Whereas the experimentally observed appearance potentials for the reaction leading to  $O^- + C$ , given in brackets above, occur at the expected position for these reactions, the formation of  $O + C^-$  is "delayed" by about 360 meV from the energetically lowest value that can give the reaction (9.84 eV). A hypothetical potential energy diagram showing some of the observed features is shown in Fig. 52.

Figure 53 shows the dissociative attachment cross section for  $O^-$  formation as measured by Stamatovic and Schulz (1970), by Chantry (1968), and by Rapp and Briglia (1965). Stamatovic and Schulz detect structure in the dissociative attachment curve near 10 eV, which can be interpreted by the presence of the  $^2\Sigma^+$  core-excited resonance (to be discussed in the following section) interacting with the potential energy curve responsible for  $O^-$  formation.

### C. Core-Excited Resonances in the 10–15 eV Region

Core-excited resonances in CO strongly resemble those of  $N_2$ . Just as in  $N_2$ , the lowest Rydberg state of CO,  $b^3\Sigma^+$ , can support a strong core-excited resonance of the Feshbach type. This resonance, discovered in a transmission experiment by Sanche and Schulz (1971a), was further studied by Comer and Read (1971c), by Swanson *et al.* (1971, 1972) and by Mazeau *et al.* (1972a). Uniform agreement exists on the location of this resonance as measured by Sanche and Schulz, i.e.,  $10.04 \pm 0.03$  eV, with a width about 45 meV. Angular distribution measurements (Mazeau *et al.*, 1972a; Pavlovic *et al.*, 1973) show that the resonance exhibits itself in the  $s$  wave and thus the symmetry is  $^2\Sigma^+$ .

Figure 54(a) shows the energy dependence of the differential cross section for the  $v=0$  and  $v=1$  exit channels of the ground electronic state at angles of 80 and 60 degrees, respectively, and Fig. 54(b) shows the elastic differential cross section at other angles of observation. The transmission experiment of Sanche and Schulz is shown in Fig. 55(A). The features are numbered and the positions of the features are listed in Appendix VI in comparison with the features observed by Comer and Read (1971c) and Mazeau *et al.* (1972a).

The principal decay channels are indicated on the energy level diagram [Fig. 55(B)], mostly based on the work of Mazeau *et al.* (1972a), Swanson *et al.* (1972), and Comer and Read (1971c). The excitation function of electronically excited states at different angles of observation is shown in Figs. 55(C) and 55(D).

The features observed in CO are discussed in greater detail below.

#### I. $^2\Sigma^+$ Resonances (10.04 eV, 10.28 eV)

Structures (1-1') to (4-4') in the derivative transmission spectrum of CO, shown in Fig. 55(A), exhibit a remarkable resemblance to the structures (1-1') to (4-4') in  $N_2$  and can be interpreted similarly. Structures 1-1' (10.04 eV) and 2-2' (10.28 eV) can be identified as two members of a vibrational sequence of Feshbach resonances whose parents are the  $b^3\Sigma^+$  and  $B^1\Sigma^+$  states of CO at 10.39 and 10.77 eV, respectively. The grandparent is the  $X^2\Sigma^+$  ground state of  $CO^+$  and the resonance itself has a symmetry  $^2\Sigma^+$ . The binding of the two  $3s\sigma_g$  electrons with respect to the grandparent state is 4.1 eV, similar to other cases studied (see summary, Table X).

The  $^2\Sigma^+$  resonance at 10.04 eV also influences dissociative attachment as has been discussed by Sanche and Schulz (1972), who reinterpreted the dissociative attachment experiments of Stamatovic and Schulz (1970) and pointed out that the structure near 10 eV in the  $O^-$  production from CO may be due to the  $^2\Sigma^+$  resonance. Also, the formation of  $C^-$  from CO can be interpreted in terms of this resonance.

Although compound state formation is expected to be similar in the isoelectronic molecules  $N_2$  and CO, the  $^2\Sigma^+$  resonance in CO has a natural width ( $\Gamma \approx 40$  meV) which is almost two orders of magnitude greater than that found for the  $^2\Sigma_g^+$  resonance at 11.48 eV in  $N_2$  ( $\Gamma \approx 0.6$  meV). The larger width in CO probably results from the partial decay of the  $^2\Sigma^+$  resonance into the  $O^-(^2P) + C(^3P)$  channel. In  $N_2$  dissociative processes are not observed and the potential energy curve corresponding to the one leading to  $O^- + C$  in CO could occur at a different energy where it would not interact with the  $^2\Sigma_g^+$  state of  $N_2^-$ . Thus the natural width of the  $^2\Sigma_g^+$  state in  $N_2$  would be small since this state decays predominantly to the ground state of the molecule.

The decay of the  $^2\Sigma^+$  resonance has been studied by

Mazeau *et al.* (1972a) and by Swanson *et al.* (1972). They find that the  ${}^2\Sigma^+$ ,  $v=0$  resonance at 10.04 shows a preference for decay into high vibrational levels of valence-excited electronic states: the  $v=3$  state of  $a\ {}^3\Pi$ , the  $v=4$  state of  $A\ {}^1\Pi$ , and the  $v=25$  or 26 state of  $a'\ {}^3\Sigma^+$ . Schematically, these observations are shown on the energy level diagram, Fig. 55(B). One can understand the experimentally determined decay scheme by considering the equilibrium internuclear separation of the various states (Mazeau *et al.*, 1972; Swanson *et al.*, 1972). The  ${}^2\Sigma^+$  compound state, being a Rydberg state, should have an equilibrium internuclear separation close to that of the positive ion  $X\ {}^2\Sigma^+$  ( $r_e=1.11\ \text{\AA}$ ) or the two parents  $b\ {}^3\Sigma^+$  ( $r_e=1.11\ \text{\AA}$ ) or  $B\ {}^1\Sigma^+$  ( $r_e=1.12\ \text{\AA}$ ); this places  $r_e$  for the compound state near 1.11  $\text{\AA}$ . The decay takes place to electronic states with a larger equilibrium internuclear separation ( $X\ {}^1\Sigma^+$ :  $r=1.13\ \text{\AA}$ ;  $a\ {}^3\Pi$ : 1.20  $\text{\AA}$ ;  $A\ {}^1\Pi$ : 1.23  $\text{\AA}$ ;  $a'\ {}^3\Sigma^+$ : 1.35  $\text{\AA}$ ). Thus, high vibrational quantum numbers will be preferred in the decay, especially when the final state has an  $r_e$  very large, as is the case for the  $a'\ {}^3\Sigma^+$  state.

### 2. Shape Resonances and Inelastic Thresholds

Structures 3 and (4-4') of Fig. 55(A) at 10.42 and 10.7 eV, respectively, are probably shape resonances, by analogy with similar structures observed in nitrogen. Angular distribution measurements in the  $b\ {}^3\Sigma^+$  decay channel indicate that the 10.7-eV resonance has a  $a\ {}^2\Pi$  symmetry. Figure 55(C) shows this measurement of the angular distribution, and also the differential excitation cross section to the  $b\ {}^3\Sigma^+$  state at 10.39 eV.

The excitation cross section to the  $b\ {}^3\Sigma^+$  state shown in Fig. 55(C) exhibits a sharp rise near threshold and a number of structures above threshold. At first sight, this excitation function appears similar to the excitation cross section to the  $E\ {}^3\Sigma_g^+$  state in  $N_2$  [Fig. 44(B)]. However, there is a notable difference: Whereas the angular distribution near the threshold of the  $E\ {}^3\Sigma_g^+$  state in  $N_2$  exhibited a  $p$ -wave dependence [see Fig. 44(C)] characteristic of the decay of a  $p$ -type shape resonance, in the case of the  $b\ {}^3\Sigma^+$  state in CO, we see from Fig. 55(C) that the angular distribution is isotropic. Thus, an  $s$  wave is indicated.

We have already pointed out in Sec. IIIB2 that the decay of the wings of the  ${}^2\Sigma^+$  resonance, lying 350 meV below the threshold of the  $b\ {}^3\Sigma^+$  state, can cause a sharp structure in the threshold behavior. This appears to be the case. The large width of  ${}^2\Sigma^+$  resonance in CO, about 45 meV (vs only 0.6 meV for the  ${}^2\Sigma_g^+$  resonance in  $N_2$  at 11.48 eV) would provide a favorable circumstance for the observation of the decay of the  ${}^2\Sigma^+$  resonance into an inelastic channel.

### 3. Band "a"

At higher energies in CO, the transmission experiment (Fig. 55) shows many overlapping resonances and

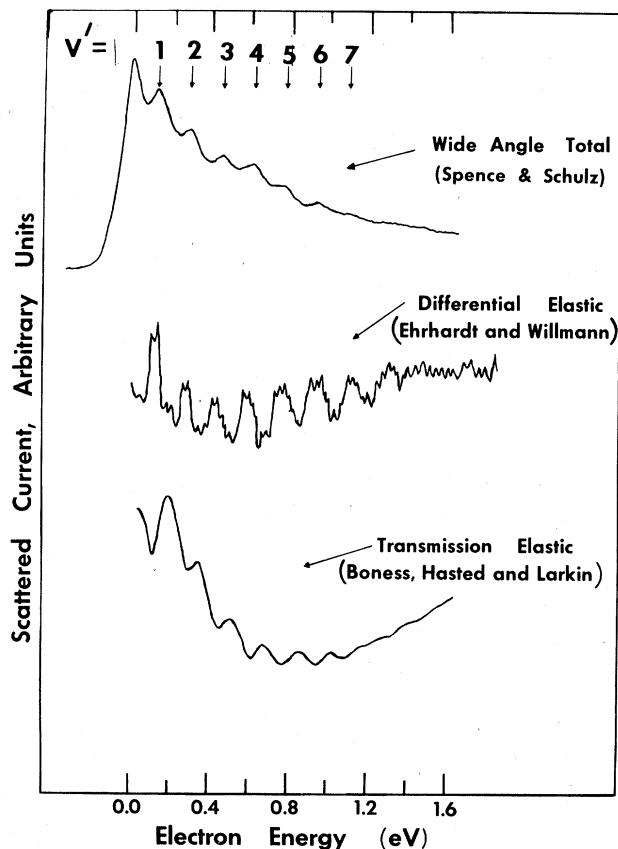


FIG. 56. Comparison of experiments on the structure in the low-energy cross section of NO. The top curve represents a recorder tracing of electrons scattered over a wide acceptance angle (mostly elastic) (Spence and Schulz, 1971b). The middle curve is the differential elastic cross section (Ehrhardt and Willmann, 1967). The bottom curve, which has been shifted by about 0.4 eV to overlap the present results, represents the transmission experiment of Boness, Hasted, and Larkin (1968). The structure is interpreted as the resonant contribution to the elastic cross section and the spacing of the structure is interpreted as the spacing of the  $NO^- \ {}^3\Sigma^-$  system. [From Spence and Schulz (1971b).]

identification of particular bands is not possible. However, one can identify six vibrational levels belonging to a common progression (band "a") near the end of the spectrum shown in Fig. 55. This progression starts at  $13.95 \pm 0.05$  eV with a spacing of 205, 190, 185, 175, and  $165 \pm 5$  meV, respectively. The probable grandparent is the  $A\ {}^2\Pi$  state of  $CO^+$ .

### D. Resonances above the Ionization Potential in CO

It was pointed out in Sec. IIID that there exist resonances above the ionization potential of nitrogen, in the range 20–24 eV. A similar process exists in carbon monoxide. Chutjian *et al.* (1972) and Truhlar *et al.* (1972) have measured the cross section for excitation of the  $v=1$  vibrational state in CO [see Fig. 55(E)] and find a broad peak around 20-eV energy. They find that theories relying on potential scattering alone are

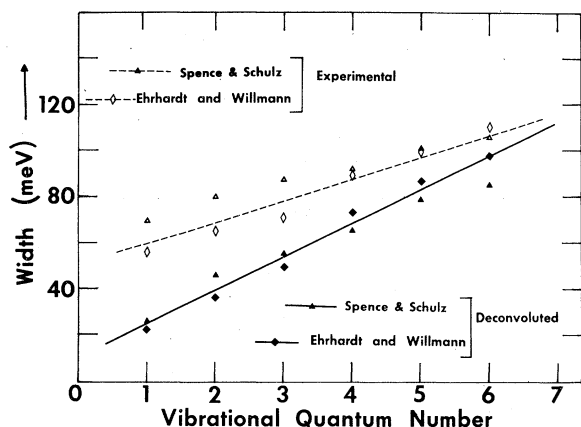


FIG. 57. Width of resonances in the elastic cross section of NO. Open symbols represent the experimental observations and the dashed line is drawn through these points. Filled-in symbols with the solid line drawn through them represent the "real" width of the resonances, obtained by deconvolution. In the deconvolution both the electron-energy distribution and the resonances are assumed to be Gaussian. The data shown are those of Spence and Schulz (1971) and of Ehrhardt and Willmann (1967). The width is defined as the full width at half-maximum. [From Spence and Schulz (1971b).]

not adequate to explain this peak and conclude that a resonance or a series of resonances must be involved to explain the cross sections near 20 eV.

## V. NITRIC OXIDE, NO

### A. Compound State at Low Energy (0–1.5 eV) $X^3\Sigma^-$

Nitric oxide, like  $O_2$ , forms a stable parent negative ion and thus NO has a positive electron affinity. The lowest negative ion state is the  $X^3\Sigma^-$  state whose zeroth vibrational level is stable with respect to autodetachment; however, the higher vibrational states autodetach since they lie energetically above the  $v=0$  state of NO ( $X^2\Pi_r$ ). For an understanding of electron

scattering, one wishes to know the electron affinity, the vibrational spacings of  $NO^-$ , the anharmonicity, and the equilibrium internuclear separation. Information regarding these parameters comes from various types of experiments, discussed below, which shed light on the nature of the shape resonance in NO.

#### 1. Elastic Scattering

The values of the vibrational spacings of the low-lying shape resonance are deduced (for both  $O_2$  and NO) primarily from electron scattering experiments: The energy dependence of the elastic cross section exhibits structure at the positions of the vibrational levels. The vibrational cross section to various states of NO also exhibits relatively sharp peaks at the positions of the vibrational states of  $NO^-$ .

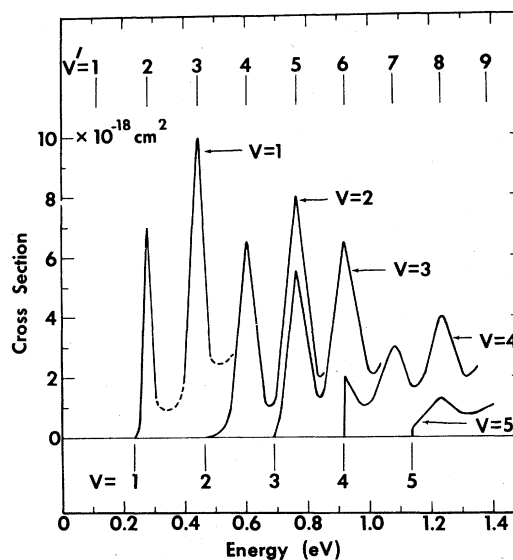


FIG. 58. Approximate cross sections for vibrational excitation of NO by electron impact. The vibrational spacing of the neutral molecule is indicated below the curves, and the vibrational spacing of  $NO^-$  above the curve. [From Spence and Schulz (1971b).]

TABLE VII. Parameters of  $NO^-(X^3\Sigma^-)$ .

	Electron scattering:	
	(Spence and Schulz)	Photodetachment: (Siegel <i>et al.</i> )
Equilibrium separation, $r_e$	1.286 Å <sup>a</sup>	1.258±0.010 Å <sup>b</sup>
Electron affinity, EA (NO)	50 meV	24(+10, -5) meV <sup>b</sup>
$\omega_e$	170±20 meV	182±25 meV
$\omega_e x_e$	1.0±0.25 meV	...

<sup>a</sup> Values obtained using Badger's rule.

<sup>b</sup> Preferred values.

Figure 56 shows the structure in the elastic cross section as observed by Spence and Schulz (1971b), by Ehrhardt and Willman (1967), and by Boness, Hasted, and Larkin (1968). The spacing of the peaks is about 160 meV and the agreement between various experiments appears good. Interestingly, the width of the observed peaks increases as the quantum number increases, from 70 meV for the first peak to 100 meV for the fifth. This effect can be clearly seen from Fig. 57. A similar broadening may also occur in  $O_2$ , but has not been observed experimentally because the width of the peaks in  $O_2$  is much narrower than in NO, and thus the experimentally observed width of the peaks in  $O_2$  are almost entirely caused by the instrumental resolution. Any changes in the natural width are hidden, in the case of  $O_2$ , by the instrumental resolution.

## 2. Vibrational Excitation (0–1.4 eV)

The vibrational cross section, as measured by Spence and Schulz (1971) using the trapped-electron method, exhibits (similar to the case of  $O_2$ ) a series of spikes superimposed on a slowly rising background (“direct”) cross section. The results are shown in Fig. 58. Here, the vibrational levels of the compound state (as determined by the elastic scattering experiments of Fig. 56) are shown by the vertical lines. The agreement between the location of the “spikes” in the vibrational cross section and the location of the compound states from elastic scattering is very good and justifies the model used.

One important result obtained by Spence and Schulz involves the observation that the  $v=4$  state of NO is accidentally coincident in energy (within  $\pm 10$  meV) with the  $v'=6$  state of  $NO^-$ . The trapped-electron method has a high sensitivity for detection of such coincidences. This comes about by plotting the positions of the peaks in the trapped-electron current as a function of well depth. If an excitation function contains a dominant spike (resulting from a resonance), then the peak of the trapped-electron current occurs at the energy of the spike and a plot of the position vs well depth is a horizontal straight line. Otherwise, such a plot is a straight line with slope of unity.

Spence and Schulz (1971b) observe that the branching ratio, i.e., the ratio of cross sections for various final states of NO via a given state of  $NO^-$ , is

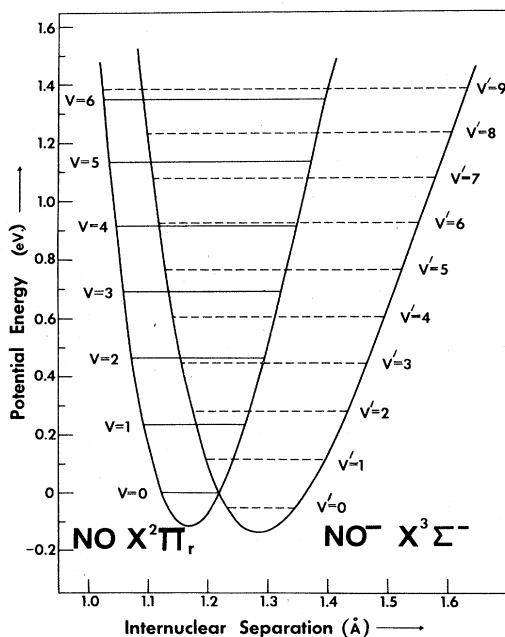


FIG. 59. Potential-energy curves for  $NO(X^2\Pi_r)$  and  $NO^-(X^3\Sigma^-)$ . The width of the levels of  $NO^-$  have been omitted. In order to bring the  $NO^-$  curve into agreement with the results of photodetachment experiments, one should shift the minimum of the  $NO^-$  curve to 1.258 Å and the spacings of the vibrational levels should be decreased. [From Spence and Schulz (1971b).]

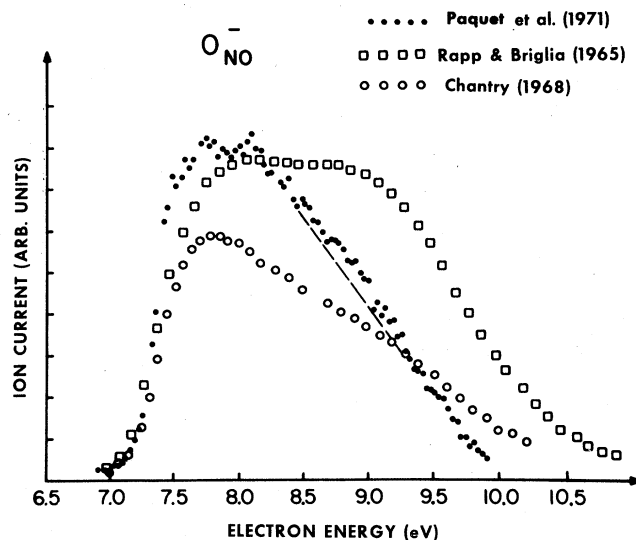


FIG. 60. Negative ion formation by dissociative attachment in NO. Shown are the results of Paquet, Marchant, and Marmet (1971), of Chantry (1968), and of Rapp and Briglia (1968). Dissociative attachment in NO leads exclusively to electronically excited N. [From Paquet, Marchand, and Marmet (1971).]

close to unity, in sharp contrast to the case of  $O_2$ . They deduce that the barrier height involved in the case of NO is lower than that in  $O_2$  and that probably a  $p$  wave dominates the electron escape. The resulting lower barrier leads to a short lifetime of  $NO^-$  ( $\sim 10^{-14}$  sec) compared to the lifetime of  $O_2^-$  ( $\sim 10^{-10}$  sec). The assumption of a  $p$ -wave barrier is consistent with the theoretical considerations of Bardsley and Read (1968) who point out that the partial waves which are being mixed are the  $p\pi$  and  $d\pi$  waves (see Sec. VII). Bardsley and Read also point out that in resonance formation and decay at low energies, a  $p$ -wave component is much more efficient than a  $d$ -wave component. The centrifugal barrier through which the incoming or outgoing electron must tunnel is much higher for  $d$  waves than for  $p$  waves. Although  $d$  waves may be more important than  $p$  waves in the interior of the molecule, this is not necessarily true near the surface.

Spence and Schulz (1971b) deduce the values of  $\omega_e$  from the spacing of the peaks in the elastic and the vibrational cross sections, and they calculate the equilibrium internuclear separation for  $NO^-$  using Badger's rule (Badger, 1935). Table VII shows a comparison of the values thus calculated with the values from photodetachment experiments. The schematic potential energy curve deduced by Spence and Schulz is shown in Fig. 59. In order to bring the  $NO^-$  curve into agreement with the results of photodetachment experiments, one should decrease  $r_e$  to 1.258 Å and should decrease the spacing of the  $NO^-$  levels somewhat so that the coincidence of the level  $v'=6$  of  $NO^-$  with  $v=4$  of NO can be maintained and so that the  $v'=0$  level comes to  $-0.024$  eV.

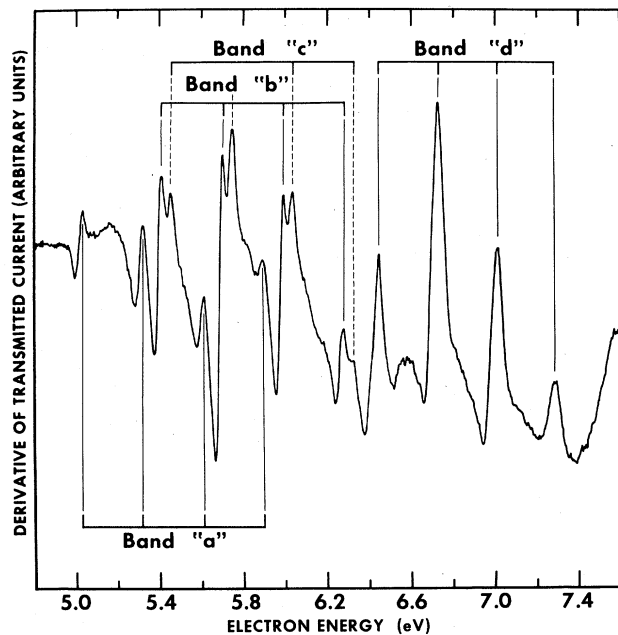


FIG. 61. Derivative of transmitted current vs electron energy in the 5–7.5 eV region in NO. Four bands belonging to a Rydberg series of  $\text{NO}^-$  states are shown; each band consists of a vibrational progression. The spacing of each vibrational progression agrees with the vibrational spacing of the  $X^2\Sigma^+$  ground state of  $\text{NO}^+$ , which is the grandparent. [From Sanche and Schulz (1972).]

### 3. Equilibrium Internuclear Separation and Electron Affinity: Photodetachment Spectroscopy

Values of the electron affinity of NO (and also of  $\text{O}_2$ ) have been in a state of violent fluctuation until very recently. But as a result of the recent photodetachment experiments of Siegel *et al.* (1972), a reliable value is now available:

$$EA(\text{NO}) = 24(+10, -5) \text{ meV.}$$

In the experiments of Siegel *et al.*, an argon-ion laser photodetaches electrons which are energy-analyzed. A Franck-Condon factor analysis of the observed cross sections determines the molecular constants for  $\text{NO}^-$ :  $\omega_e = 1470 \pm 200 \text{ cm}^{-1}$ ;  $r_e = 1.258 \pm 0.010 \text{ \AA}$ ; and  $B_e = 1.427 \pm 0.02 \text{ cm}^{-1}$ , and also the electron affinity quoted above (24 meV). The very recent value of McFarland *et al.* (1972) is  $28 \pm 14 \text{ meV}$ , in good agreement with Siegel. Older values of the electron affinity of NO are listed by Siegel *et al.* (1972) but they all seem less reliable: The other values are  $900 \pm 100 \text{ meV}$  (Farragher *et al.*, 1964),  $650 \text{ meV}$  (Stockdale *et al.*, 1969),  $90 \pm 100 \text{ meV}$  (Berkowitz *et al.*, 1971),  $0$  (Lacman and Herschbach, 1970), and  $50 \text{ meV}$  (Spence and Schulz, 1971b).

### B. Dissociative Attachment (7–10 eV)

Dissociative attachment in NO, leading to the formation of  $\text{O}^-$ , indicates the existence of a repulsive potential energy curve in the region 7–10 eV, as shown by the

negative ion production of Fig. 60. The structure observed by Paquet *et al.* (1971) may well be due to the traversal of the repulsive curve responsible for  $\text{O}^-$  production through the potential energy curves responsible for the core-excited resonances. Noteworthy is the conclusion of Chantry (1968), who determined from kinetic energy measurements of the  $\text{O}^-$  ion, that the dissociative attachment process leads exclusively to the formation of electronically excited N, i.e.,  $e + \text{NO} \rightarrow \text{O}^- + \text{N}(^2D)$ .

### C. Core-Excited Resonances in NO

Fewer experiments on core-excited resonances are available in NO than in the molecules previously discussed. Differential measurements have not yet become available. Nevertheless it was the NO molecule which revealed the interpretation of core-excited resonances in terms of Rydberg compound states (Sanche and Schulz, 1971). Figures 61 and 62 show a plot of the derivative of the transmitted current vs electron energy in the energy range 5–18 eV. The features on Fig. 61 are given letter designations and are discussed below.

#### 1. Bands "a" to "d"

The location of four bands of resonances, "a", "b", "c", and "d", is indicated in Fig. 61 by vertical lines

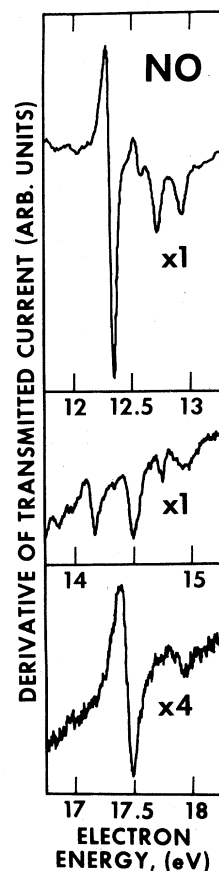


FIG. 62. Electron transmission spectra for NO in the 12–13 eV, 14–15 eV, and 17–18 eV regions. Each segment shows resonances associated with the  $b^3\Pi$ ,  $A^4\Pi$ , and  $B^4\Pi$  excited states of  $\text{NO}^+$  which are the respective grandparents. The binding of the first compound state in each segment relative to the corresponding grandparent state is nearly constant. [From Sanche and Schulz (1972).]

pointing to each vibrational member of a given band. The first 3 bands have four vibrational members and the bands start at 5.04, 5.41, and 5.46 eV, respectively. Band "d" starts at 6.45 eV and six vibronic states belonging to that band have been observed; four of these are shown in Fig. 61. The vibrational spacings of each band and the Franck-Condon probabilities for bands "a", "b", and "d" are compared with the corresponding values for the  $X^1\Sigma^+$  ground state of  $\text{NO}^+$  in Appendix VII. Bands "a", "b", and "c" have about the same spacing, which agrees well with the spacing of the grandparent  $\text{NO}^+$  core. Band "d" deviates slightly from the grandparent spacing. Franck-Condon probabilities for bands "a", "b", and "d" agree qualitatively with those of the  $\text{NO}^+$  ion core, even though bands "a", "b", and "c" overlap. All Franck-Condon probabilities listed are normalized to  $v=1$  for comparison purposes.

The comparisons suggest that all four bands in NO are composed of two Rydberg electrons temporarily bound to the same  $X^1\Sigma^+$  core of  $\text{NO}^+$ . The parent of band "a" is probably the  $A^2\Sigma^+$  Rydberg state of NO which lies at 5.48 eV. The A state, whose electron affinity from the above argument is 0.45 eV, corresponds to an electron in a Rydberg orbital of the symmetry  $3s\sigma$  bound to the  $X^1\Sigma^+$  core of  $\text{NO}^+$ . The addition of another  $3s\sigma$  electron to the core gives the  $^1\Sigma^+$  symmetry for band "a".

Bands "b" and "c" which lie 0.07 and 0.02 eV below the  $A^2\Sigma^+$  state of NO, respectively, could result from the addition of a  $3p\sigma$  or  $3p\pi$  electron to the A state. Alternatively, the parents of bands "b" and "c" could be the  $C^2\Pi$  and  $D^2\Sigma^+$  states of NO, which lie at 6.49 and 6.60 eV, respectively. As far as band "d" is concerned the only likely parents are the C and D states of NO.

Paquet, Marchand, and Marmet (1971) have

FIG. 63. The energy level diagram of relevant  $\text{NO}^+$  grandparent states (left side of diagram) compared with the energy level diagram of the  $\text{NO}^-$  states observed in the present experiment (right side of diagram). The two energy scales have been displaced by the binding energy of the lowest member of band "a" with respect to its grandparent  $X^1\Sigma^+$  state of  $\text{NO}^+$ . Each state of  $\text{NO}^+$ , shown on the left of the diagram, gives rise to a Rydberg series of  $\text{NO}^-$  states. [From Sanche and Schulz (1972).]

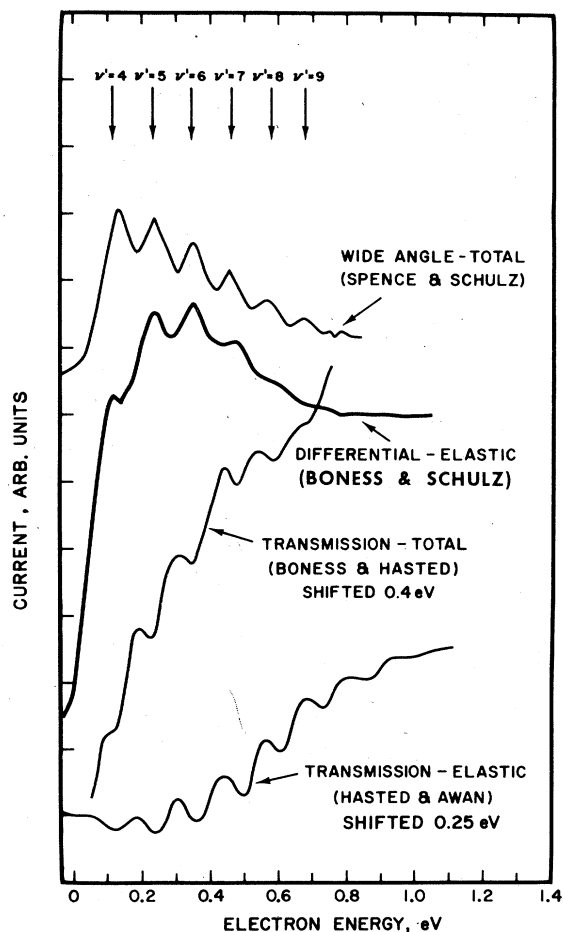
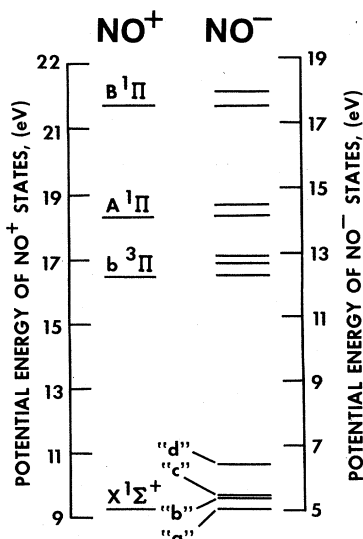


FIG. 64. Comparison of four experiments on the structure in the electron impact cross section in  $\text{O}_2$ . The top curve shows the wide-angle total cross section (Spence and Schulz, 1970), the next curve shows the differential elastic cross section (Boness and Schulz, 1970). The bottom two curves represent transmission experiments. The curve by Boness and Hasted (1966) is shifted by 0.4 eV and the curve by Hasted and Awan (1969) is shifted by 0.25 eV, both to lower energies. The agreement in the spacing of the structures is considered good. The indicated quantum numbers refer to the  $\text{O}_2^-(X^2\Pi_g)$  state. [From Boness and Schulz (1970).]

recently postulated the presence of two long-lived bound negative ion states at 7.8 and 8.2 eV, in order to explain two peaks they observe in the cross section for  $\text{O}^-$  formation from NO at these energies. The postulated states should appear in the total scattering cross section. The 5th vibrational member of band "d," which lies at 7.83 eV, could possibly account for the 7.8-eV peak in the  $\text{O}^-$  data at Paquet *et al.*

## 2. Region 12 eV-18 eV

The resonances shown in Fig. 62 for the energy range 12-18 eV seem to have as their grandparents excited states of  $\text{NO}^+$ . At least ten bound excited states of  $\text{NO}^+$  are known at the present time and four of these, namely the  $b^3\Pi$ ,  $A^1\Pi$ ,  $c^3\Pi$ , and  $B^1\Pi$  ion states, can be con-

TABLE VIII. Molecular orbital configuration of the ground states and of shape resonances in diatomic molecules. The extra electron, which is responsible for the shape resonance, occupies the lowest vacant orbital shown in the fourth column.<sup>a</sup>

Molecule	Molecular orbitals of ground state	Ground state	Lowest vacant orbital	Compound state	Dominant partial wave
H <sub>2</sub>	(1sσ <sub>g</sub> ) <sup>2</sup>	<sup>1</sup> Σ <sub>g</sub> <sup>+</sup>	2pσ <sub>u</sub>	<sup>2</sup> Σ <sub>u</sub> <sup>+</sup>	pσ
N <sub>2</sub>	(1sσ <sub>g</sub> ) <sup>2</sup> (2pσ <sub>u</sub> ) <sup>2</sup> (2sσ <sub>g</sub> ) <sup>2</sup> (3pσ <sub>u</sub> ) <sup>2</sup> (3sσ <sub>g</sub> ) <sup>2</sup> (2pπ <sub>u</sub> ) <sup>4</sup>	<sup>1</sup> Σ <sub>g</sub> <sup>+</sup>	3dπ <sub>g</sub>	<sup>2</sup> Π <sub>g</sub>	dπ
O <sub>2</sub>	----- (3dπ <sub>g</sub> ) <sup>2</sup>	<sup>3</sup> Σ <sub>g</sub> <sup>-</sup>	3dπ <sub>g</sub>	<sup>2</sup> Π <sub>g</sub>	dπ
CO	(1sσ) <sup>2</sup> (2sσ) <sup>2</sup> (2pσ) <sup>2</sup> (2pπ) <sup>4</sup> (3sσ) <sup>2</sup> (3pσ) <sup>2</sup>	<sup>1</sup> Σ <sup>+</sup>	3pπ	<sup>2</sup> Π	dπ + pπ
NO	----- (3pπ)	<sup>2</sup> Π <sub>r</sub>	3pπ	<sup>2</sup> Σ <sup>-</sup>	dπ + pπ

<sup>a</sup> The notation used is the "united atom" notation of Herzberg (1950). See also Bardsley and Mandl (1968). The notation used in the column entitled "dominant partial wave" is dπ, pπ, and pσ. The first, Latin letter, refers to the angular momentum of the electron partial wave at infinity, i.e., *l* = 2, and 1, respectively. The Greek letter refers to the component of this angular momentum along the internuclear axis of the molecule as the electron comes close to the molecule.

sidered as possible candidates for compound state formation from the ground state since their internuclear distances lie close to the internuclear distance of the NO ground state. These states are listed in Appendix VIII where their energies are given. Also shown in Appendix VIII are the position of the resonances in the energy range 12–18 eV. In the last column of Appendix VIII we calculate the "binding" energy by taking the difference between the energies of the assumed grandparent and the lowest value of the resonance. The constancy of the binding energy indicates that the proper grandparents have been assigned and that the potential well which binds the two 3sσ electrons does not change. The binding energy of band "a" (previously discussed) with respect to the X <sup>1</sup>Σ<sup>+</sup> ground state is 4.23 eV, in very good agreement with the other values for the binding energy shown in Appendix VIII.

The various structures listed in Appendix VIII have been interpreted by Sanche and Schulz (1972) as core-excited Feshbach resonances or as core-excited shape resonances, and their parents have been suggested. For example, the 12.57-eV feature listed in Appendix VIII is interpreted as the *v* = 1 state belonging to the progression starting at 12.36 eV, since the spacing and the Franck-Condon factors agree with those of the *b* <sup>3</sup>Π grandparent state.

An energy level diagram of the zeroth vibronic level of each NO<sup>-</sup> state is shown on the right side of Fig. 63. On the left side of this figure the energy levels of the NO<sup>+</sup> grandparent states are shown. The two scales have been displaced by the difference in energies between the lowest member of band "a" with respect to its grandparent, the X <sup>1</sup>Σ<sup>+</sup> core of NO<sup>+</sup> (4.23 eV), in order to show the relationship between the NO<sup>+</sup> state and its grandchildren NO<sup>-</sup> states. This comparison demonstrates that the binding energy of two 3sσ Rydberg electrons does not depend on the configuration of the positive ion core. It also illustrates that in NO

only Rydberg excited states give rise to core-excited resonances in the total scattering cross section.

## VI. OXYGEN

### A. Compound State at Low Energy: X <sup>2</sup>Π<sub>g</sub> (0–1 eV)

The lowest compound state of O<sub>2</sub> is the X <sup>2</sup>Π<sub>g</sub> state. The vibrational states *v*' = 0 to *v*' = 3 of O<sub>2</sub><sup>-</sup> (X <sup>2</sup>Π<sub>g</sub>) lie below the *v* = 0 state of O<sub>2</sub> (X <sup>3</sup>Σ<sub>g</sub><sup>-</sup>) and cannot auto-detach. These vibrational states of O<sub>2</sub><sup>-</sup> are therefore stable. For higher quantum numbers, autodetachment can take place and these higher vibrational states form the lowest compound state of O<sub>2</sub>. As in the case of NO, a variety of experiments must be brought to bear on the problem in order to gain a full picture which has recently emerged. The important experiments are elastic scattering, inelastic scattering (i.e., vibrational excitation), photodetachment, various measurements of the electron affinity, and three-body attachment.

The molecular orbital notation for the lowest states of O<sub>2</sub> and O<sub>2</sub><sup>-</sup> is given in Table VIII, Sec. VII.

#### 1. Elastic Scattering

The structure, consisting of peaks, in the elastic differential and total cross sections of electrons on O<sub>2</sub> gives us the information on the position of the vibrational levels of the O<sub>2</sub><sup>-</sup> system. Figure 64 shows a compilation of several experiments, suitably presented. The spacings are also listed in Appendix IX. The assignment of the proper vibrational quantum number does not come from the elastic experiment alone. Rather, the electron affinity of O<sub>2</sub> must be known in order to achieve such an assignment and a backward extrapolation, using the measured spacings and the anharmonicity, must be performed. Until recently the value for the electron affinity was being questioned (see Sec. VI A3) but we can now be confident that the values of Pack and Phelps (1966) (0.43 ± 0.02 eV) and of Celotta *et al.* (1972) (0.440 ± 0.008 eV) are correct.

When the backward extrapolation is performed and terminated at the electron affinity of 0.44 eV, one obtains a value of 132 meV (Spence and Schulz, 1972) or 135 meV (Linder and Schmidt, 1971b) or 140 meV (Gray *et al.*, 1971) for the spacing of the lowest vibrational states, i.e.,  $v'=0 \rightarrow v'=1$  of  $O_2^-$ . These values compare to a value of 135 meV deduced by Holzer *et al.* (1968) from Raman spectroscopy of alkali halide crystals in which  $O_2^-$  is trapped. The agreement between all these values appears to be good.

A high-resolution (10 meV) transmission experiment by Land and Raith (1973) shows that the  $v'=4$  peak is split by spin-orbit coupling into  ${}^2\Pi_{3/2}$  and  ${}^2\Pi_{1/2}$  components, separated by  $20 \pm 2$  meV. The center of the  $v'=4$  state is determined to be at  $91 \pm 5$  meV.

## 2. Vibrational Excitation of $O_2$ at Low Energy (0–1.0 eV)

The vibrational cross section in  $O_2$  should consist of a "direct" component and a "compound-state" component at the position of the compound state,  $O_2^-$ .

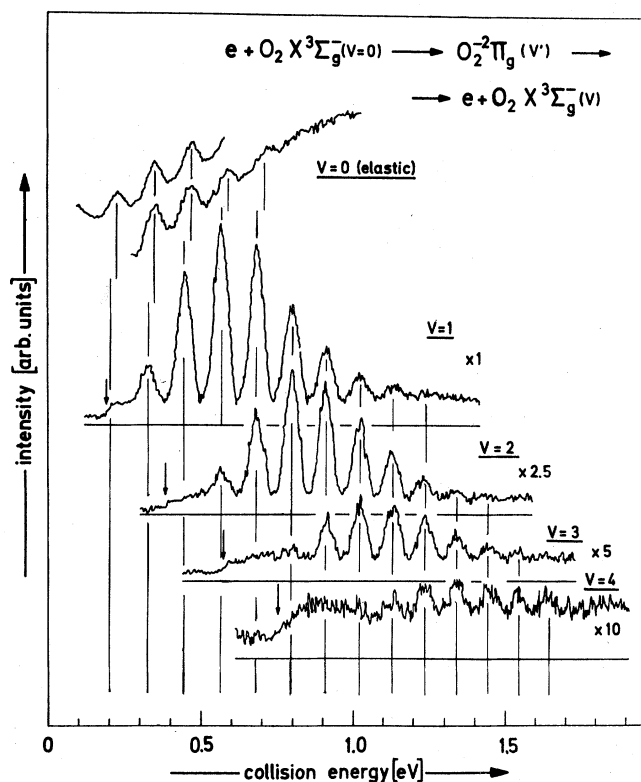


FIG. 65. Measured vibrational cross sections to  $v=1, 2, 3, 4$  of  $O_2$ . The horizontal line at each curve indicates the zero line of the stored signal. Two runs of the energy dependence of elastic scattering are also shown in the upper part of the figure. The scattering angle is  $60^\circ$  for all curves. The vertical lines indicate the energy position of the resonance peaks. The threshold onsets of the excitation functions are marked by small arrows. Energy-integrated cross sections in absolute units are listed in Appendix X. [From Linder and Schmidt (1971b).]

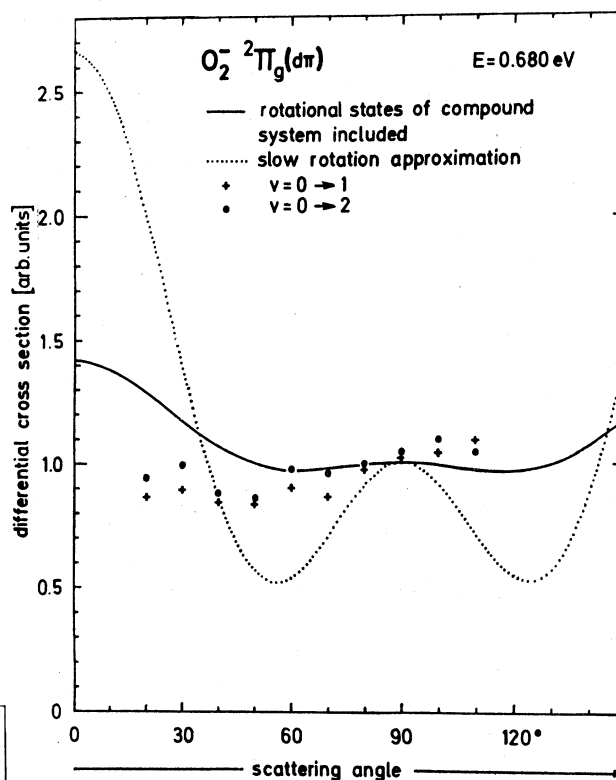


FIG. 66. Angular distribution of electrons having excited the  $v=1$  and  $v=2$  vibrational states in  $O_2$ . The points are experimental (error  $\sim 10\%$ ). The lines represent theoretical models with and without rotational states of the compound state. The curves have been normalized at or near  $90^\circ$ . [From Linder and Schmidt (1971b).]

This model was invoked by Hake and Phelps (1967) and by Schulz and Dowell (1962) to explain swarm and trapped-electron experiments, respectively.

Recent trapped-electron experiments by Spence and Schulz (1970) led to the conclusion that the vibrational cross sections in  $O_2$  consist of series of spikes at the position of the compound state which had been previously established from elastic scatterings. This finding is corroborated by the differential cross section measurements of Linder and Schmidt (1971), whose data are shown in Fig. 65.

The trapped-electron method possesses a high sensitivity for detecting when a level of  $O_2$  and a level of  $O_2^-$  occur accidentally at the same energy. Spence and Schulz find that the  $v'=8$  level of  $O_2^-$  is coincident in energy with the  $v=3$  level of  $O_2$ , thus fixing the relative positions of the vibrational levels of the two systems. This coincidence has been confirmed by Linder and Schmidt, who find that the coincidence between these two levels is within 1 meV, as well as by Land and Raith (1973).

In order to obtain an absolute magnitude from their differential cross section, Linder and Schmidt have to know the angular distribution of the scattered electrons. Figure 66 shows that the experimentally ob-

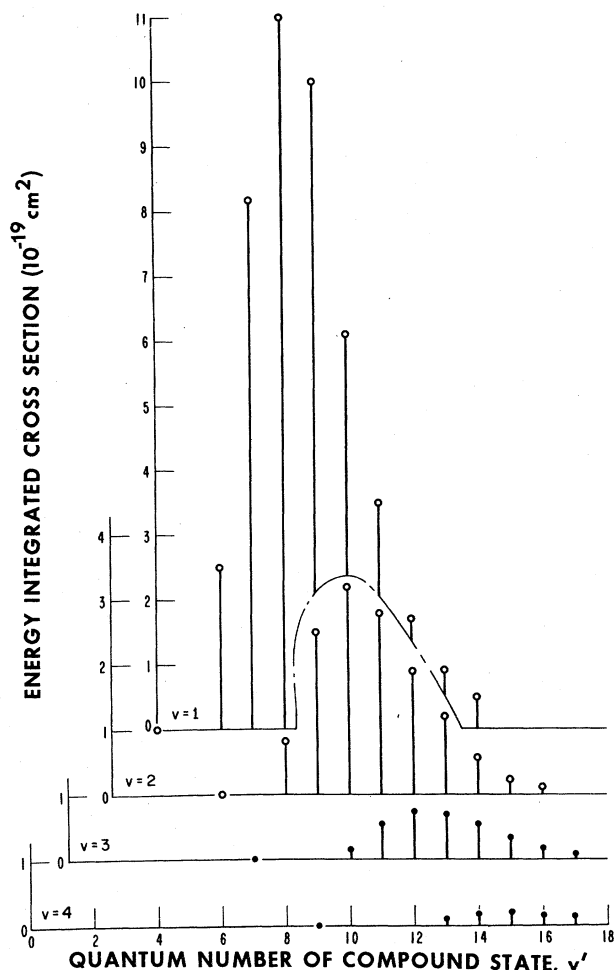


FIG. 67. Plot of energy-integrated cross section for vibrational excitation to  $v=1, 2, 3, 4$  vs quantum number of compound state, as measured by Linder and Schmidt (1971b). The cross sections consist of a series of narrow spikes at the positions of the vibrational levels,  $v'$ , of the compound state.

served angular distribution is isotropic. The lifetime of the  $X^2\Pi_g$  compound state,  $O_2^-$ , is long (i.e.,  $\sim 10^{-10}$  sec for the lowest vibrational member,  $v'=4$ ), as will be discussed below. For such a long-lived object, one has to include rotation in the theory and the result of such a theory yields a near-isotropic angular distribution, as shown in Fig. 66. It is pointed out in Sec. VII that the partial wave in which the resonance occurs is  $d\pi$ .

The absolute magnitude of the energy-integrated vibrational cross sections for the  $v=1, 2, 3, 4$  state of  $O_2$  are shown in Fig. 67 and are listed in Appendix X. Spence and Schulz also measured the energy-integrated cross sections, but their set of measurements is less complete than that of Linder and Schmidt.

Disturbingly, Spence and Schulz' values are by a factor of 10 lower than the values of Linder and Schmidt for those states which are measured in both experiments. No clear-cut criticism can be found in either experiment. However, the values of Linder and

Schmidt must be preferred at this time since they agree better in order of magnitude with the analysis of swarm experiments (Hake and Phelps, 1967) although a detailed comparison is not yet possible because the analysis of swarm experiments has not been performed with the proper set of relative cross sections.

An interesting feature of the data can be brought out by plotting the branching ratio of the cross sections for  $v=2$  to  $v=3$  and  $v=1$  to  $v=2$  vs quantum number of the compound state as is done in Fig. 68. Both curves show an enormous rise as the quantum number  $v'$  is lowered, indicating that a given compound state (especially for low quantum numbers,  $v'$ ) prefers to decay to the lowest possible state of the neutral molecule. The lowest possible state of the neutral molecule is reached by the emission of an electron with the highest possible energy, in the reaction  $O_2^- \rightarrow O_2(v) + e$ . A high-energy electron penetrates the potential barrier with a higher probability than a low-energy electron. Thus the emission of a high-energy electron is favored. For  $d$ -wave scattering which is involved in the present reaction, the barrier penetration is proportional to  $E^{5/2}$  (Blatt and Weisskopf, 1952), where  $E$  is the energy of the electrons.

When the ratio of electron energies of the ejected electrons leading to various decay channels is large (as is the case at low quantum numbers  $v'$ ) a large branching ratio results. It should be noted that the branching ratio for low-lying vibrational states in  $N_2$  and CO is close to unity. This results from the fact that

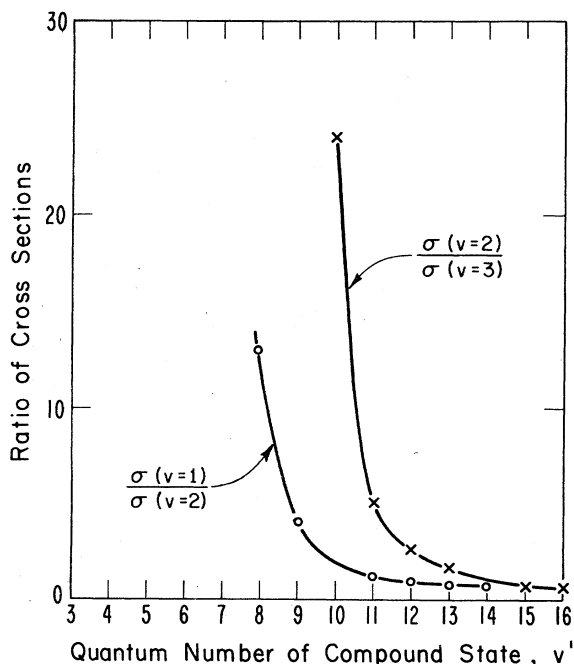


FIG. 68. Ratio of vibrational cross sections vs quantum number,  $v'$ , of compound state. From data of Linder and Schmidt (1971b).

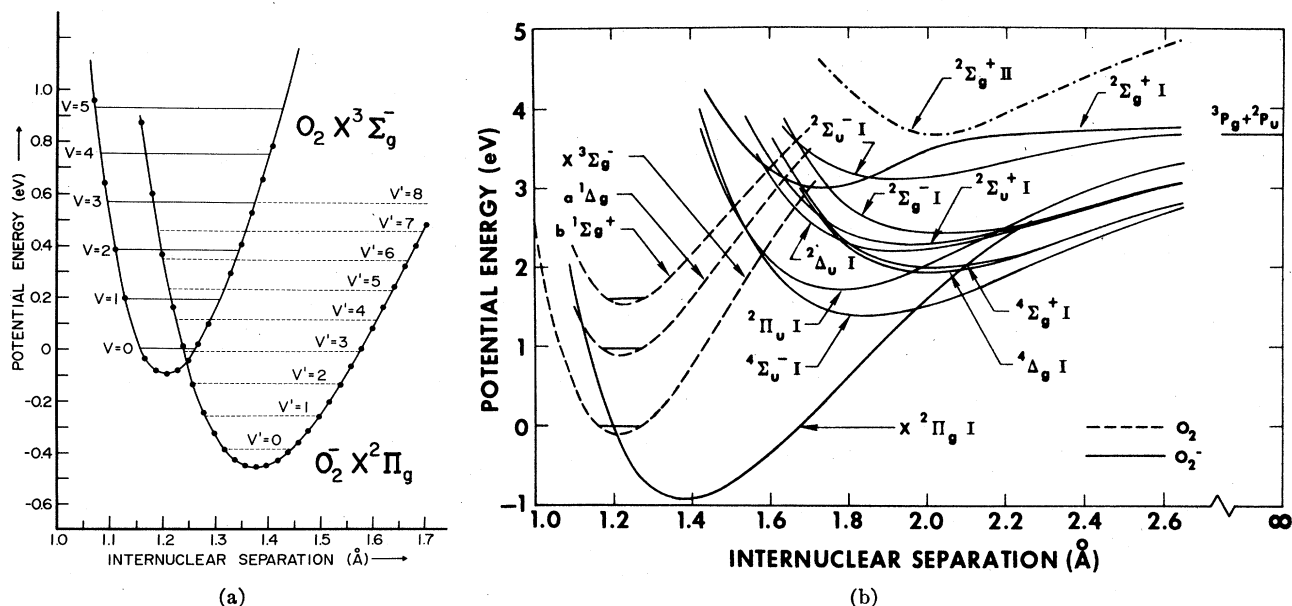


FIG. 69. (a) Approximate potential energy curves for  $O_2$  and  $O_2^-$ . The  $O_2^-$  curve should have its minimum at 1.341 Å (Celotta *et al.*, 1972). The center of the  $v'=4$  state is located at  $0.091 \pm 0.005$  eV and it has a fine structure splitting ( $\Pi_{3/2}-\Pi_{1/2}$ ) of  $20 \pm 2$  meV (Land and Raith, 1973). The  $v=3$  level of  $O_2(X^3\Sigma_g^-)$  is coincident in energy with the  $v'=8$  level of  $O_2^-(X^2\Pi_g)$  (Spence and Schulz, 1970). [From Boness and Schulz (1970).] (b) *Ab initio* calculations of adiabatic potential energy curves for  $O_2^-$ . [From Michels and Harris (1971).]

the ratio of energies of the ejected electrons is also close to unity since the compound state in  $N_2$  is located near 2.3 eV and the spacing of vibrational levels is about 0.3 eV. Thus the barrier penetration in  $N_2$  does not differ much for the decay channels leading to the low vibrational states.

The widths of the  $v'=4-10$  vibrational states of  $O_2^-(X^2\Pi_g)$  have been calculated by Koike and Watanabe (1973) who find a value of 0.004 meV for the  $v'=4$  state. This value has a confidence limit of a factor of about two (Watanabe, private communication) and thus it is in good agreement with the estimate of 0.002 meV made by Herzenberg (1969) from the absolute magnitude of the vibrational cross section in  $O_2$ . The calculated values of Koike and Watanabe are listed in Appendix X.

### 3. Potential Energy Curve for $O_2^-(X^2\Pi_g)$

Using a Morse-function representation together with parameters derived from electron spectroscopy, Boness and Schulz (1970) derived the potential energy curve for the  $O_2^-(X^2\Pi_g)$  state. This curve, together with the curve for the ground state of  $O_2(X^3\Sigma_g^-)$ , is shown in Fig. 69(a). The curve is drawn so that the  $v=3$  level of  $O_2(X^3\Sigma_g^-)$  coincides in energy with the  $v'=8$  level of  $O_2^-(X^2\Pi_g)$ . This coincidence has been established by Spence and Schulz (1970) and by Linder and Schmidt (1971). In order to bring the  $O_2^-$  curve into agreement with the results of Celotta *et al.* (1972), it should be shifted to smaller internuclear separations by 0.036 Å,

so that the minimum of the potential energy curve would be at 1.341 Å.

*Ab initio* calculations for the low-lying potential energy curves have been performed by Michels and Harris (1971) and by Krauss, Neumann, Wahl, Das, and Zemke (1973). The agreement between the two sets of theoretical calculations appears to be good. The set by Michels and Harris is shown in Fig. 69(b).

### 4. Equilibrium Internuclear Separation and Electron Affinity: Photodetachment Spectroscopy

As in the case of NO, the electron affinity of  $O_2$  was a matter of dispute for a long period of time. The various values have been summarized, as of 1970 by Boness and Schulz (1970). At that time it appeared that only the value of Pack and Phelps (1966), obtained from drift-tube studies of attachment and detachment coefficients in thermal equilibrium, was free of serious objections. The value of Pack and Phelps (0.43 eV) has recently been confirmed in a conclusive experiment involving photodetachment. The value of Celotta *et al.* (1972) is  $0.440 \pm 0.008$  eV.

Other recent values for the electron affinity converge on the above value. Among these are the experiments of Nalley and Compton (1971), and those of Berkowitz *et al.* (1971) as interpreted by Chantray (1971).

The photodetachment experiment of Celotta *et al.* (1972) also gives a value of the equilibrium internuclear separation,  $r_e = 1.341 \pm 0.010$  Å, making obsolete

TABLE IX. Parameters of  $O_2^-(X^2\Pi_g)$ .<sup>a</sup>

	Celotta <i>et al.</i> (1972)	Boness and Schulz (1970)	Linder and Schmidt (1971b)	Gray <i>et al.</i> (1971)
Equilibrium separation, $r_e$ Å	$1.341 \pm 0.010$	...	...	...
Electron affinity, eV	$0.440 \pm 0.008$	...	...	...
$B_e$ ( $cm^{-1}$ )	$1.17 \pm 0.02$	...	...	...
$\hbar\omega_e$ (meV)	...	135	135	140
$\hbar\omega_e x_e$ (meV)	...	1.5	1.0	3.0

<sup>a</sup> Additional features: The fine-structure splitting is  $22 \pm 2$  meV (Land and Raith, 1972).

the previous determination of Boness and Schulz (1970), obtained by use of Badger's rule from the vibrational spacings of  $O_2^-$ .

Table IX lists the parameters for  $O_2^-(X^2\Pi_g)$  deduced from photodetachment spectroscopy and from electron impact spectroscopy. It is seen that the values deduced from these two types of experiments complement each other. The value deduced by Boness and Schulz (1970) from the vibrational spacing of  $O_2^-$  using Badger's rule (i.e.,  $r_e = 1.377$  Å) is not listed since the value deduced from photodetachment spectroscopy is considered more reliable.

From the foregoing discussion it should be fairly obvious that photodetachment spectroscopy is a powerful tool for determining electron affinities and the structure of negative ions. In both of the cases in which a stable negative ion exists, namely  $O_2$  and NO, no evidence exists for excited negative ions lying below the neutral species, i.e., only one electronic state exhibits a positive electron affinity. Photodetachment experiments do not, however, rule out the possibility of the existence of excited states of  $O_2^-$  which have a large equilibrium internuclear separation. The calculations of Michels and Harris (1971) show that only the  $X^2\Pi_g$  state of  $O_2^-$  lies below the ground state of  $O_2$ . Thus one must conclude that the only stable state of  $O_2^-$  which lies energetically below the ground state of  $O_2$  is the  $X^2\Pi_g$  state.

Figure 69(b) shows the potential energy curves for  $O_2^-$  as calculated by Michels and Harris (1971). In addition to the  $X^2\Pi_g$  state, Michels and Harris find 12 other attractive states arising from the limit  $O+O^-$ . All these states are qualitatively similar, exhibiting shallow potential wells at large internuclear separations (1.8–2.0 Å). The existence of a large number of autodetaching states,  $O_2^-$ , is consistent with the experiments, on associative detachment (Ferguson, 1968). The thermal rate constant for the associative detachment reaction,  $O^- + O \rightarrow O_2^- \rightarrow O_2 + e$ , is large [Ferguson (1968) gives a value of  $3 \times 10^{-10}$   $cm^3$   $sec^{-1}$  at 300°K], and it is reasonable to suppose that some of the  $O_2^-$  states shown in Fig. 69(b) serve as intermediates.

Recently, Lineberger and Patterson (1972), using two-photon photodetachment spectroscopy, discovered an excited state of a negative ion which lies below the ground state of the neutral molecule. The molecule is  $C_2$ . The ground state of the negative ion,  $C_2^-(^2\Sigma_g^+)$  lies  $\sim 3.5$  eV below the neutral ground state,  $C_2$   $^1\Sigma_g^+$ . About 2 eV above  $C_2^-(^2\Sigma_g^+)$  there is an excited state of the negative ion,  $C_2^-(^2\Sigma_u^+)$ . It may be of interest to study such systems using electron spectroscopy to obtain complementary data.

### 5. Three-Body Attachment in $O_2$

Three-body attachment, i.e., the reaction  $e + 2O_2 \rightarrow O_2^- + O_2$ , is now known to proceed via the  $X^2\Pi_g$  compound state of  $O_2$ . The reaction can therefore be written as a two-step process:  $e + O_2 \rightarrow O_2^{-*}$ , followed by

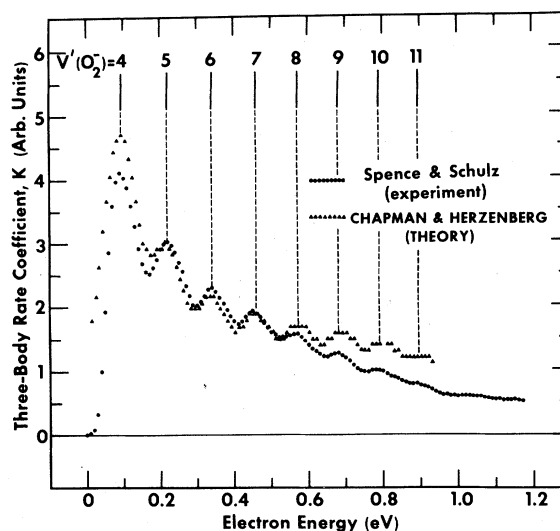
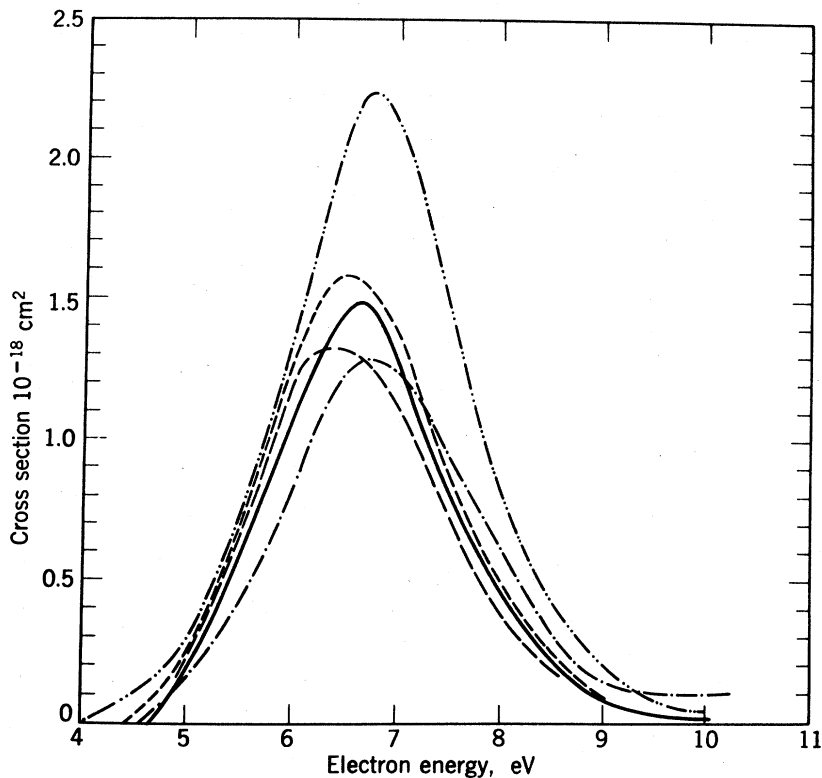


FIG. 70. The three-body attachment coefficient of production of  $O_2^-$  in  $O_2$  in comparison with the theory. The theory is normalized to the experimental data at the second peak. The vibrational levels of the  $O_2^-(X^2\Pi_g)$  state are indicated by the lines on top. The structure in the three-body attachment coincides with the positions of the vibrational states of  $O_2^-$ . This figure shows that three-body attachment on  $O_2$  proceeds via the low-lying compound state of  $O_2$ . [From Spence and Schulz 1972].]

FIG. 71. The cross section for O<sup>-</sup> formation by dissociative attachment in O<sub>2</sub>. The value of Craggs *et al.* (1957) (-·-·-) is undoubtedly too high. The values of Buchelnikova (1959) (- - -), of Schulz (1962b) (- · - ·), of Rapp *et al.* (1965) (- - -), and of Christophorou *et al.* (1965) (—) all agree very well. [From Chen (1969).]

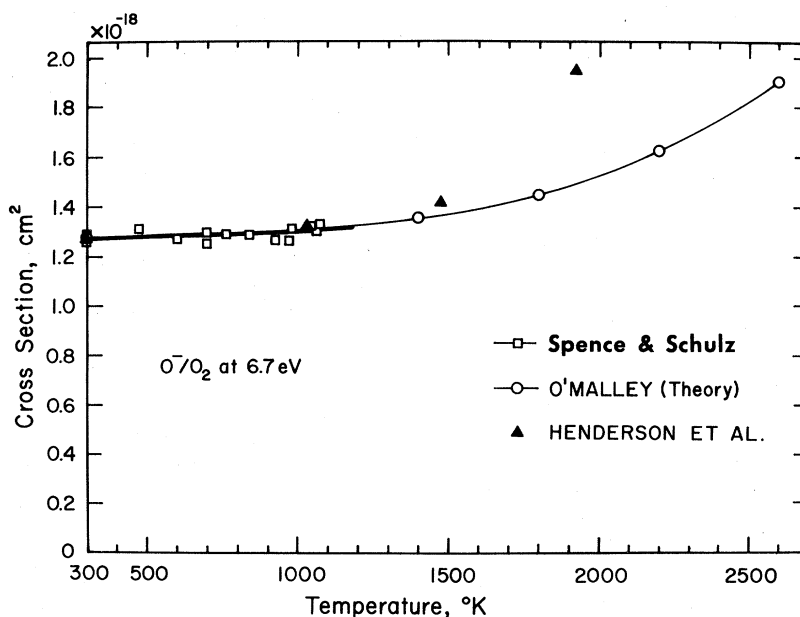


$O_2^{-*} + O_2 \rightarrow O_2^- + O_2$ . Here,  $O_2^{-*}$  denotes a particular vibrational level of the  $O_2^{-}(X^2\Pi_g)$  state. The general features of this model have been deduced by Chanin, Phelps, and Biondi (1962) who clearly established the three-body nature of the process from their swarm data. The modern approach to the theoretical considerations

is due to Herzenberg (1969). The swarm experiments of Chanin *et al.* show a smooth variation with energy of the three-body attachment coefficient as would be expected for swarm experiments.

If one performs an experiment with essentially monoenergetic electrons, the three-body attachment coeffi-

FIG. 72. The dependence on temperature of the peak dissociative attachment cross section in O<sub>2</sub>. Shown are the results of Spence and Schulz (1969), of O'Malley (1967), and of Henderson, Fite, and Brackmann (1969). [From Spence and Schulz (1969).]



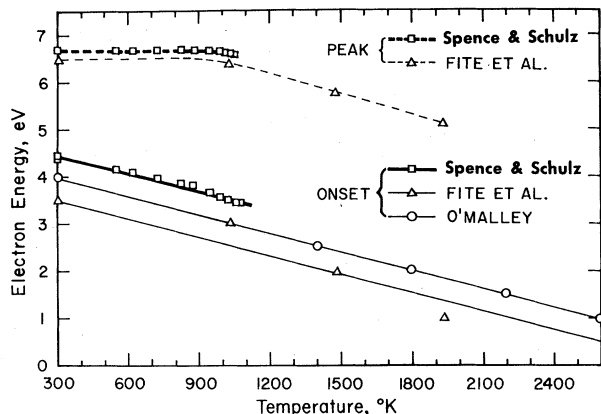


FIG. 73. Temperature dependence of energies of onset and energies at which peak of dissociative attachment occurs in  $O_2$ . Shown are the results of the same authors as Fig. 72. [From Spence and Schulz (1969).]

cient shows pronounced structure at the positions of the vibrational levels of the  $O_2^-$  system. The experimental results of Spence and Schulz (1972) are shown in Fig. 70, in comparison with the theory. The good agreement between the energy levels of the  $O_2^-$  system obtained from elastic scattering (shown on top of Fig. 70) and the positions of the peaks is convincing evidence that the process proceeds via the  $O_2^-(X^2\Pi_g)$  state.

**B. Dissociative Attachment (4.4–10 eV):  $^2\Pi_u$  State**

Dissociative attachment in  $O_2$  has been studied in great detail and Fig. 71 shows that good agreement

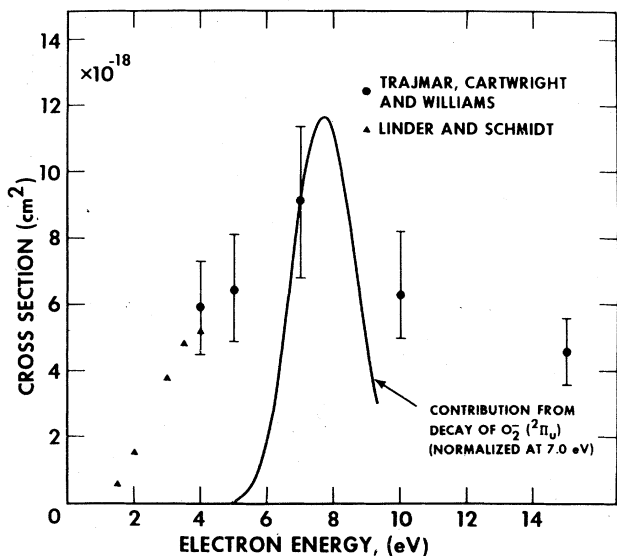


FIG. 74. Cross section for excitation of the  $O_2(a^1\Delta_g)$  metastable state. Shown by the points are the data of Linder and Schmidt (1971) and of Trajmar, Cartwright, and Williams (1971). The solid curve, due to Burrow, shows that portion of the cross section to the  $a^1\Delta_g$  state which proceeds via the  $O_2(^2\Pi_u)$  state. The calculated curve represented by the solid line is normalized to the experimental value of Trajmar *et al.* at 7 eV. [From Burrow (1973).]

exists between the results of various experiments. The cross section for  $O^-$  production starts rising near 4.4 eV, reaches a maximum of about  $1.3 \times 10^{-18} \text{ cm}^2$  at 6.7 eV, and then drops. No structure of any kind has been detected in this cross section, nor is there a signal below 4.4 eV at room temperature (the theoretical onset for the reaction is about 3.6 eV), to a sensitivity 0.1% of the peak cross section. Spence and Schulz (1969) and Chen (1969) have reviewed the subject matter recently.

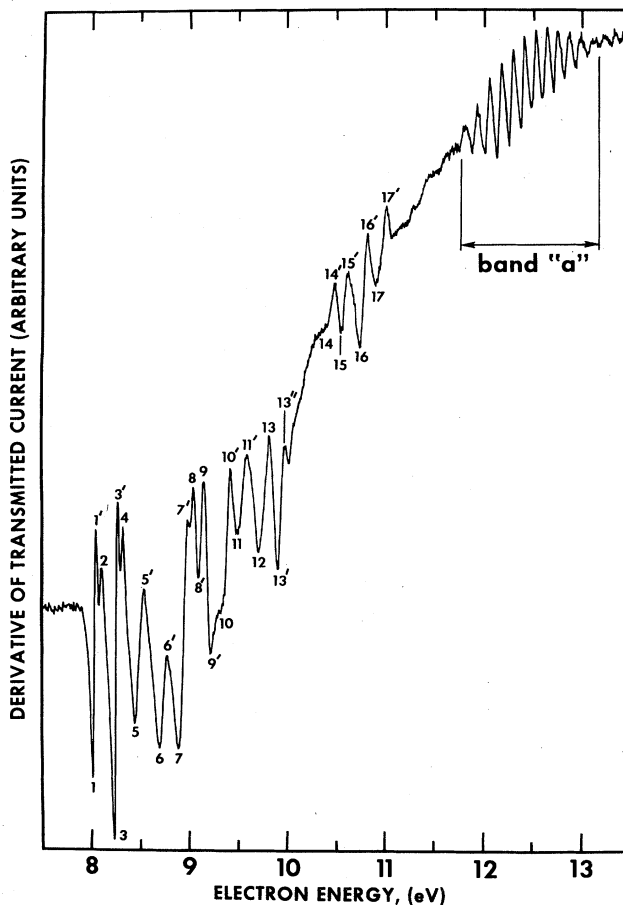


FIG. 75. Derivative of transmitted current vs electron energy in  $O_2$ . Structures 1–17 are interpreted as resonances whose grandparent is the ground state of  $O_2^+$ . A well-developed progression of ten resonances, marked band "a", appears near the end of the spectrum. The grandparent of band "a" is the  $a^4\Pi_u$  state of  $O_2^+$ . [From Sanche and Schulz (1972).]

Noteworthy are the studies of the dependence on gas temperature of the onset and the absolute magnitude of the dissociative attachment cross section. These studies, performed by Henderson, Fite, and Brackmann (1969) and by Spence and Schulz (1969) show that the magnitude of the cross section increases as the gas temperature is raised and that the onset is lowered at higher temperatures. Figures 72 and 73 show the results of these studies.

The single peak at 6.7 eV suggests that a single compound state,  ${}^2\Pi_u$ , is responsible for dissociative attachment around 6.7 eV, although many more compound states exist in this energy range. This view is reinforced by the parametrization study of O'Malley (1967), who used the shape and the magnitude of the experimental cross section at room temperature and the temperature dependence to arrive at the shape of a single potential energy curve and the value for the width of the state. It is pointed out by O'Malley, and confirmed experimentally by Henderson *et al.* (1969) that the temperature effects in  $O^-/O_2$  production can be explained solely on the basis of the vibrational excitation of the target molecule, and that rotational excitation does not play a significant role.

Vibrationally excited molecules have a large Franck-Condon region and if the electron is captured while the  $O_2$  molecule is at a large internuclear separation, the survival probability for negative ion formation is enhanced. As a result, the dissociative attachment cross section increases for higher vibrational states.

The angular distribution of the  $O^-$  ions resulting from electron impact on  $O_2$  in the energy range 5.75–8.40 eV has been studied by Van Brunt and Kieffer (1970). They find that the experimentally observed angular distributions can be explained most simply in terms of a transition to a single  ${}^2\Pi_u$  repulsive state of  $O_2^-$ . They arrive at this conclusion by comparing the experimentally observed angular distributions with the theory of O'Malley and Taylor (1968) and the symmetry arguments of Dunn (1962). The interpretation in terms of a single compound state is consistent with the evidence coming from the temperature dependence of dissociative attachment and also with the measurements of the  $O^-$  kinetic energy (Schulz, 1962b; Chantry and Schulz, 1967). Van Brunt and Kieffer (1970) do not exclude the possibility that another closely spaced resonance also contributes, but they find this alternative less attractive.

Burrow (1973) has recently measured the dissociative attachment cross section from the  $a^1\Delta_g$  state of  $O_2$ , i.e., the reaction  $e + O_2(a^1\Delta_g) \rightarrow O_2^-({}^2\Pi_u) \rightarrow O^-({}^2P) + O(^3P)$  and finds that this cross section is larger by a factor of about  $3.5 \pm 1$  compared to the ground-state dissociative attachment cross section. This measurement, coupled with an analysis based on O'Malley's theory, enables Burrow to calculate that portion of the excitation cross section to the  $a^1\Delta_g$  state which proceeds via the  ${}^2\Pi_u$  state, i.e., the reaction  $e + O_2(X^3\Sigma_g^-) \rightarrow O_2^-({}^2\Pi_u) \rightarrow O_2(a^1\Delta_g) + e$ . The contribution from the decay of the compound state is found to be a large portion of the total excitation cross section at its maximum. The energy range over which this mechanism is important, together with experimental measurements of the  $a^1\Delta_g$  excitation function, are shown in Fig. 74.

The most likely means of excitation to the  ${}^1\Delta_g$  state from threshold to 5 eV and above 15 eV is pro-

vided by nonresonant exchange scattering. The cross section for this process has been calculated by Julienne and Krauss (1972) using the Ochkur-Rudge approximation to the exchange amplitude. The calculated cross section is somewhat smaller than the experimentally measured values.

Wong, Boness, and Schulz (1973) have recently observed vibrational excitation to the  $v=1, 2, 3$ , and 4 levels of the electronic ground state of  $O_2$ , in the energy range 4–15 eV, with a peak near 9 eV. For an interpretation of this process, Wong *et al.* invoke some of the  $O_2^-$  compound states which exist in this energy range, e.g.,  ${}^2\Sigma_u^-$ ,  ${}^4\Sigma_u^-$ , and  ${}^2\Pi_u$  states and possibly others.

### C. Core-Excited Resonances

The only information regarding core-excited resonances in  $O_2$  comes from the transmission experiments of Sanche and Schulz (1972). Figure 75 shows the derivative of the transmitted current vs electron energy in the range 8–13 eV. The structures are labelled and are listed in Appendix XI. Because of the extreme complexity of the spectrum, especially in the energy range 8.5–12 eV, Sanche and Schulz were not able to identify the structures in detail.

The structures (1–1') and (3–3'), spaced 220 meV apart probably have as a grandparent the  $O_2^+(X^2\Pi_g)$  state, which has a spacing of 232 meV. These two resonances thus consist of two electrons in ( $3s\sigma_g$ ) Rydberg orbitals, attached to the  $X({}^2\Pi_g)$  core. The "binding" of the two electrons, i.e., the energy difference between the lowest resonance (8.04 eV) and the  $O_2^+(X^2\Pi_g)$  state, is 4.02 eV, a number similar to that found in other molecules (see Table X).

Structures 2 and 4 lie  $40 \pm 5$  meV above structures (1–1') and (3–3'), respectively. They could reflect spin-orbit splitting of the  ${}^2\Pi_g$  state of  $O_2^-$  into a  ${}^2\Pi_{3/2}$  configuration for resonances (1–1') and (3–3') and a  ${}^2\Pi_{1/2}$  configuration for resonances 2 and 4. The observed doublet spacing is larger than the value of 24 meV for the splitting of the ground state of  $O_2^+$ .

#### 1. Band "a"

At higher energies a well-developed progression of ten resonances appears in the spectrum starting at  $11.81 \pm 0.05$  eV. Sanche and Schulz (1972) compare the vibrational spacings and Franck-Condon probabilities of band "a" with those of the  $a^4\Pi_u$  grandparent state of  $O_2^+$ . They find that there is remarkable agreement, whereas no such correspondence can be found when the experimental data are compared with other states of  $O_2^+$ , i.e., the  $X^2\Pi_g$ ,  $A^2\Pi_u$ ,  $b^4\Sigma_g^-$ , and  $B^2\Sigma_g^-$  of  $O_2^+$ .

This suggests that band "a" results from vibrational structure of a  ${}^4\Pi_u$  Rydberg negative ion, formed by the addition of two Rydberg electrons of the  $3s\sigma_g$  orbital symmetry to a  $O_2^+$  core in the  $a^4\Pi_u$  valence excited state. The likely parents of the  $O_2^-$  state could be

formed by the addition of a single  $3s\sigma_g$  electron to the  $O_2^+(a^4\Pi_u)$  core, thus forming  $^3\Pi$  and  $^5\Pi$  Rydberg states. These states lie at 12.50 eV ( $^3\Pi$ ) and 12.24 eV ( $^5\Pi$ ), respectively, and the observed progression lies about 0.6 eV below the  $^5\Pi$  state. Since a value of 0.6 eV is a reasonable value for the electron affinity, Sanche and Schulz (1972) consider this a further confirmation that the  $^3,^5\Pi$  states of  $O_2$  are the parents of band "a". Again, the "binding" of the two  $3s\sigma_g$  electrons to the grandparent is about 4.4 eV.

The quantum number of each vibrational level listed in Appendix XI is determined by fitting the Franck-Condon probabilities of the  $O_2$  ion to those of the  $O_2^+$  ion. The zeroth level of the  $O_2^-$  progression cannot be observed because its Franck-Condon probability is small.

## 2. Band "b"

Another band of  $O_2^-$  states (band "b") consisting of a progression of four vibrational members has been observed above ionization (Sanche and Schulz, 1972) and is listed in Appendix XI. In this case the vibrational spacings are close to those of the  $b^2\Sigma^-$  state of  $O_2^+$ . The  $^3\Sigma_u^-$  state which lies 0.210 eV above the zeroth level of band "b" and constitutes the lowest Rydberg excited state belonging to the  $b^4\Sigma_g^-$  state of the positive ion system is the suggested parent for this progression.

## VII. CONCLUSIONS

In this section we summarize some of the features discussed in the text, not by molecular species, but by the process involved.

### A. Shape Resonances

All molecules discussed in this review exhibit shape resonances associated with the ground electronic state. These can be understood by referring to Table VIII. Listed are the molecular orbital configurations of the ground state of the respective molecule; the designation of the ground state; the lowest vacant orbital into which the electron attaches to form the shape resonance; the designation of the compound state; and the dominant electron partial wave responsible for forming the compound state.

The angular distribution measurements and the widths of compound states can be understood in terms of the partial wave which is dominant. In homonuclear diatomic molecules, having a center of symmetry, the allowed values of the angular momentum in the partial wave are either all even or all odd. Therefore it is unlikely that higher allowed partial waves, beyond those indicated, provide a significant contribution. In heteronuclear diatomic molecules, where there is no center of symmetry, one has to consider mixtures of partial waves. The dominant mixtures are indicated in Table VIII. For those molecules for which the lifetime of the compound state is short compared to the rotation

time (all listed molecules except  $O_2$ ), the angular distribution measurements show the behavior characteristic of the partial waves indicated. In heteronuclear molecules, the admixture of the two components must be adjusted properly in order to obtain agreement with the experiments, as has been done by Read (1968) for CO. Read (1968) has shown that "pure" partial waves, i.e.,  $p\sigma$ ,  $p\pi$ ,  $d\sigma$ ,  $d\pi$ , and  $d\delta$  exhibit the characteristic shapes for  $p$  waves and  $d$  waves, in the sense that a minimum exists at  $90^\circ$  for the  $p\sigma$  and  $p\pi$  waves and a maximum exists at  $90^\circ$  for the  $d\sigma$ ,  $d\pi$ , and  $d\delta$  waves. However, the detailed shape is somewhat different from that of  $p$  and  $d$  waves: the  $p\sigma$  and  $p\pi$  waves do not lead to zero cross sections at  $90^\circ$ , and neither do the  $d\sigma$ ,  $d\pi$ , and  $d\delta$  waves show a zero near  $60^\circ$ .

When the lifetime of the compound state is comparable to or long compared to the rotational time, then the angular distribution becomes nearly isotropic, as is the case in  $O_2$ , and little information can be gained from angular distribution measurements, beyond the lifetime considerations.

The mixture of partial waves which one has to consider in the case of CO and NO contains  $p$ -wave components in the partial wave. Because the  $p$ -wave component leads to a much lower barrier than a  $d$  wave, the decay via the  $p$ -wave barrier is favored over escape via the  $d$ -wave barrier. Although  $d$  waves may be more important in the interior of the molecule, the  $p$  wave may dominate the decay and thus be responsible for the angular distribution and lifetime. These considerations explain the shorter lifetimes of the compound states in CO and NO, compared to  $N_2$  and  $O_2$ .

### B. Core-Excited Shape Resonances

Singly or doubly excited states of molecules also can bind an extra electron by the centrifugal barrier, thus forming shape resonances. The most extensive study has been made for the case of  $N_2$ , in which the singly excited valence states,  $A^3\Sigma_u^+$  and  $B^3\Pi_g$ , have associated shape resonances. The progression of vibrational levels of these shape resonances are often long, exhibiting up to 18 vibrational states. These core-excited shape resonances have properties which are very similar to shape resonances associated with the ground state.

Core-excited resonances consisting of a doubly excited core plus an electron also have been postulated, for example in  $N_2$  near 22-eV energy.

Although other molecules have not been studied in sufficient detail, it can be expected that core-excited shape resonances are the rule rather than the exception and that future energy level diagrams of negative molecular ions will show a fantastic number of compound states.

It should be noted that repulsive states of molecules also can have associated shape resonances, as is the case in  $H_2$ .

### C. Binding of Rydberg Resonances

A recurrent theme throughout this review is the observation that most core-excited Feshbach resonances are associated with Rydberg excited states of the molecule. These states can be considered as being formed by the attachment of two electrons in Rydberg orbitals to the positive ion core, which we call the "grandparent." The *lowest configuration* that is possible contains the positive ion core plus two  $3s\sigma_g$  electrons. Table X lists the "binding energy" of these two electrons to the various positive ion cores of  $H_2$ , NO, CO,  $N_2$ , and  $O_2$ . The "binding energy" is determined by taking the difference between the energy of a particular state of the positive ion and the experimentally observed energy of a particular resonance which we associate with this positive ion core. The association between the positive ion core and the resonance comes from a comparison of the vibrational spacings and Franck-Condon factors. The data used for constructing Table X are taken from Sanche and Schulz (1972) and are fully discussed in the body of this review.

It is obvious from Table X that all the molecules listed have binding energies for the two  $3s\sigma_g$  electrons of about 4 eV.

TABLE X. "Binding" energy of two  $3s\sigma_g$  electrons to grandparents.

Molecule	Positive ion		Associated resonance energy eV	"Binding" energy eV
	State	Energy eV		
$H_2$	$X^2\Sigma_g^+$	15.42	11.32	4.1
$N_2$	$X^2\Sigma_g^+$	15.51	11.48	4.03
	$A^2\Pi_u$	16.62	12.64	3.98
CO	$X^2\Sigma^+$	14.1	10.04	4.1
	$A^2\Pi$	16.6	13.95	...
NO	$X^1\Sigma^+$	9.27	5.04	4.23
	$b^3\Pi$	16.56	12.36	4.20
	$A^1\Pi$	18.32	14.19	4.23
	$B^1\Pi$	21.72	17.51	4.21
$O_2$	$X^2\Pi_g$	12.06	8.04	4.02
	$a^4\Pi_u$	16.10	~11.69 <sup>a</sup>	4.4
	$b^2\Sigma_g^-$	18.16	14.27 <sup>b</sup>	3.9

<sup>a</sup> The level  $v=0$  is not observed. The value given is an extrapolation.

<sup>b</sup> The assignment as  $v=0$  is uncertain.

### D. Thresholds of Inelastic Cross Sections

It is pointed out in Sec. IIIB2 that the threshold behavior of inelastic cross sections is often dominated by nearby resonances. Both core-excited shape resonances (which lie above the electronic state) and Feshbach resonances (which lie below their parent) are important. Sometimes, the influence of these two types of resonances can be distinguished and energy ranges can be specified which are dominated by the influence of one or the other resonance. This is the case for the  $2^3S$  excitation function of helium. In other cases, the threshold is dominated only by a nearby shape resonance ( $E^3\Sigma_g^+$  state in  $N_2$ ). In still other cases the threshold behavior is dominated by a Feshbach resonance lying below the respective excited state ( $b^3\Sigma^+$  state in CO). The width of the Feshbach resonance appears to be a dominant factor.

### ACKNOWLEDGMENTS

The author is indebted to many people and to many agencies who made possible his participation, over the past eighteen years, in the exciting developments partially described in this report. Support for this work came at various stages from the Westinghouse Research Laboratories (1954-1966), from the National Science Foundation, the Defense Atomic Support Agency, the Advanced Research Projects Agency, and the Army Research Office, Durham. To these agencies go the thanks of the author for providing the funds which enabled him and his colleagues to participate in the progress of this field. Needless to say, many other advances, not reported in this survey, resulted from the above-mentioned support.

The scientists from whom the author learned about atomic collision processes along the way include U. Fano, E. Gerjuoy, A. Herzenberg, A. V. Phelps, H. S. Taylor, and many others.

The author received comments, suggestions, and corrections from J. Comer, U. Fano, E. Ferguson, F. Linder, C. Kuyatt, C. Lineberger, P. D. Burrow, A. Herzenberg, A. V. Phelps, H. S. Taylor, and M. J. W. Boness and wishes to express his thanks to them for reading portions of the manuscript.

A portion of this review was written while the author enjoyed the hospitality of JILA and special thanks go to L. J. Kieffer for his interest in this review, for carefully reading the whole manuscript, and for suggesting many changes and corrections. Mrs. L. H. Volsky of JILA and Mrs. M. R. Harrison of Yale provided editorial assistance. Lastly, the author is greatly indebted to his wife, Rose, who selflessly tended to the problems of life, the family, and the home, and gave up a great many things for the cause of science.

## APPENDIX I

Comparison of the values obtained by different authors for the  $H_2^-$  states (eV).

Vibrational quantum number ( $H_2^-$ )	Transmission		Inelastic		Theory	
	Sanche and Schulz (1972)	Kuyatt <i>et al.</i> (1966)	Comer and Read (1971a)	Weingart- shofer <i>et al.</i> (1970)	Eliezer <i>et al.</i> (1967) <sup>a</sup>	
		Bands "a" and "d"				
0	11.32	11.28	11.30	11.30	11.32	
1	11.62	11.56	11.62	11.62	11.62	
2	11.91	11.84	11.91	11.92	11.91	
3	12.19	12.11	12.19	12.20	12.18	
4	12.44	12.37	12.45	12.46	12.44	
5	12.68	12.62	12.68	12.70	12.68	
6		12.86	12.89	12.93		
7			13.10			
8			13.28			
		Band "b"				
2			11.27			
3			11.47			
4			11.63			
5			11.75			
6			11.85			
7			11.96			
		Bands "c" and "e"				
0	11.43	11.46	11.19 <sup>b</sup>	11.50	11.46	
1	11.74	11.72	11.50 <sup>b</sup>	11.79	11.75	
2	12.03	11.99	11.80 <sup>b</sup>	12.08	12.03	
3	12.32	12.27	12.07 <sup>b</sup>	12.38	12.31	
4	12.58	12.53			12.58	
5	12.83	12.77			12.84	
6	13.06	12.97				
		Band "f"				
		Golden (1971)				
0	13.66	13.62		13.63		
1	13.94	13.91		13.93		
2	14.20	14.19		14.20		
3	14.45	14.46		14.47		
4	14.69	14.72		14.70		
5	14.93	14.97		14.92		
6	15.18	15.21				
7	15.43	15.44				
8	15.65	15.66				
9	15.85	15.87				
10		16.07				
11		16.26				
		Band "g"				
	15.09					
	15.32					
	15.57					
	15.77					

<sup>a</sup> The theoretical values of Eliezer, Taylor, and Williams (1967) for band "a" were incremented by 0.25 eV for purposes of direct comparison with the experimental values of Sanche and Schulz (1972).

<sup>b</sup> From Joyez, Comer, and Read (1973).

**APPENDIX II**

 Comparison of the values obtained by different authors for  $D_2^-$  states (eV).

Vibrational quantum number ( $D_2^-$ )	Transmission		Inelastic Comer and Read (1971a)	Vibrational quantum number ( $D_2^-$ )	Transmission		Inelastic Comer and Read (1971a)
	Sanche and Schulz (1972)	Kuyatt <i>et al.</i> (1966)			Sanche and Schulz (1972)	Kuyatt <i>et al.</i> (1966)	
Band "a"				Band "c"			
0	11.34	11.28	11.32	1	11.67		11.65
1	11.56	11.48	11.54	2	11.89		11.87
2	11.76	11.69	11.75	3	12.09		12.07
3	11.97	11.89	11.96	4	12.26		12.23
4	12.17	12.09	12.15	Sanche and Schulz (1972)			
5	12.36	12.28	12.32	Band "f"		Band "g"	
6	12.55	12.47	12.48	0	13.66	15.05	
7	12.71	12.64	12.61	1	13.86	15.22	
8	12.88	12.85	12.75	2	14.06	15.39	
9	13.05			3	14.25	15.55	
10	13.22			4	14.43	15.71	
				5	14.57		

**APPENDIX III**

 Relative branching ratios for the decay of resonance series "a" in  $H_2$  in terms of absolute cross sections ( $10^{-17} \text{ cm}^2$ ). The estimated error for the cross sections is in the order of 20%.

Exit channel	$v'=0$	$v'=1$	$v'=2$	$v'=3$	$v'=4$	$v'=5$
$B^1\Sigma_u^+$						
$v=2$	...	0.27	0.39	0.09	0.14	0.14
$v=1$	...	0.41	0.29	0.39	0.18	0.10
$v=0$	0.67	1.4	0.76	0.21	...	...
$b^3\Sigma_u^+^a$						
11.02 eV	...	0.11	0.10	0.042	0.020	0.008
10.76 eV	0.031	0.087	0.063	0.039	0.015	...
10.47 eV	0.042	0.063	0.048	0.024	0.007	...
10.17 eV	0.033	0.045	0.022	0.011	0.004	...
$b^3\Sigma_u^+$ —Integrated values	2.0	2.5	2.5	1.4	1.0	
$X^1\Sigma_g^+$						
$v=5$	...	0.09	...	...	...	...
$v=4$	0.04	0.2	0.06	0.02	...	...
$v=3$	0.14	0.23	0.02	...	...	...
$v=2$						
$v=1$						
$v=0$	Pronounced interference structure					

<sup>a</sup> Within an energy band of  $\Delta E \approx 60$  meV. From Weingartshofer *et al.* (1970).

## APPENDIX IV

Energies of resonances in N<sub>2</sub> (11–15 eV).

Feature number	Transmission		Differential elastic and inelastic	Trapped electron	Total metastable	$E^3\Sigma_g^+$ , $a''^1\Sigma_g^+$
	Sanche and Schulz (1972)	Heideman <i>et al.</i> (1966a)				
Fig. 42			Comer and Read (1971b)	Hall <i>et al.</i> (1970)	Lawton and Pichanick (1973)	Mazeau <i>et al.</i> (1972b)
"b"	11.47–11.51	11.48	11.48	} band "b"		
	11.74–11.78	11.75	11.75			
			12.02			
3	11.92	11.87	11.87	11.87		11.90
4–4'	12.18–12.27		12.205	12.25	12.12/12.25	12.14
5	12.64				12.59	12.54
6	12.87		Ehrhardt and Willmann ( $^1\Sigma_g^+$ )		12.80	12.78
"c"	13.00			13.0		13.03
	13.23				13.24	13.21
	13.50				13.52	13.44
	13.70					13.66
"d"	13.88					
	14.12		14.2			13.73
	14.36					13.86
	14.57					

All structures are Feshbach-type resonances except structures 3 and 4–4', which are identified as shape resonances. Additional shape resonances have been observed by Mazeau *et al.* (1972b) at 12.40 eV in the  $E^3\Sigma_g^+$  ( $v=1$ ) channel and at 12.70 eV in the  $E^3\Sigma_g^+$  ( $v=0$ ) channel.

## APPENDIX V

Energies and spacings of shape resonances connected with the  $B^3\Pi_g$  state in N<sub>2</sub>.

Transmission (Sanche and Schulz, 1972)		$B^3\Pi_g$ decay channel (Mazeau <i>et al.</i> , 1972c)				
Energy, <sup>a</sup> eV	Spacing, <sup>b</sup> meV	Energy, <sup>c</sup> eV				
		$v=1$	$v=2$	$v=3$	$v=4$	$v=5$
		9.070				
9.23		9.220	9.155			
9.35	130	9.360	9.300			
9.49	125	9.500	9.445	9.400	9.365	
9.61	120	9.635	9.590	9.540	9.505	
9.73	120	9.760	9.730	9.675	9.645	9.600
9.85	115	9.885	9.860	9.810	9.780	9.730
9.96	115	10.005	9.980	9.940	9.910	9.860
10.07	110	10.120	10.095	9.065	10.035	9.990
10.18	105		10.200	9.175	10.155	10.115
10.29	105		10.305	9.285	10.265	10.230
10.39	100		10.405	9.395	10.375	10.345
10.49	100		10.505	9.495	10.480	10.450
10.58	90			9.595	10.575	10.555
10.67	90			9.695	10.670	10.655
10.76	90				10.765	10.745
10.85	85				10.850	10.835
10.93	85				10.930	10.920
11.02	85					11.000
						11.075
						11.150

**APPENDIX V—Continued**

 Energies of shape resonances connected with the  $A\ ^3\Sigma_u^+$  state.  
 $A\ ^3\Sigma_u^+$  decay channel (Mazeau *et al.*, 1972c)<sup>d</sup>

$v=2$	3	4	5	6
8.225 (15)				
8.315 (15)	8.307 (10)			
8.415 (10)	8.415 (10)	8.395 (10)		
8.515 (10)	8.522 (10)	8.503 (5)		
8.610 (10)	8.620 (10)	8.595 (5)	8.603 (5)	8.553 (5)
8.705 (10)	8.715 (5)	8.690 (15)	8.698 (5)	8.653 (10)
8.800 (10)	8.800 (10)	8.778 (15)	8.785 (5)	8.745 (10)
	8.880 (5)	8.878 (15)	8.870 (5)	8.837 (10)
	8.960 (10)	8.950 (15)	8.958 (5)	8.925 (5)
	9.040 (5)	9.030 (15)	9.040 (5)	9.008 (5)
	9.120 (10)	9.110 (15)	9.115 (5)	9.088 (5)
	9.195 (10)	9.178 (15)	9.183 (10)	9.168 (5)
	9.263 (10)	9.245 (15)	9.250 (5)	9.238 (5)
		9.312 (15)	9.315 (5)	9.300 (5)
		9.375 (15)	9.373 (5)	9.358 (5)
		9.428 (15)	9.430 (10)	9.418 (5)
		9.480 (10)	9.482 (10)	9.468 (5)
			9.538 (10)	9.515 (5)
			9.575 (10)	9.562 (10)

<sup>a</sup> Absolute error of the energy is  $\pm 0.05$  eV. Relative error  $\pm 0.003$  eV.

<sup>b</sup> The spacings are given to the nearest 5 meV.

<sup>c</sup> Error approximately  $\pm 10$  meV (see Mazeau *et al.*, 1972c).

<sup>d</sup> In parentheses are given the probable errors, in meV.

**APPENDIX VI**

Energies of features in CO (10–15 eV).

Feature number	Transmission Sanche and Schulz (1972)	Differential Comer and Read (1971c)		Mazeau <i>et al.</i> (1972a) $b\ ^3\Sigma^+, v=0^a$	Designation
		$v=1$	$v=2$		
1-1'	9.98-10.04	10.02	10.02	10.04 <sup>b</sup>	$^2\Sigma^+ v=0$
2-2'	10.24-10.29		10.28		$v=1$
3	10.42	10.38	10.46		
4-4'	10.65-10.72	10.80		10.7	$^2\Pi$
5	11.27			11.3	
6	12.17			12.2	
Band "a"	13.95				
	14.155				
	14.345				
	14.530				
	14.705				
	14.870				

<sup>a</sup> The threshold for the  $b\ ^3\Sigma^+$  state is 10.39 eV.

<sup>b</sup> Determined from elastic scattering at  $90^\circ$ . The calibration is performed against the  $(1s2s^2)^2S$  resonance in helium which the authors locate at  $19.35 \pm 0.02$  eV. [Sanche and Schulz find  $19.34 \pm 0.02$  eV.]

## APPENDIX VII

Comparison of vibrational spacings and Franck-Condon probabilities observed for four bands of NO<sup>-</sup> with appropriate values for NO<sup>+</sup>(X<sup>1</sup>Σ<sup>+</sup>) Sanche and Schulz (1972).

Δ <i>v</i>	Vibrational spacings (meV)				NO <sup>+</sup> (X <sup>1</sup> Σ <sup>+</sup> )	
	NO <sup>-</sup> band <sup>a</sup>				Experimental	Theoretical
	"a"	"b"	"c"	"d"		
0-1	286	290	292	282	290	
1-2	286	290	288	284	287	
2-3	282	284	286	275	283	
3-4				275	278	
4-5				275	273	

<i>v</i>	Franck-Condon probabilities				NO <sup>+</sup> (X <sup>1</sup> Σ <sup>+</sup> )	
	NO <sup>-</sup> band <sup>a</sup>				Experimental	Theoretical
	"a"	"b"	"c"	"d"		
0	0.84	0.57	...	0.66	0.7	0.48
1	1	1	...	1	1	1
2	0.62	0.64	...	0.7	0.7	0.92
3	0.16	0.24	...	0.19	0.5	0.49

<sup>a</sup> "a", "b", "c", "d" represent designations of bands, which start at 5.04, 5.41, 5.46, and 6.44±0.05 eV, respectively.

## APPENDIX VIII

Resonances in NO and their grandparents (12-18 eV) (Sanche and Schulz, 1972).

Resonance <sup>a</sup> NO <sup>-</sup> energy eV	Grandparent NO <sup>+</sup>		
	Designation	Energy eV	Binding eV
12.36( <i>v</i> =0)	<i>b</i> <sup>3</sup> Π	16.56	4.20
12.57( <i>v</i> =1)			
12.73( <i>s</i> )			
12.94( <i>s</i> )			
14.19( <i>v</i> =0)	<i>A</i> <sup>1</sup> Π	18.32	4.13
14.52( <i>s</i> )			
...	<i>C</i> <sup>3</sup> Π	20.46	...
17.51( <i>v</i> =0)	<i>B</i> <sup>1</sup> Π	21.72	4.21
17.94( <i>s</i> )			
5.04( <i>v</i> =0)	<i>X</i> <sup>1</sup> Σ <sup>+</sup>	9.27	4.23

<sup>a</sup> The features marked (*v*=0) are interpreted as the lowest states of core-excited Feshbach resonances. The features marked (*s*) are interpreted as core-excited shape resonances.

## APPENDIX IX

Spacing of vibrational states of O<sub>2</sub><sup>-</sup> X<sup>(2)</sup>Π<sub>g</sub> in meV.<sup>a</sup>

Vibrational transition	Spence and Schulz (1970)	Linder and Schmidt (1971b)	Gray <i>et al.</i> (1971)
4→5	117	125	128
5→6	113	123	125
6→7	110	120	121
7→8	108	119	118
8→9	106	117	115
9→10		115	113
10→11		113	109
11→12		111	105
12→13		110	
13→14		107	
14→15		104	
15→16		103	
16→17		101	
17→18		99	
Extrapolated: 0-1	135	135	140

<sup>a</sup> The state *v*'=8 is located near 569 meV (Linder and Schmidt, 1971b) and it is nearly coincident with the *v*=3 state of O<sub>2</sub> (Spence and Schulz, 1970).

## APPENDIX X

Resonance energies of  $O_2^-(X^2\Pi_g)$ , widths of  $O_2^-(X^2\Pi_g)$  and energy-integrated vibrational cross sections. [Energies and cross sections from Linder and Schmidt (1971b); widths from Koike and Watanabe (1973).]

$v'^a$	4 <sup>b</sup>	5	6	7	8	9	10	11	12	13	14	15	16	17	18
$E$ [eV] <sup>b</sup>	0.082	0.207	0.330	0.450	0.569	0.686	0.801	0.914	1.025	1.135	1.242	1.346	1.449	1.550	1.649
$\Delta E$ [meV] <sup>c</sup>	125	123	120	119	117	115	113	111	110	107	104	103	101	99	99
$\Gamma$ [meV]	0.004	0.036	0.12	0.26	0.46	0.74	1.1								
$\bar{Q}_v$ (in $10^{-20}$ cm <sup>2</sup> ×eV) <sup>e</sup>															
$v=1$	x <sup>g</sup>	...	25	82	110	100	61	35	17	9	5	...	...	...	...
$v=2$	x	x	x	...	8.5	25	32	28	19	12	5.8	2.4	1.0	...	...
$v=3$	x	x	x	x	...	...	1.3	5.5	7.3	7.0	5.8	3.3	1.8	1.0	...
$v=4$	x	x	x	x	x	x	...	...	...	1.0	1.9	2.0	1.7	1.0	1.0

<sup>a</sup>  $v'$  is the vibrational quantum number of the  $O_2^-(X^2\Pi_g)$  compound state.

<sup>b</sup>  $E$  is the energy of the compound state in the  $v'$  level (in eV).

<sup>c</sup>  $\Delta E$  is the spacing of the vibrational levels (in meV) of the compound state.

<sup>d</sup>  $\Gamma$  is the width of the vibrational level  $v'$  (in meV).

<sup>e</sup>  $\bar{Q}_v$  is the energy-integrated cross section to the final vibrational state,  $v$ , of  $O_2(X^3\Sigma_g^-)$ , which proceeds via  $O_2^-(v')$  [in units of  $10^{-20}$  cm<sup>2</sup>×eV].

<sup>f</sup> The symbol x indicates that the state is energetically inaccessible.

<sup>g</sup> Using a time-of-flight spectrometer, Land and Raith (1973) locate the center of the  $v'=4$  state at  $0.090 \pm 0.004$  eV, i.e., 8 meV above the value given in this table. The splitting of the  $v'=4$  state of  $O_2^-(X^2\Pi_g)$  is  $\Delta E = 22 \pm 2$  meV.

<sup>h</sup>  $v$  is the quantum number of vibrational states of  $O_2(X^3\Sigma_g^-)$ .

## APPENDIX XI

Core-excited resonances in O<sub>2</sub> as observed in a transmission experiment (Sanche and Schulz, 1972).

1-1'	2	3-3'	4	5-5'
8.03-8.06	8.12	8.24-8.28	8.34	8.47-8.54
6-6'	7-7'	8-8'	9-9'	10-10'
8.71-8.78	8.90-8.98	9.08-9.11	9.16-9.23	9.36-9.44
11-11'	12	13-13'-13	14-14'	15-15'
9.53-9.61	9.73	9.86-9.92-9.98	10.43-10.48	10.55-10.61
16-16'	17-17'			
10.74-10.82	10.91-11.00			
Band "a"				
11.81	11.93	12.05	12.17	12.29
<i>v</i> =1	<i>v</i> =2	<i>v</i> =3	<i>v</i> =4	<i>v</i> =5
12.40	12.51	12.62	12.73	12.84
<i>v</i> =6	<i>v</i> =7	<i>v</i> =8	<i>v</i> =9	<i>v</i> =10
Band "b"				
14.27	14.43	14.58	14.72	

\*The writing of this review was supported by the National Bureau of Standards, Office of Standard Reference Data, as part of the National Standard Reference Data Program.

†This paper is scheduled for reprinting in the National Standard Reference Data series being published by the National Bureau of Standards Office of Standard Reference Data through the U. S. Government Printing Office. For availability information write to the Office of Standard Reference Data, National Bureau of Standards, Washington, D. C. 20234.

Abram, R. A., and A. Herzenberg, 1969, *Chem. Phys. Lett.* **3**, 187.  
 Badger, R. M., 1935, *J. Chem. Phys.* **3**, 710.  
 Bardsley, J. N., A. Herzenberg, and F. Mandl, 1966a, *Proc. Phys. Soc. Lond.* **89**, 305.  
 Bardsley, J. N., A. Herzenberg, and F. Mandl, 1966b, *Proc. Phys. Soc. Lond.* **89**, 321.  
 Bardsley, J. N., and F. H. Read, 1968, *Chem. Phys. Lett.* **2**, 333.  
 Bardsley, J. N., and F. Mandl, 1968, *Rep. Prog. Phys.* **31**, 472.  
 Bates, D. R., and H. S. W. Massey, 1954, *Philos. Mag.* **45**, 111.  
 Berkowitz, J., W. A. Chupka, and D. Gutman, 1971, *J. Chem. Phys.* **55**, 2733.  
 Birtwistle, D. T., and A. Herzenberg, 1971, *J. Phys.* **B 4**, 53.  
 Black, K. F., and N. F. Lane, 1971, in *Electronic and Atomic Collisions*, Abstracts of Papers of the VIIth International Conference on the Physics of Electronic and Atomic Collisions (North-Holland, Amsterdam), p. 332 (1971).  
 Blatt, J. M., and V. F. Weisskopf, 1952, *Theoretical Nuclear Physics* (Wiley, New York), p. 360 (1952).  
 Boness, M. J. W., and J. B. Hasted, 1966, *Phys. Lett.* **21**, 526.  
 Boness, M. J. W., J. B. Hasted, and I. W. Larkin, 1968, *Proc. R. Soc. A* **305**, 493.  
 Boness, M. J. W., and G. J. Schulz, 1970, *Phys. Rev. A* **2**, 2182.  
 Borst, W. L., and E. C. Zipf, 1971, *Phys. Rev. A* **3**, 979.  
 Breig, E. L., and C. C. Lin, 1965, *J. Chem. Phys.* **43**, 3839.

Brongersma, H. H., A. J. H. Boerboom, and J. Kistemaker, 1969, *Physica (Utr.)* **44**, 449.  
 Brongersma, H. H., and L. J. Oosterhoff, 1967, *Chem. Phys. Lett.* **1**, 169.  
 Browne, J. C., and A. Dalgarno, 1969, *J. Phys.* **B 2**, 885.  
 Buchelnikova, I. S., 1959, *Sov. Phys.-JETP* **8**, 783.  
 Burke, P. G., and A. L. Sinfailam, 1970, *J. Phys.* **B 3**, 641.  
 Burke, P. G., 1968, *Adv. At. Mol. Phys.* **4**, 173.  
 Burrow, P. D., 1973 (unpublished).  
 Burrow, P. D., and L. Sanche, 1972, *Phys. Rev. Lett.* **28**, 333.  
 Burrow, P. D., and G. J. Schulz, 1969, *Phys. Rev.* **187**, 97.  
 Celotta, R. J., R. A. Bennett, J. L. Hall, M. W. Siegel, and J. Levine, 1972, *Phys. Rev. A* **6**, 631.  
 Chang, E. S., and U. Fano, 1972, *Phys. Rev. A* **6**, 173.  
 Chanin, L. M., A. V. Phelps, and M. A. Biondi, 1962, *Phys. Rev.* **128**, 219.  
 Chantry, P. J., 1968, *Phys. Rev.* **172**, 125.  
 Chantry, P. J., 1971, *J. Chem. Phys.* **55**, 2746.  
 Chantry, P. J., and G. J. Schulz, 1967, *Phys. Rev.* **156**, 134.  
 Chen, J. C. Y., 1964a, *J. Chem. Phys.* **40**, 3507.  
 Chen, J. C. Y., 1964b, *J. Chem. Phys.* **40**, 3513.  
 Chen, J. C. Y., 1966a, *J. Chem. Phys.* **45**, 2710.  
 Chen, J. C. Y., 1966b, *Phys. Rev.* **146**, 61.  
 Chen, J. C. Y., 1969, *Adv. Radiative Chem.* **1**, 245.  
 Chen, J. C. Y., and J. L. Peacher, 1967, *Phys. Rev.* **163**, 103.  
 Chen, J. C. Y., and J. L. Peacher, 1968a, *Phys. Rev.* **167**, 30.  
 Chen, J. C. Y., and J. L. Peacher, 1968b, *Phys. Rev.* **168**, 56.  
 Christophorou, L. G., and R. N. Compton, G. J. Hurst, and P. W. Reinhardt, 1965, *J. Chem. Phys.* **43**, 4273.  
 Chutjian, A., D. G. Truhlar, W. Williams, and S. Trajmar, 1972, *Phys. Rev. Lett.* **29**, 1580.  
 Clampitt, R., and A. S. Newton, 1969, *J. Chem. Phys.* **50**, 1997.  
 Claydon, C. R., G. A. Segal, and H. S. Taylor, 1970, *J. Chem. Phys.* **52**, 3387.  
 Comer, J., and F. H. Read, 1971a, *J. Phys.* **B 4**, 368.  
 Comer, J., and F. H. Read, 1971b, *J. Phys.* **B 4**, 1055.  
 Comer, J., and F. H. Read, 1971c, *J. Phys.* **B 4**, 1678.  
 Craggs, J. D., C. Thorburn, and B. A. Tozer, 1957, *Proc. R. Soc. A* **240**, 473.

- Crawford, O. H., and A. Dalgarno, 1971, *J. Phys. B* **4**, 494.
- Crompton, R. W., D. K. Gibson, and A. I. McIntosh, 1969, *Aust. J. Phys.* **22**, 715.
- Crompton, R. W., D. K. Gibson, and A. G. Robertson, 1970, *Phys. Rev. A* **2**, 1386.
- Crompton, R. W., and A. G. Robertson, 1971, *Aust. J. Phys.* **24**, 543.
- Dalgarno, A., 1961, *Ann. Geophys.* **17**, 16.
- Demkov, Yu. N., 1964, *Zh. Eksp. Teor. Fiz.* **46**, 1126. [*Sov. Phys.-JETP* **19**, 762.].
- Demkov, Yu. N., 1965, *Phys. Lett.* **15**, 235.
- Dowell, J. T., and T. E. Sharp, 1968, *Phys. Rev.* **167**, 124.
- Dunn, G. H., 1962, *Phys. Rev. Lett.* **8**, 62.
- Ehrhardt, H., 1969, *Physics of One- and Two-Electron Atoms*, edited by F. Bopp and H. Kleinpoppen (North-Holland, Amsterdam) (1969).
- Ehrhardt, H., L. Langhans, F. Linder, and H. S. Taylor, 1968, *Phys. Rev.* **173**, 222.
- Ehrhardt, H., and F. Linder, 1968, *Phys. Rev. Lett.* **21**, 419.
- Ehrhardt, H., and A. Weingartshofer, 1969, *Z. Phys.* **226**, 33.
- Ehrhardt, H., and K. Willmann, 1967, *Z. Phys.* **204**, 462.
- Eliezer, I., H. S. Taylor, and J. K. Williams, 1967, *J. Chem. Phys.* **47**, 2165.
- Englehardt, A. G., and A. V. Phelps, 1963, *Phys. Rev.* **131**, 2115.
- Englehardt, A. G., A. V. Phelps, and C. G. Risk, 1964, *Phys. Rev.* **135**, A1566.
- Faisal, F. H. M., and A. Temkin, 1972, *Phys. Rev. Lett.* **28**, 203.
- Farragher, A. L., F. M. Page, and R. C. Wheeler, 1964, *Discuss. Faraday Soc.* **37**, 205.
- Ferguson, E. E., 1968, *Adv. Electron. Electron Phys.* **24**, 1.
- Ferguson, E. E., 1970, *Acc. Chem. Res.* **3**, 402.
- Feshbach, H., 1958, *Ann. Phys. (N.Y.)* **5**, 357.
- Feshbach, H., 1962, *Ann. Phys. (N.Y.)* **19**, 287.
- Franck, J., and W. Grotrian, 1921, *Z. Phys.* **4**, 89.
- Frommhold, L., 1968, *Phys. Rev.* **172**, 118. ; see also D. J. Kouri, W. N. Sams, and L. Frommhold, 1969, *Phys. Rev.* **184**, 252.
- Gilmore, F. R., 1965, *J. Quant. Spectrosc. Radiat. Transfer* **5**, 369.
- Golden, D. E., 1966, *Phys. Rev. Lett.* **17**, 847.
- Golden, D. E., 1971, *Phys. Rev. Lett.* **27**, 227.
- Golden, D. E., and H. W. Bandel, 1965, *Phys. Rev. Lett.* **14**, 1010.
- Golden, D. E., H. W. Bandel, and J. A. Salerno, 1966, *Phys. Rev.* **146**, 40.
- Golden, D. E., N. F. Lane, A. Temkin, and E. Gerjuoy, 1971, *Rev. Mod. Phys.* **43**, 642.
- Golden, D. E., and H. Nakano, 1966, *Phys. Rev.* **144**, 71.
- Gray, R. L., H. H. Haselton, D. Krause, Jr., and E. A. Soltysik, 1971, in *Electronic and Atomic Collisions*, Abstracts of Papers of the VIIth International Conference on the Physics of Electronic and Atomic Collisions (North-Holland Amsterdam), p. 347 (1971).
- Haas, R., 1957, *Z. Phys.* **148**, 177.
- Hake, R. D., and A. V. Phelps, 1967, *Phys. Rev.* **158**, 70.
- Hall, R. I., M. Mazeau, J. Reinhardt, and C. Shermann, 1970, *J. Phys. B* **3**, 991.
- Hara, S., 1969, *J. Phys. Soc. Jap.* **27**, 1592.
- Hasted, J. B., and A. M. Awan, 1969, *J. Phys. B* **2**, 367.
- Heideman, H. G. M., C. E. Kuyatt, and G. E. Chamberlain, 1966a, *J. Chem. Phys.* **44**, 355.
- Heideman, H. G. M., C. E. Kuyatt, and G. E. Chamberlain, 1966b, *J. Chem. Phys.* **44**, 440.
- Henderson, W. R., W. L. Fite, and R. T. Brackmann, 1969, *Phys. Rev.* **183**, 157.
- Henry, R. J. W., 1970, *Phys. Rev. A* **2**, 1349.
- Henry, R. J. W., and E. S. Chang, 1972, *Phys. Rev. A* **5**, 276.
- Henry, R. J. W., and N. F. Lane, 1969, *Phys. Rev.* **183**, 221.
- Herzberg, G., 1950, *The Spectra of Diatomic Molecules* (Van Nostrand, Princeton, N. J.) (1950)
- Herzenberg, A., 1967, *Phys. Rev.* **160**, 80.
- Herzenberg, A., 1968, *J. Phys. B* **1**, 548.
- Herzenberg, A., 1969, *J. Chem. Phys.* **51**, 4992.
- Herzenberg, A., 1970, *Methods and Problems of Theoretical Physics*, edited by J. E. Bowcock (North-Holland, Amsterdam), p. 131 (1970).
- Herzenberg, A., 1971, *Phys. Bull. Inst. Phys. Soc. Lond.* **22**, 521.
- Herzenberg, A., and F. Mandl, 1962, *Proc. R. Soc. A* **270**, 48.
- Holzer, W., W. F. Murphy, H. J. Bernstein, and J. Rolfe, 1968, *J. Mol. Spectrosc.* **26**, 543.
- Joyez, G., J. Comer, and F. H. Read, 1973, *Eighth International Conference on the Physics of Electronic and Atomic Collisions: Abstracts of Papers* (Belgrade, Yugoslavia). Paper to be published in *J. Phys. B*.
- Julienne, P. S., and M. Krauss, 1972, *J. Res. Natl. Bur. Stand. (U.S.)* **76A**, 661.
- Kisker, E., 1972, *Z. Phys.* **257**, 51.
- Koike, F., and T. Watanabe, 1973, *J. Phys. Soc. Jap.* **34** (1022).
- Kolos, W., and L. Wolnicwicz, 1965, *J. Chem. Phys.* **43**, 2429.
- Kouri, D. J., 1968, *J. Chem. Phys.* **49**, 5205.
- Krauss, M., and F. H. Mies, 1970, *Phys. Rev. A* **1**, 1592.
- Krauss, M., and D. Neumann, 1972, *Chem. Phys. Lett.* **14**, 26.
- Krauss, M., D. Neumann, A. C. Wahl, G. Das, and W. Zemke, 1973, *Phys. Rev. A* **7**, 69.
- Kuyatt, C. E., S. R. Mielczarek, and J. A. Simpson, 1964, *Phys. Rev. Lett.* **12**, 293.
- Kuyatt, C. E., J. A. Simpson, and S. R. Mielczarek, 1966, *J. Chem. Phys.* **44**, 437.
- Lacmann, K., and D. R. Herschbach, 1970, *Chem. Phys. Lett.* **6**, 106.
- Land, J. E., and W. Raith, 1973, *Phys. Rev. Lett.* **30**, 193.
- Lane, N. F., and S. Geltman, 1967, *Phys. Rev.* **160**, 53.
- Lawton, S. A., and F. M. J. Pichanick, 1973, *Phys. Rev. A* **7**, 1004.
- Lassette, E. N., A. Skerbele, M. A. Dillon, and K. J. Ross, 1968, *J. Chem. Phys.* **48**, 5066.
- Linder, F., 1969, in *Sixth International Conference on the Physics of Electronic and Atomic Collisions: Abstracts of Papers* (North-Holland, Amsterdam), p. 141 (1969a).
- Linder, F., and H. Schmidt, 1971a, *Z. Naturforsch.* **26a**, 1603.
- Linder, F., and H. Schmidt, 1971b, *Z. Naturforsch.* **26a**, 1617.
- Lineberger, W. C., and T. A. Patterson, 1972, *Chem. Phys. Lett.* **13**, 40.
- Massey, H. S. W., and E. H. S. Burhop, 1969, *Electronic and Ionic Impact Phenomena* (Clarendon, Oxford), Vol. II. (1969).
- Mauer, J. L., and G. J. Schulz, 1973, *Phys. Rev. A* **7**, 593.
- Mazeau, J., F. Gresteau, G. Joyez, R. Reinhardt, and R. I. Hall, 1972a, *J. Phys. B* **5**, 1890.
- Mazeau, J., R. I. Hall, G. Joyez, M. Landau, and J. Reinhardt, 1972b, private communication and *J. Phys. B* **6**, 873 (1973).
- Mazeau, J., F. Gresteau, R. I. Hall, G. Joyez, and J. Reinhardt, 1972c, private communication and *J. Phys. B* **6**, 862 (1973).
- McFarland, M., D. B. Dunkin, F. C. Fehsenfeld, A. L. Schmeltekopf, and E. E. Ferguson, 1972, *J. Chem. Phys.* **56**, 2358.
- McGowan, J. W., and J. F. Williams, 1969, in *Sixth International Conference on the Physics of Electronic and Atomic Collisions: Abstract of Papers* (MIT, Cambridge, Mass.), p. 506 (1969).
- Menendez, M. G., and H. K. Holt, 1966, *J. Chem. Phys.* **45**, 2743.
- Michels, H. H., and F. E. Harris, 1971, in *Seventh International Conference on the Physics of Electronic and Atomic Collisions: Abstract of Papers*, (North-Holland, Amsterdam), Vol. II, p. 1170. (1971).

- Moruzzi, J. L., J. W. Ekin, Jr., and A. V. Phelps, 1968, *J. Chem. Phys.* **48**, 3070.
- Mulliken, R. S., 1957, in *The Threshold of Space*, edited by M. Zelikoff (Pergamon, New York) (1957).
- Nalley, S. J., and R. N. Compton, 1971, *Chem. Phys. Lett.* **9**, 529.
- Ogawa, M., and Y. Tanaka, 1962, *Can. J. Phys.* **40**, 1593.
- Oksyuk, Yu. D., 1966, *Sov. Phys.-JETP* **22**, 873.
- Olmsted, J., A. S. Newton, and K. Street, 1965, *J. Chem. Phys.* **42**, 2321.
- O'Malley, T. F., 1967, *Phys. Rev.* **155**, 59.
- O'Malley, T. F., and H. S. Taylor, 1968, *Phys. Rev.* **176**, 207.
- Pack, J. L., and A. V. Phelps, 1966, *J. Chem. Phys.* **44**, 1870.
- Paquet, C., P. Marchand, and P. Marmet, 1971, *Can. J. Phys.* **49**, 2013.
- Pavlovic, Z., M. J. W. Boness, A. Herzenberg, and G. J. Schulz, 1972, *Phys. Rev. A* **6**, 676.
- Pavlovic, Z., and M. J. W. Boness, 1973 (unpublished).
- Phelps, A. V., 1968, *Rev. Mod. Phys.* **40**, 399.
- Pichanick, F. M. J., S. A. Lawton, and R. D. Dubois, 1971, in *Electronic and Atomic Collisions*, Abstract of Papers of the VIIth International Conference on the Physics of Electronic and Atomic Collisions (North-Holland, Amsterdam), p. 339 (1971).
- Raith, W., and J. E. Land, 1972, in *Third International Conference on Atomic Physics* (University of Colorado, Boulder)(1972). See Land and Raith, 1973.
- Ramien, H., 1931, *Z. Phys.* **70**, 353.
- Ramsauer, C., and R. Kollath, 1931, *Ann. Phys. (Leipz.)* **10**, 143.
- Rapp, D. and D. D. Briglia, 1965, *J. Chem. Phys.* **43**, 1480.
- Rapp, D., T. E. Sharp, and D. D. Briglia, 1965, *Phys. Rev. Lett.* **14**, 533.
- Read, F. H., 1968, *J. Phys. B* **1**, 893.
- Reinhardt, J., G. Joyez, J. Mazeau, and R. I. Hall, 1972, *J. Phys. B* **5**, 1884.
- Rosen, B., 1970, *Spectroscopic Data Relative to Diatomic Molecules* (Pergamon, New York) (1970).
- Sampson, D. H., and R. C. Mjolsness, 1965, *Phys. Rev.* **140**, A1466.
- Sanche, L., Z. Pavlovic, M. J. W. Boness, and G. J. Schulz, 1971, in *Electronic and Atomic Collisions*, Abstracts of Papers of the VIIth International Conference on the Physics of Electronic and Atomic Collisions (North-Holland, Amsterdam), p. 350 (1971).
- Sanche, L., and G. J. Schulz, 1971a, *Phys. Rev. Lett.* **26**, 943.
- Sanche, L., and G. J. Schulz, 1971b, *Phys. Rev. Lett.* **27**, 1333.
- Sanche, L., and G. J. Schulz, 1972, *Phys. Rev. A* **6**, 69. Note that the bands in the transmission spectrum of N<sub>2</sub> (their Fig. 10) are improperly labelled. The proper designation appears in the Erratum, *Phys. Rev. A* **6**, 2500 (1972) and also in Fig. 42 of the present text.
- Schmeltekopf, A. L., F. C. Fehsenfeld, and E. E. Ferguson, 1967, *Astrophys. J.* **148**, L155.
- Schulz, G. J., 1959a, *Phys. Rev.* **113**, 816.
- Schulz, G. J., 1959b, *Phys. Rev.* **116**, 1141.
- Schulz, G. J., 1962a, *Phys. Rev.* **125**, 229.
- Schulz, G. J., 1962b, *Phys. Rev.* **128**, 178.
- Schulz, G. J., 1964a, *Phys. Rev.* **135**, A988.
- Schulz, G. J., 1964b, *Phys. Rev.* **136**, A650.
- Schulz, G. J., and R. K. Asundi, 1967, *Phys. Rev.* **158**, 25.
- Schulz, G. J., and J. T. Dowell, 1962, *Phys. Rev.* **128**, 174.
- Schulz, G. J., and H. C. Koons, 1966, *J. Chem. Phys.* **44**, 1297.
- Sharp, T. E., 1971, *At. Data* **2**, 119.
- Siegel, M. W., R. J. Celotta, J. L. Hall, J. Levine, and R. A. Bennett, 1972, *Phys. Rev. A* **6**, 607.
- Spence, D., and G. J. Schulz, 1970, *Phys. Rev. A* **2**, 1802.
- Spence, D., and G. J. Schulz, 1971a, *J. Chem. Phys.* **53**, 5424.
- Spence, D., and G. J. Schulz, 1971b, *Phys. Rev. A* **3**, 1968.
- Spence, D., and G. J. Schulz, 1972, *Phys. Rev. A* **5**, 724.
- Stamatovic, A., and G. J. Schulz, 1970, *J. Chem. Phys.* **53**, 2663.
- Swanson, N., C. E. Kuyatt, J. W. Cooper, M. Krauss, 1972, *Phys. Rev. Lett.* **28**, 948.
- Stockdale, J. A. D., R. N. Compton, G. S. Hurst, and P. W. Reinhardt, 1969, *J. Chem. Phys.* **50**, 2176.
- Swanson, N., J. W. Cooper, and C. E. Kuyatt, 1971, in *Electronic and Atomic Collisions*, Abstracts of Papers of the VIIth International Conference on the Physics of Electronic and Atomic Collisions (North-Holland, Amsterdam), p. 344 (1971).
- Takayanagi, K., and S. Geltman, 1965, *Phys. Rev.* **138**, A1003.
- Takayanagi, K., and Y. Itikawa, 1970, *Adv. At. Mol. Phys.* **6**, 105.
- Taylor, H. S., 1970, *Adv. Chem. Phys.* **18**, 91.
- Taylor, H. S., G. V. Nazarov, and A. Golebiewski, 1966, *J. Chem. Phys.* **45**, 2872.
- Trajmar, S., D. C. Cartwright, and W. Williams, 1971, *Phys. Rev. A* **4**, 1482.
- Trajmar, S., D. G. Truhlar, J. K. Rice, and A. Kuppermann, 1970, *J. Chem. Phys.* **52**, 4516.
- Truhlar, D. G., S. Trajmar, and W. Williams, 1972, *J. Chem. Phys.* **57**, 3250.
- Van Brunt, R. J., and L. J. Kieffer, 1970, *Phys. Rev.* **A2**, 1899.
- Weingartshofer, A., H. Ehrhardt, V. Hermann, and F. Linder, 1970, *Phys. Rev. A* **2**, 294.
- Weiss, A. W., and M. Krauss, 1970, *J. Chem. Phys.* **52**, 4363.
- Wong, S. F., M. J. W. Boness, and G. J. Schulz, 1973 (unpublished).